THE GENETIC AND PROTEOMIC DETEREMINANTS OF THE RISK OF CORONARY ARTERY DISEASE

NAIF AHMAD ALMONTASHIRI

Thesis submitted to the

Faculty of Graduate and Postdoctoral Studies

In partial fulfillment of the requirements for the degree of

Doctor of Philosophy (Ph.D.) in Biochemistry-Human and Molecular Genetics

Department of Biochemistry, Microbiology and Immunology

Faculty of Medicine, University of Ottawa

© Naif Ahmad Almontashiri, Ottawa, Canada, 2015

ABSTRACT

Coronary artery disease (CAD) remains the number one cause of morbidity and mortality in the world. CAD or atherosclerosis of the coronary arteries, results from the interaction of environmental and genetic risks factors and it is postulated that 50% of the susceptibility to CAD is genetic. With knowledge of specific genetic predispositions, people at risk could be screened earlier before the disease onset. I used information from genome wide association studies (GWASs) approach to characterize some of the genetic polymorphisms that increase the risk of CAD in large case-control studies. From the first top hit of the GWASs of CAD, I found that the CAD risk polymorphisms at the 9p21.3 risk locus are associated with increased human aortic smooth muscle cells (HAoSMCs) proliferation and down regulation of the expression of genes in the vicinity of the 9p21.3 risk locus, CDKN2A (p16) and CDKN2B (p15). Extensive bioinformatics scanning of the 58 kb long 9p21.3 risk locus identified two polymorphisms that disrupt the binding of TEA-domain (TEAD) transcription factors that play a role in controlling cell cycle. Over-expression of TEAD3 or TEAD4 in HAoSMCs homozygous for the non-risk allele led to increased expression of p16, while cells homozygous for the risk allele failed to respond. TEAD factors interact with SMAD3 to mediate TGFβ induction of p16 expression. HAoSMCs homozygous for the risk allele failed to induce p16 in response to TGFβ treatment. The disrupted binding of TEAD factors to its sites at the 9p21.3 risk locus is responsible for the impaired TEAD/ TGFβ induction of p16 at the 9p21.3 risk locus.

From another hit of GWASs, I characterized a gain-of-function polymorphism (rs12960) in a mitochondrial protease called spastic paraplegia 7 (SPG7). This variant escaped a novel phosphorylation regulated processing which rendered SPG7 constitutively

active. HAoSMCs carrying the risk alleles showed increased protease activity and mitochondrial reactive oxygen species production (mROS). Increased mROS production led to increased cellular proliferation and mitochondrial fusion. Cellular proliferation and mROS production are potential risk factors for CAD.

GWASs discovered variants at PCSK9 that are linked to the risk of CAD. The mechanism on how PCSK9 has a major effect on the incidence of CAD-associated events relative to his effect on LDL-C is not clear. To address this, I measured plasma PCSK9 levels in two large angiographic case-control studies using ELISA. I found that plasma PCSK9 was significantly higher in patients with acute myocardial infarction (AMI) compared to those with CAD only or CAD with a previous (non-acute) MI. The association between plasma PCSK9 levels and AMI was independent of LDL-C. My work suggests that plasma PCSK9 levels could affect AMI by mechanisms independent of LDL-C.

My PhD work points to the importance of backing up the GWASs and genetics data with functional studies to understand the mechanism of how these variants and genes increases the risk of CAD.

ACKNOWLEDGMENTS

I would like to thank my supervisor Dr. Alexandre Stewart who was very nice, friendly and smart mentor. He helped me to achieve my aims that once were just dreams. In addition, his sense of humor when I feel bored or upset helped me to get back on track. I wish to thank Drs. Patrick Burgon and Daniel Sparks for their guidance and support as members of my TAC committee. Special thanks to my lab mates, Tiffany Ho, Ragnar Vilmundarson and Darlene Antoine for helping me get through the difficult times, and for all the emotional support that I received during the time I spent with them.

My mother, Zahra, deserves more than gratitude and respect for her unlimited support, prayers and infinite love. To my brothers and sisters, I send my respect and appreciation for caring about me and my educational progress.

My sweet and special thanks to my beloved wife, Khulud, for her help and generous emotional support that made my success visible. My daughter, Sadeen, although she has no idea what I am doing, her presence in my life made me different, stronger and patient man.

I dedicate this dissertation to the memory of my father, Ahmad Almontashiri. I really miss him and I wish him with me especially for this moment.

TABLE OF CONTENTS

ABSTRACT ..... **ii**

ACKNOWLEDGMENTS ..... **iv**

TABLE OF CONTENTS ..... **v**

LIST OF ORIGINAL PUBLICATIONS ..... **vii**

ABBREVIATIONS ..... **ix**

LIST OF FIGURES ..... **xiv**

LIST OF TABLES ..... **xvi**

CHAPTER 1 ..... **1**

General introduction **1**

The pathophysiology of atherosclerosis 2

Cell proliferation in atherosclerosis 4

TGFβ and VSMCs proliferation in atherosclerosis 5

The genetics of CAD 7

9p21.3 CAD risk locus as the first hit of GWAS 9

Mitochondrial reactive oxygen species (mROS) and coronary atherosclerosis 11

Rationale 12

Research objectives and introduction to manuscripts 13

CHAPTER 2 ..... **20**

Abstract **21**

Introduction **22**

Materials and Methods **23**

Results **25**

Interferon-γ markedly increases p16 and p15 protein levels 25

Discussion **28**

CHAPTER 3 ..... **34**

Abstract **35**

Introduction **36**

Methods **38**

Results **39**

The effect of the 9p21.3 locus on cultured primary HAoSMC proliferation and senescence 39

TEAD transcription factor binding is disrupted at the 9p21.3 locus 40

Disruption of TEAD regulation of p16 at the 9p21.3 risk locus 48

9p21.3 risk locus impairs TGFβ induction of p16 49

Conclusions **60**

Acknowledgements **60**

Source of funding **61**

Disclosures **61**

Clinical perspective **61**

Supplemental information **61**

CHAPTER4 ..... **84**
Abstract **85**
Highlights **85**
Introduction **86**
Experimental procedures **88**
A variant of SPG7 (Q688) associates with CAD risk 91
SPG7 protein processing and maturation is enhanced in individuals who carry the Q688 allele 91
Stable HEK293 cells expressing the Q688 SPG7 variant also show increased SPG7 maturation 95
The Q688 form of SPG7 is a gain-of-function variant 95
Molecular modeling suggests a stabilizing influence of the Q688 variant 96
The Q688 SPG7 variant increases ATP production 99
The Q688 SPG7 variant Alters the stoichiometry of components of the electron transport chain and proton leak from fatty acid oxidation 102
The Q688 SPG7 variant increases mROS levels 106
The Q688 SPG7 variant increases cell proliferation 110
Forskolin blocks processing of the R688 SPG7 but not the Q688 variant 110
Discussion **116**
Supplemental experimental procedures **121**

CHAPTER 5 ..... **143**
Introduction **145**
Materials and Methods **146**
Results **150**
Statins elevate plasma PCSK9 150
Plasma PCSK9 levels are not associated with coronary atherosclerosis in the OHGS for individuals not taking a statin 150
Plasma PCSK9 levels are elevated with acute MI, but not with prior MI, in the OHGS 153
PCSK9 levels are associated with coronary atherosclerosis in the EmCB study 153
Plasma PCSK9 levels are also elevated with acute MI, but not with prior MI, in the EmCB study 156
Discussion **157**
Conclusion **160**

CHAPTER 6 ..... **170**
General discussion **170**
The regulation of gene expression at the 9p21.3 CAD risk locus 171
Mitochondrial ROS signaling and atherosclerosis 174
The pathogenic roles of PCSK9 in CAD 176
Future insights 177

Appendices **180**
Appendix 1. Permission from the Journal of the American College of Cardiology to reprint paper (105) in the PhD dissertation. **180**

REFERENCES **181**

LIST OF ORIGINAL PUBLICATIONS

1) Chen, H. H., Almontashiri, N. A., Antoine, D. & Stewart, A. F. Functional genomics of the 9p21.3 locus for atherosclerosis: clarity or confusion? *Curr Cardiol Rep* 16, 502, doi:10.1007/s11886-014-0502-7 (2014).
2) Naif A. M. Almontashiri, Hsiao-Huei Chen, Ryan J. Mailloux, Takashi Tatsuta, Allen C. T. Teng, Ahmad B. Mahmoud, Tiffany Ho , Nicolas A. S. Stewart, Peter Rippstein, Mary Ellen Harper, Robert Roberts, Christina Willenborg and Jeanette Erdmann for the CARDIoGRAM consortium, Annalisa Pastore, Heidi McBride, Thomas Langer, Alexandre F. R. Stewart. SPG7 Variant Escapes Phosphorylation-Regulated Processing by AFG3L2, Elevates Mitochondrial ROS and Associates with Multiple Clinical Phenotypes. *Cell Reports*, doi:S2211-1247(14)00248-4 [pii] 10.1016/j.celrep.2014.03.051 (2014).
3) Naif A. M. Almontashiri, Meng Fan, Robert Roberts, Alexandre F. R. Stewart. Interferon-γ activates expression of p15 and p16 regardless of 9p21.3 coronary artery disease risk genotype.*J Am Coll Cardiol.* Jan 15 2013;61(2):143-147. (Impact factor: 14.16). (This paper received an editorial commentary in a different journal, Circulation Cardiovascular Genetics: Musunuru K. Enduring mystery of the chromosome 9p21.3 locus. *Circ Cardiovasc Genet.* Apr 1 2013;6(2):224-225).
4) Allen C.T. Teng, Naif A. M. Almontashiri, Brian L.M. Cheng, Philip Lou, Pinar Ozmizrak, Hsiao-Huei Chen, and Alexandre F.R. Stewart (2011). Identification of Nuclear Localization Signal in IRF2BP2. PLoS ONE, 6(8), e24100. (Impact factor: 4.09).

5) Naif A. M. Almontashiri, Ragnar O. Vilmundarson, Nima Ghasemzadeh, Hsiao-Huei Chen, Robert Roberts, Arshed Quyyumi, Alexandre F. R. Stewart. Plasma PCSK9 levels are elevated with acute myocardial infarction in two independent retrospective cross-sectional angiographic studies. PLoS One 9, e106294, doi:10.1371/journal.pone.0106294 . PONE-D-14-15937 [pii] (2014).

ABBREVIATIONS

CAD: coronary artery disease

MI: myocardial infarction

T2DM: type 2 diabetes mellitus

SNPs: single nucleotide polymorphisms

GWASs: genome-wide association studies

LD: linkage disequilibrium

CARDIoGRAM : Coronary ARtery DIsease Genome-Wide Replication And Meta-Analysis

OHGS: ottawa heart genomics study

EmCB: Emory cardiology biobank

CDKN2A: cyclin dependent kinase inhibitors 2A

CDKN2B: cyclin dependent kinase inhibitors 2B

MTAP: methylthioadenosine phosphorylase

chr4$^{\Delta 70kb/\Delta 70kb}$ mice: deletion of the human 9p21.3 homologous region in mice

shRNA: short hairpin RNA

STAT1: signal transducers and activators of transcription family of transcription factor 1

ANRIL: antisense noncoding RNA at the ink4 locus non-coding gene

PRC1 and PRC2: polycomb repressor complex 1 and 2

DNMT1: DNA methyltransferase

HAoSMCs: human aortic smooth muscle cells

AoSMCs: aortic smooth muscle cells

VSMCs: vascular smooth muscle cells

WBCs: white blood cells

HUVECs: human umbilical vein endothelial cells

LCLs: lymphoblastoid cell lines

HEK293: human embryonic kidney

THP-1: Tamm-Horsfall protein 1

EMSA: electrophoretic mobility shift

TEAD: TEA-domain

ECM: extracellular matrix

CDKs: cyclin-dependent kinases

CKIs: cyclin dependent kinase inhibitors

E2F1: E2 promoter binding factor 1

TGFβ: transforming growth factor beta

TGFBR: TGFβ receptor

MRPS6: mitochondrial ribosomal protein S6

CYP17A1: cytochrome P450, family 17, subfamily A, polypeptide 1

ETC: electron transport chain

ATP5G1: ATP synthase, H+ transporting, mitochondrial Fo complex, subunit C1

PEMT: phosphatidylethanolamine N-methyltransferase

ROS: mitochondrial reactive oxygen species

Trx2: thioredoxin 2

PRDX3: peroxiredoxin 3

SOD2: superoxide dismutase 2

TrxR2: thioredoxin reductase 2

AFG3L2: ATPase family gene 3-like 2

SPG7: spastic paraplegia 7

HSP: hereditary spastic paraplegia

SCA28: spinocerebellar ataxia 28

hMRPL32: human mitochondrial ribosomal protein L32

m-AAA: matrix-ATPases associated with diverse cellular activities

LON: ATP-dependent protease La

OPA1: optic atrophy 1

MFN2: mitofusin 2

HNF1α: hepatocyte nuclear factor 1 homeobox A

PCNA: proliferating cell nuclear antigen

TCA cycle: tricarboxylic acid cycle

COX1: cytochrome c oxidase subunit 1

COX2: cytochrome c oxidase subunit 2

COX3: cytochrome c oxidase subunit 3

COX4: cytochrome c oxidase subunit 4

GAPDH: glyceraldehyde-3- phosphate dehydrogenase

pRB: phosphorylated retinoblastoma

NO: nitric oxide

peNOS-Thr495: phosphorylated inhibitory threonine at position 495

eNOS: endothelial nitric oxide synthase

p-AMPK: phosphyrlated AMP-activated protein kinase

BN-PAGE: blue native-polyacrylamide gel electrophoresis

HEt: hydroethidium

BrdU: bromodeoxyuridine

PI: propidium iodide

FACS: fluorescence-activated cell sorting

DCFH-DA: 2',7'-dichlorfluorescein-diacetate

TMRE: tetramethylrhodamine ethyl ester

OCR: oxygen consumption rate

ECAR: extracellular acidification rate

FCCP: carbonilcyanide p triflouromethoxyphenylhydrazone

MPP: mitochondrial processing peptidase

PBMCs: peripheral blood mononuclear cells

DRP1: dynamin-related protein 1

TFAM: mitochondrial transcription factor A

MCAD: medium-chain acyl-CoA dehydrogenase

TOM 20: translocase of the outer membrane 20

NAC: N-acetyl cysteine

PKA: protein kinase A

ANOVA: analysis of variance

ANCOVA: analysis of covariance

SD: standard deviation

SEM: standard error of the mean

OR: odds ratio

IQR: inter-quartile range

OMA1: oocyte maturation defective metallopeptidase

ELISA: enzyme-linked immunosorbent assay

PCSK9: proprotein convertase subtilisin/kexin type 9

LDL-C: low density lipoprotein-cholesterol

HDL-C: high density lipoprotein-cholesterol

LDL-R: LDL receptor

LRP8: LDL-R related protein 8

ApoE: apolipoprotein E

HMG-CoA reductase: 3-hydroxy-3-methyl-glutaryl-CoA reductase

SREBP-2: sterol regulatory element-binding protein 2

BMI: body mass index

TG: riglycerides

HTN: hypertension

LIST OF FIGURES

Chapter 1

Figure 1. Schematic diagram of the effect of the 9p21.3 risk locus on the cell cycle suppressor genes and cell proliferation 16
Figure 2. Schematic diagram of the hypotheses and findings generated from the GWASs of CAD. 18

Chapter 2

Figure 1. Interferon-γ activates p16 and p15 expression regardless of 9p21.3 genotype. 26
Figure 2. Effect of interferon-γ on p15 and p16 levels in different cell types. 29

Chapter 3

Figure 1. The 9p21 coronary artery disease risk allele is associated with reduced p16 and p15 protein expression and increased cellular proliferation in HAoSMCs. 41
Figure 2. The rs10811656 and rs4977757 polymorphisms disrupt a functional TEAD factor binding site. 44
Figure 3. The rs4977757 and rs10811656 risk alleles disrupt functional binding sites for TEAD3 and TEAD4 at the 9p21.3 CAD risk locus. 46
Figure 4. TEAD3 and TEAD4 regulate the expression of p16 but not p15 at the 9p21.3 locus. 50
Figure 5. TGFβ induced p16 expression is TEAD-dependent and disrupted by the 9p21.3 risk allele. 52
Figure 6. TGFβ regulation of p16 expression is dependent on TEAD3 transcription factor and disrupted by 9p21.3 risk alleles rs4977757 and rs10811656. 56
Figure S1. Gel mobility shift assay reveals that the STAT1 does not bind to rs10757278. 67
Figure S2. EMSA analysis shows that rs1333045 dose not contain a functional Smad3 binding site. 69
Figure S3 71
Figure S4. EMSA analysis shows that rs10811656 and rs4977757 polymorphisms disrupt the binding the endogenous TEADs factors to its binding sites. 73
Figure S5. TEAD4 does not affect the response to TGFβ of luciferase reporters bearing rs10811656 and rs4977757. 75
Figure S6 77

Chapter 4

Figure 1. Q688 variant of SPG7 associates with risk of CAD and alters proteolytic processing of SPG7. 92
Figure 2. The SPG7 Q688 variant rescues loss of function AFG3L2 mutants in yeast. 97
Figure 3. The SPG7 Q688 variant alters mitochondrial bioenergetics. 100
Figure 4. Effect of SPG7 Q688 variant on cellular bioenergetics measured in living cells. 104
Figure 5. The SPG7 Q688 variant increases mROS production and cellular proliferation. . 107
Figure 6. SPG7 processing is controlled by AFG3L2 phosphorylation. 111
Figure 7. Model of SPG7 processing. 114
Figure S1. Quantification of over-expressed SPG7 R688 and Q688 proteins in HEK293 cells. 131
Figure S2. Knockdown of SPG7 shows that both bands detected in mitochondria by immunoblot are SPG7. 133

Figure S3. Effect of TCA cycle substrates glutamine and pyruvate on aerobic respiration (oxygen consumption rate, OCR) and glycolysis (extracellular acidification, ECAR) in HEK293 cells transfected with wild type R688 or variant Q688. 135
Figure S4. Effect of fatty acid oxidation on aerobic respiration (oxygen consumption rate, OCR) and glycolysis (extracellular acidification, ECAR) in HEK293 cells transfected with wild type R688 or variant Q688. 137
Figure S5. 139
Figure S6. Specificity of immunoprecipitation. 141

Chapter 5

Figure 1. Mean PCSK9 levels do not differ with atherosclerosis burden. 151
Figure 2. Plasma PCSK9 levels are increased with acute MI. 154

LIST OF TABLES

Chapter 2

Table 1 Imputation of rs10757278 using flanking SNPs in high linkage disequilibrium. 33

Chapter 3

Table S1 Characteristics of the primary HAoSMCs used in this study. 78
Table S2 Summary of the bioinformatics scan and functional validation of SNPs with possibly disruptive effect. 79
Table S3 The oligonucleotides used for EMSA to test transcription factors binding to different SNPs. 80
Table S4 Control oligonucleotides used as competitors in EMSA for different transcription factors. 81
Table S5 Oligonucleotides used to generate different reporter constructs carrying the risk and non risk variants that are shown. 82
Table S6 Sequences of the lentiviral shRNAs used to knock down human TEAD3 and TEAD4 83

Chapter 5

Table 1 Clinical characteristics of OHGS CAD cases and controls. 162
Table 2 Linear regression analysis of the relationships between explanatory variables and the level of PCSK9 in the OHGS. 163
Table 3 Logistic regression analysis of the association of PCSK9 with CAD in the OHGS cohort, stratified by statin use. 164
Table 4 Logistic regression analysis of the association of PCSK9 with acute MI in the OHGS cohort, stratified by statin use. 165
Table 5 Clinical characteristics of CAD cases and controls from 166
Table 6 Linear regression analysis of the relationships between explanatory variables and the level of PCSK9 in the EmCB sub-study. 167
Table 7 Logistic regression analysis of the association of PCSK9 with CAD in the EmCB sub-study. 168
Table 8 Logistic regression analysis of the association of PCSK9 with acute MI in the EmCB sub-study. 169

CHAPTER 1

General introduction

The major cause of CAD is atherosclerosis which is the result of plaque build up and narrowing of the inner wall of the coronary arteries that supply heart muscle with blood leading to limited blood flow and therefore ischemia. Plaque consists mainly of fat (cholesterol and fatty acids)-laden macrophages, vascular smooth muscle cells (VSMCs), cellular debris, and minerals such as calcium. The white blood cells (WBCs) component of the plaque produces inflammatory cytokines that recruit more inflammatory cells at the site of the plaque. Although this process is meant to be protective, it further contributes to the plaque size and inflammation (1). CAD is a very common and complex chronic disease with traditional and genetic risk factors. The traditional risk factors of CAD include age, gender, obesity, dyslipidemia, diabetes, hypertension and smoking. These factors act independently or in concert with each other to increase the risk of CAD. Controlling of the known risk factors for CAD such as smoking, hypercholesterolemia is shown by the randomized clinical trials to associate with about 30% to 40% reduction in the clinical events such as myocardial infarction and subsequent death (2). The other 40% to 60% of the risk for CAD is heritable as shown by the epidemiological, twins and family studies. Heritability of CAD is the part of CAD risk explained by genetic factors (3). In a landmark case-control study, CAD is shown to have a strong heritability ranging from 56 % (when patients with monogenic heart disease are excluded) to 63 % (including patients with monogenic heart diseases) (4). Moreover, the first degree relatives showed higher risk index for ischemic heart disease and stroke (3, 1 respectively) than the second degree relatives (1, 0.5 respectively). The heritability in this

study was calculated using the method of falconer used in twin studies to determine the heritability of a certain traits or phenotypes based on the difference between twins. Among the first degree relatives with CAD, the heritability was estimated to be about 100% in patient under age 46; whereas the heritability ranged from 15% to 30% in late onset cases of CAD (5). The younger the CAD patient at the diagnosis of the first event of MI, the more common was CAD in his relatives of parents and siblings.

CAD is a polygenic and complex disease that requires the action and presence of several risk variants to express the phenotype (6). Some of the traditional risk factors are influenced by genetic variations in their gene components. For example, variants in *APOE* or *PCSK9* genes affect the levels of low density lipoprotein-cholesterol (LDL-C) and increase the risk of CAD through mechanisms dependent on LDL-C (7). However, some of the genetic variations exert their effect independent of the traditional risk factors such as the 9p21.3 CAD risk locus (8). Therefore, deep knowledge of these variants and how they interact with each other or with the traditional risk factors is prerequisite for a comprehensive prevention strategy in the future.

The pathophysiology of atherosclerosis

Atherosclerosis is an asymptomatic chronic late onset disease. The atherosclerotic plaques are divided into stable or unstable. The stable plaque is often asymptomatic and contains collagen-rich extracellular matrix produced mainly by smooth muscle cells. The collagen-rich extracellular matrix (ECM) makes the stabilizing fibrous cap that separates the plaque from the lumen of the vessel. In contrast, unstable plaque is rich in foam cells and collagen-poor ECM making it unstable and vulnerable to rupture. The rupture of the plaque

and the release of its thrombogenic components trigger the thrombosis and formation of blood clots that occlude arteries and trigger MI (9).

The major players in the pathogenesis of atherosclerosis are the endothelial cells, macrophages and VSMCs. These cells are involved in plaque development and rupture (10). A very interesting recent study on human coronary atherosclerotic sections from hearts showed that 50% of the total foam cells in the human coronary atherosclerosis were derived from intimal smooth muscle cells (11). One of the major and sufficient drivers of atherosclerosis and plaque development is the higher levels of plasma LDL-C. LDL-C particles migrate from the circulation to the intima of the arteries. Macrophages in the intima release the atherogenic NO that oxidizes LDL-C (ox-LDL) and makes them hard to degrade (indigestible) by macrophages forming fat-laden macrophages (12). The necrotic death of these macrophages in the growing plaque releases pro-inflammatory cytokines and destabilizes the plaque, making it vulnerable to rupture and leading to myocardial infarction (MI) (10). LDL-C is cleared from the circulation by the LDL receptor (LDL-R) on the surface of the liver hepatocytes. Disruption of this mechanism of clearance is associated with hypercholesterolemia and atherosclerosis. Mutations in LDL-R receptor or a gain of function in the proprotein convertase subtilisin/kexin type 9 (*PCSK9*), the protein that helps to degrade LDL-R, are associated with high levels of plasma LDL-C and linked to familial hypercholesterolemia, premature CAD, and MI (13). PCSK9 binds to the LDL-R through the EGF-a (epidermal growth factor) domain, resulting into lysosomal degradation of the complex through unknown mechanisms. Higher levels of PCSK9 result in increased plasma levels of LDL-C as a result of the increased degradation of LDL-R (14).

Loss-of-function mutations in PCSK9 are associated with 88% reduction in CAD-associated events and only 30% reduction in plasma LDL-C (15). The uptake of PCSK9 by

hepatic LDL-receptors accounts for most, but not all, of the clearance mechanism that removes PCSK9 from plasma (16). Statins can reduce LDL-C by 20-40% in a dose dependent manner (17). This effect of statins on LDL-C is associated with less than 30% reduction in mortality from CAD (18). Plasma PCSK9 is associated with periodontitis, a risk factor for MI, independent of LDL-C levels (19). Periodontitis is a risk factor for CAD and MI (20). Altogether, these observations suggest that PCSK9 may have additional effects beyond LDL-C.

Statins are the drugs of choice for lowering LDL-C in patients with hypercholesterolemia. They work by inhibiting the rate limiting enzyme, HMG-CoA reductase, for cholesterol synthesis in the liver (21). Statins also induce the expression of plasma PCSK9 through the induction of its transcription activators, SREBP2 and HNF1α (22-25). Therefore, reducing or inhibiting PCSK9 is expected to have a greater impact on lowering LDL-C in patients taking statins. In fact, monoclonal antibodies to block PCSK9 interaction with LDL-R is a strategy already in the late stage clinical trials and was shown to be successful at lowering LDL-C in patients taking statins (26,27).

Cell proliferation in atherosclerosis

The process of cell proliferation is regulated by a group of proteins called cyclin-dependent kinases (CDKs) and cyclin dependent kinase inhibitors (CKIs). Activation of cell cycle phase-specific CDKs drive the progression through this phase. For example, the CKIs p15 and p16 interact with and inactivate CDK4 and CDK6, preventing them from binding and activating cyclin D. Inactive cyclin D cannot phosphorylate the cytoplasmic retinoblastoma protein (RB) and release the sequestered E2 promoter binding factor 1 (E2F1) to enter the nucleus and activate the transcription of genes involved in the progression from G1 to S phase (28,29).

Epigenetic modifications such as hypermethylation were found to be enriched in the aorta and PBMCs and to play causative role in the process of atherosclerosis development in mouse model of CAD (30). Hypermethylation is significantly associated with the risk of CAD (31,32). Hypermethylation of the upstream regions of TGFBR3 genes were found to be significantly enriched in those patients (31). Risk factors such as dyslipidemia and hyperhomocysteinemia are key mediators of hypermethylation seen in patients with CAD (30,32). Higher methylation levels were detected in the promoter of estrogen receptor beta gene in tissues and plaques from CAD patients (33). The expression of the estrogen receptor beta gene was restored upon DNA-methyltransferase inhibition. Perturbed expression of *CDKN2A* and *CDKN2B* is associated with several tumors (34-36). Methylation of *CDKN2A* and *CDKN2B* is associated with CAD in human (37). Methylation, although not significantly correlated to the 9p21.3 risk locus, was linked to the *ANRIL* transcript expression. The 9p21.3 CAD risk locus is associated with reduced expression of p15 and p16 and increased cell proliferation (38). Excessive cell proliferation within the walls of the arteries contributes to the enlargement of the plaque and restenosis after angioplasty (39). The VSMCs and macrophages are the main proliferating cell types in the human atherosclerotic plaques (40).

TGFβ and VSMCs proliferation in atherosclerosis

The proliferation of VSMCs is very critical for repair and healing processes after vascular injury or insult. However, if the insult persists, as in atherosclerosis, the mitogenic stimulus continues and the proliferation of VSMCs becomes atherogenic (41). The VSMCs produce ECM that stabilizes the plaque. Migration and proliferation of arterial smooth-muscle cells enlarge the atherosclerotic lesion (39). TGFβ inhibits VSMCs migration, proliferation and induces collagen-rich ECM production (42,43). In the walls of normal vessels, the VSMCs

mainly express type II TGFβ receptor (*TGFBR),* as opposed to type I TGFβ receptor in VSMCs from atherosclerotic vessels (42). In response to TGFβ, normal VSMCs that express type II TGFβ receptor massively induce the expression of contractile proteins and minimal production of the ECM. In contrast, diseased VSMCs expressing type I TGFβ receptor increase the expression of the collagen rich-ECM but fail to induce contractile proteins expression in response to TGFβ. If fresh VSMCs are maintained in TGFβ containing media, they maintain type II TGFβ receptor (44). Low concentrations of TGFβ increase proliferation of VSMCs, consistent with the fact that low levels of plasma TGFβ are associated with a poor outcome in CAD (45,46). Conversely, at higher concentrations, TGFβ inhibits VSMCs proliferation (45) and reduces atherosclerosis (47). The levels of plasma TGFβ are reduced at sites of lesion development in the intima of the coronary arteries and human aorta (48,49). Altogether, these studies demonstrate that TGFβ is critical for maintaining the contractility of the VSMCs and to inhibit their proliferation and migration to the intima of the arteries. Therefore, impaired or lack of TGFβ signaling is atherogenic. Mutations in *TGFBR1* and *TGFBR2* genes that cause congenital heart disease and arterial aneurysms are linked to increased VSMCs proliferation, increased collagen expression and reduced contractile proteins (SMC α-actin, β-myosin, and calponin) expression (50,51).

TGFβ induces the expression of p16 and p15 through Smad proteins such as Smad2 and Smad3, to control cell cycle and induce cellular senescence (28,52,53). Smad3 interacts with the TEA-domain (TEAD) family of transcription factors and particularly with TEAD3 and TEAD4 (54). TEAD family has a common N-terminal domain that enables them to bind a specific DNA element called M-CAT (5'-CATTCC-3') and a transactivation domain to interact with co-activators such as Smad proteins. TEAD transcription factors play a key role in the expression of cardiac, smooth and skeletal muscle specific genes (such as SMC α-actin,

β-myosin) (55). They play a major role in tumor suppression and cell cycle control (56). The major role of TEAD factors in the VSMCs and cardiac development explain their involvement in the congenital and developmental heart diseases (57).

The genetics of CAD

Most genetic differences within the human genome are caused by changes in single nucleotides in the sequence of DNA called single nucleotide polymorphism (SNP). At certain positions, one nucleotide is replaced by another and this change occurs at a certain frequency in the human population. The group of SNPs that are clustered and co-inherited together (in linkage disequilibrium) is called a haplotype. Genotyping one SNP of the haplotype to reliably predict the genotype of the other SNPs is called imputation (58). Most of these changes are benign but sometimes they prevent certain proteins that bind to DNA from doing so and alter how nearby genes are transcribed and expressed. SNPs known to be benign and well tolerated in a monogenic disorder, can increase the risk of polygenic and complex disorder such as CAD though the pleiotropic nature of these SNPs (59,60). The advent of technology and the availability of the microarrays to detect many of the SNPs (1,000,000 SNPs) across the genome made the search for risk variants that increase and associate with the risk of CAD possible through the genome-wide association studies (GWAS). GWASs compares the frequency of bialleleic common SNPs (minor allele frequency of $\geq$ 1% in the population) between angiographically defined cases of CAD and controls (61). The significance of the difference in allele frequency between CAD cases and controls is tested using logistic regression analysis. GWAS can also be done to find SNPs that affect quantitative traits such as LDL-C, HDL-C, blood pressure or any quantitative trait known to be a risk factor for CAD in a case-control or population study designs. The mean values of these parametric traits in each

study group are compared statistically using continuous tests, such as *t* test or linear regression analyses (62). Variants that meet the genome wide significance threshold of $< 5 \times 10^{-8}$ with replication in an independent population of a relatively large sample size will be considered significant. GWAS is unbiased approach that enabled us to scan the genome for susceptibility loci without preconception which gene or SNP associate with the risk or protection against CAD.

This overly conservative threshold of significance due to the Bonferroni correction for multiple testing could result in the loss of some genetic variants (the missing heritability) that do not reach this level of significance (63). This is (the below threshold significance for some of the variants), in part, because of the relatively low frequency of these variants and the small sample size of the study. Another major reason is that they associate with other multiple phenotypes (pleiotropy) that were not adjusted for when the GWAS for CAD is performed (63). Pleiotropy occurs when a one gene influences multiple phenotypes but is caused by one gene polymorphism or mutation. The necessity for larger sample sizes to detect variants with bigger effects but low frequencies led to sample pooling and formation of consortia with bigger sample sizes such as CARDIoGRAM (Coronary Artery Disease Genome-wide Replication and Meta Analysis) for CAD variants that involves 14 GWASs (64). So far, GWASs have discovered 50 risk loci with the majority of these conferring risk of CAD through unknown mechanisms (38). Importantly, using 12 of these loci was shown to improve cardiovascular risk prediction beyond the traditional risk factors (65). Using the 50 SNPs in combination for risk prediction is likely to confer greater predictive capabilities for CAD than the risk predicted by the individual SNPs. Another form of variations in the human genome is the copy number variants (CNVs). Although such variations are linked to other human diseases (66), no CNVs were found to be significantly associated with risk of CAD.

The 50 genetic risk variants account for only 15% to 20% of the heritability of CAD due to the missing heritability (63). It is also possible that some of the common genetic variants are not yet discovered. Gene-gene and gene-environment interactions (epistasis) in CAD are possible causes of the falsely small risk effect of some of the variants which could account for the missing heritability (67). *Shirts et al.* (2011) examined gene-age interaction in HDL-C, LDL-C, and TG levels and showed age dependent association between *SORT1* and LDL (68). In early onset acute MI, the 9p21.3 CAD risk locus showed strong association with the progression of atherosclerosis and coronary revascularization (69). Loci that related to known environmental factors for CAD such as alcoholism (6p21.31) and smoking habit (9p24.12 and 17q21.32) showed a robust association with CAD by GWAS (7). It is very important for the next GWAS to take into consideration these interactions that could yield meaningful improvement in risk prediction and account for some of the heritability

9p21.3 CAD risk locus as the first hit of GWAS

Using microarrays of SNPs to genotype large numbers of cases and controls, the first common genetic variants at chromosome 9p21.3 that confer the risk for CAD was identified (70). This risk locus is also associated with other diseases such as type 2 diabetes (71), CAD-associated MI, abdominal aortic and intracranial aneurysm (72). Several other large GWAS confirmed this association with CAD (73-75). The minor allele frequency (MAF) in different populations is as follows: European (50%), Sub-Saharan African (50%), African American (24%), Asian (47%), and Han Chinese (37%). The mechanism whereby these genetic variants contribute to the risk of CAD has remained elusive (76). The 9p21 risk alleles predict the severity of CAD as measured by the burden of arterial atherosclerosis: the 9p21 risk allele was found more frequently in patients with narrowing of 3 coronary arteries than in those with a single affected

artery (77). No significant association in the frequency of 9p21.3 risk locus between CAD patients with or without MI (77). This suggests that the 9p21.3 risk locus works through plaque development not rupture. This locus contains as many as 33 enhancers that are known to contain either CAD or T2D risk variants (78).Gene expression profiling of macrophages did not show significant 9p21.3 genotype dependent-differential expression of the genes in the vicinity (79). The 9p21.3 locus contains 59 linked SNPs located 100,000 base pairs upstream the cell cycle suppressor genes, *CDKN2A* (codes for p16 and p14) and *CDKN2B* (codes for p15). This locus overlaps the 3` region of the *ANRIL* (antisense noncoding RNA at the ink4 locus non-coding gene). 9p21.3 risk variants overlapping the 3` of *ANRIL* is associated with induced expression of different splicing isoforms of ANRIL and with reduced expression of *CDKN2A* and *CDKN2B* (80) Polycomb repressor complex 1 and 2 (PRC1 and PRC2) along with polycomb complex protein EZH2 are recruited to *ANRIL* which in turn leads to recruitment of DNA methyltransferase (*DNMT1*) and this would also increase DNA methylation and inactivation *CDKN2A* locus (81). However, increased expression of *ANRIL* transcript and methylation of the *CDKN2A and CDKN2B* locus were significantly associated with CAD in angiographic defined patients but not tightly correlated to the 9p21.3 risk locus (37).

Several studies showed reduced expression of p16 and p15 in the presence of the 9p21.3 CAD risk locus in aortic smooth muscle cells (AoSMCs) (80,82,83). This reduced expression of p16 and p15 at the risk locus is linked to increased HAoSMCs proliferation and failure to enter senescence. p16 and p15 are well known tumor suppressors and cellular senescence markers through the retinoblastoma pathway (34-36). Thus, the 9p21 risk allele appears to promote the deposition of atherosclerotic plaque in the coronary arteries, maybe by the accumulation of fat-laden foam cells and proliferation of VSMCs in the intima, rather than

weakening of the extracellular matrix to cause plaque rupture and myocardial infarction (see figure 1).

Mitochondrial reactive oxygen species (mROS) and coronary atherosclerosis

Four of the 23 loci associated with CAD that are identified by CARDIoGRAM consortium were found at or near genes encoding mitochondrial proteins (including MRPS6, CYP17A1, ATP5G1, and PEMT) demonstrating a mitochondrial involvement (7). However, the mechanisms by which these variants increase the risk of CAD are unknown. Mitochondria produce mROS as a byproduct of ATP generation from oxidative phosphorylation. The ability of healthy mitochondria to keep this process under control is a key requirement for the integrity of the healthy mitochondria under normal physiology. Mitochondrial damage by ROS happens through oxidation and then inactivation of key mitochondrial proteins such as those of the electron transport chain (ETC) (84). Several human diseases including CAD are linked to perturbed mitochondrial dynamics and bioenergetics (85,86). The mROS is one of the early events that trigger the endothelial dysfunction and VSMC proliferation seen in atherosclerosis. The level of the generated mROS was significantly higher in patients with unstable angina compared to those with stable angina (87). ROS also induces the expression of the adhesion molecules required for the recruitment of the inflammatory fat-laden macrophages to the intima of the atherosclerotic arteries (88,89). ROS-mediated LDL-C oxidation leads to the formation of the atherogenic foam cells and proliferation of VSMCs, impairment of the ECM of the atherosclerotic site of the artery. Such biological events are expected to affect plaque stability (90).

Mitochondria are equipped with an antioxidant system that maintains them in a reduced state and enables them to continuously buffer the levels of generated ROS (91,92). The

antioxidant enzymes such as superoxide dismutase 2 (*SOD2*) and peroxiredoxins (*PRDXs*) are located in the inner membrane of mitochondria as a first line of defense to scavenge excessive mROS production from ETC. For example, PRDX3 protects against mROS in the AoSMCs and against mROS-induced myocardial ischemia and left ventricular remodeling (93,94). SOD2 activity in the myocardium is essential to protect against ischemia and reperfusion-induced cardiac arrhythmias and infarction (95). Mutations in SOD2 are associated with dilated cardiomyopathy (96).

The quality control function of the mitochondrial matrix proteases such as m-AAA (matrix ATPase associated with diverse cellular activities) and the Lon proteases is critical for the mitochondria to get rid of the proteins of the ETC and other proteins damaged or oxidized by mROS (97,98). The m-AAA is also required for mitochondrial ribosomal assembly, and therefore the synthesis of essential mitochondrial protein complexes such as those of ETC (99,100). The m-AAA protease can be formed as an AFG3L2 homohexamer or an AFG3L2 and SPG7 heterohexamer (101). AFG3L2 is autocatalytic, while SPG7 is dependent on AFG3L2 for its processing and activation (102). Loss-of-function mutations in either protein are associated with neurodegenerative disorders, defective mitochondrial respiration and cortical vascular lesions (103-105).

Rationale

CAD is a very common disease and considered to be the number one killer in the world. CAD is a multi-factorial and polygenic disorder with more than 50% of the risk from genetic predisposition. Therefore, identifying the genetic modifiers that increase the risk of CAD will help to understand the complex process of the disease, and in preventing or treating the disease if the mechanisms of action and pathogenesis for these variants are fully understood. The solo

job of GWASs is to scan the human genome looking for common variants (SNPs) that are more common in cases of CAD than control, or vice versa (protective SNPs), in very large sample sizes. The GWASs have been successful in discovering 50 loci that associate with the risk of CAD. The majority of these variants are associated with the risk of CAD independent of the traditional risk factors. However, except for few variants, the mechanisms of how many of these variants increase the risk of CAD are not known.

Research objectives and introduction to manuscripts

The objective of my studies is to understand the functional mechanisms of how genes or SNPs shown by our group, Ottawa Heart Genomics Study (OHGS), are associated with increased risk of CAD. My studies were focused on three hypotheses derived from GWAS data (see figure 2).

1- SNPs at the 9p21.3 CAD risk locus disrupt transcription factor binding and affect the expression of genes in the vicinity.

2- The gain-of–function variant, rs12960, in the mitochondrial protease SPG7 increases the risk of CAD and other clinical phenotypes by increasing the protease activity and the production of mROS.

3- Plasma PCSK9 levels are associated with the risk of CAD and MI by mechanisms other than the LDL-C hypothesis.

In the first part of my study (Chapter 2 & 3- Manuscripts # 1 & 2), I challenged the findings by *Harismendy et al*. (2011) (78) that claimed that the interferon gamma induction of genes in the vicinity of the 9p21.3 risk locus is impaired by the disruption of STAT1 binding at the 9p21.3 risk locus (106). My work showed that interferon gamma activates the expression of p15 and p16 regardless of the 9p21.3 risk locus **(Chapter 2- Manuscript# 1)**. Moreover, I

showed that the DNA element containing rs10757278 is a weak and non-functional STAT1 site **(Chapter 3- Manuscript# 2)**. To understand the real mechanism of the 9p21.3 risk locus, I hypothesized that SNPs that disrupt the binding for transcription factors, could account for the observed reduction in the expression of p15 and p16 and the increased HAoSMCs proliferation linked to the 9p21.3 risk locus **(Chapter 3- Manuscript# 2)**. To examine this hypothesis, I scanned the all 59 SNPs at the risk locus and found two SNPs (rs10811656 and rs4977757) that disrupt binding of TEAD3 and TEAD4 transcription factors. TEAD3 and TEAD4 induce the expression of p16 and this induction is disrupted by the homozygosity to the risk locus in HAoSMCs. Importantly, I showed that the 9p21.3 risk locus disrupts TEAD3-dependent TGFβ regulation of p16 expression and cell cycle control in HAoSMCs. This mechanism accounts for the reduced expression of p16 linked to the risk locus.

In the second part of my work **(Chapter 4- Manuscript# 3)**, I tried to understand the mechanism by which the SPG7 functional variant, rs12960, is associated with the increased risk of CAD and other clinical phenotypes (59). I hypothesized that this gain-of-function variant increases the ATP-dependent activity of the SPG7 protease and also increases mROS production as a by-product of the increased ATP production. Indeed I found that this variant is a gain-of-function polymorphism that escapes the novel phosphorylation regulation of SPG7 processing by AFG3L2. This variant increases ATP and mROS production, which led to increased cellular proliferation. Excessive production of mROS and cell proliferation are known biological phenotypes that are linked to atherosclerosis.

GWAS and genetic linkage studies showed a disproportionate correlation between the effect of PCSK9 variants on CAD-associated events rather than its effect on LDL-C. Loss of function variants are associated with 88% reduction in CAD-associated events but only reduce LDL-C by 25-30% (15). An equivalent reduction of LDL-C achieved by statins reduced the

myocardial events by only 25%. This indication leads to the hypothesis that PCSK9 increases the risk of CAD-associated events by mechanisms that include, but are not limited to LDL-C. To address this hypothesis **(Chapter 5- Manuscript# 4)**, I measured plasma PCSK9 levels in two independent retrospective angiographically defined studies using ELISA. I found that plasma PCSK9 levels were not associated with CAD or CAD severity compared to controls (107). However, when I stratified our cohorts by MI status, I discovered for the first time that plasma PCSK9 levels in patients with acute MI are significantly elevated with acute MI compared to patients with CAD but no MI or with previous MI history. Consistent with our hypothesis, plasma PCSK9 levels were an independent predictor of the acute MI independent of LDL-C levels. This supports the notion that PCSK9 may exert its pathological effect on MI by mechanisms not limited to LDL-C. However, given the cross-sectional design of our study, I could not tell if PCSK9 levels are elevated prior to or before the acute MI. Future longitudinal studies are warranted to test if plasma PCSK9 is a culprit or a consequence for acute MI.

Figure 1. Schematic diagram of the effect of the 9p21.3 risk locus on the cell cycle suppressor genes and cell proliferation

9p21.3 Risk Locus

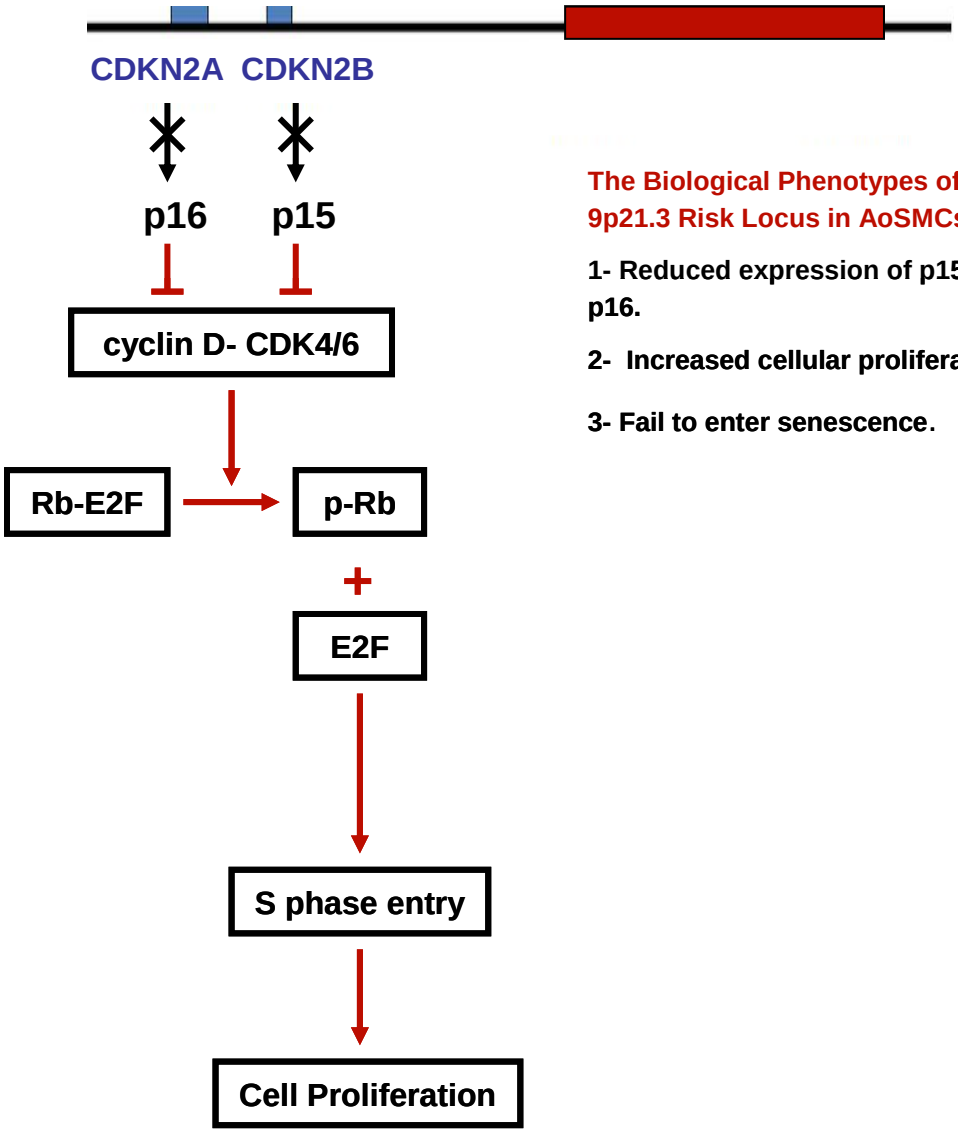

The Biological Phenotypes of the 9p21.3 Risk Locus in AoSMCs:

1- Reduced expression of p15 and p16.

2- Increased cellular proliferation.

3- Fail to enter senescence.

Figure 2. Schematic diagram of the hypotheses and findings generated from the GWASs of CAD.

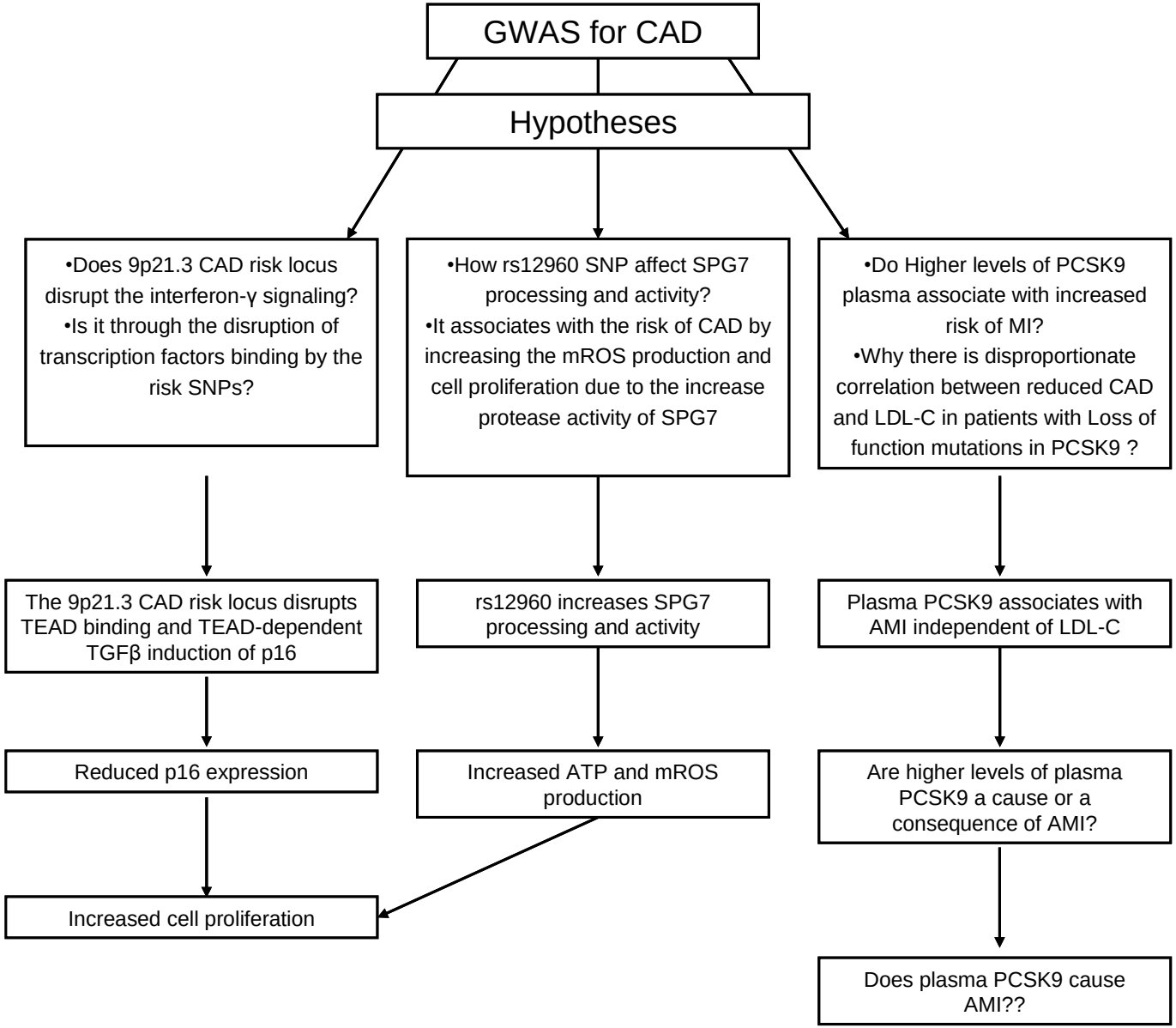
GWAS for CAD
Hypotheses
•Does 9p21.3 CAD risk locus disrupt the interferon-γ signaling?
•Is it through the disruption of transcription factors binding by the risk SNPs?
•How rs12960 SNP affect SPG7 processing and activity?
•It associates with the risk of CAD by increasing the mROS production and cell proliferation due to the increase protease activity of SPG7
•Do Higher levels of PCSK9 plasma associate with increased risk of MI?
•Why there is disproportionate correlation between reduced CAD and LDL-C in patients with Loss of function mutations in PCSK9 ?
The 9p21.3 CAD risk locus disrupts TEAD binding and TEAD-dependent TGFβ induction of p16
rs12960 increases SPG7 processing and activity
Plasma PCSK9 associates with AMI independent of LDL-C
Reduced p16 expression
Increased ATP and mROS production
Are higher levels of plasma PCSK9 a cause or a consequence of AMI?
Increased cell proliferation
Does plasma PCSK9 cause AMI??

CHAPTER 2

Interferon-γ activates expression of p15 and p16 regardless of 9p21.3 coronary artery disease risk genotype

Naif A. M. Almontashiri, MSc[*, †], Meng Fan, PhD[*], Brian L. M. Cheng, BSc[*], Hsiao-Huei Chen, PHD,[§], Robert Roberts, MD[*], Alexandre F. R. Stewart, PhD[*]

Naif A. M. Almontashiri, MSC,*†‡ Meng Fan, PHD,† Brian L. M. Cheng, BSC,† Hsiao-Huei Chen, PHD,§ Robert Roberts, MD,†_ Alexandre F. R. Stewart, PHD*†_

*Department of Biochemistry, Microbiology and Immunology, University of Ottawa, Ottawa, Ontario, Canada; †John and Jennifer Ruddy Canadian Cardiovascular Genetics Centre, University of Ottawa Heart Institute, Ottawa, Ontario, Canada; ‡Center of Genetics and Inherited Diseases, Faculty of Applied Medical Sciences, Taibah University, Almadinah, Saudi Arabia; §Neuroscience, Ottawa Hospital Research Institute, Ottawa, Ontario, Canada; and the Department of Medicine, University of Ottawa, Ottawa, Ontario, Canada.

Address for correspondence: Alexandre Stewart, 40 Ruskin Street H3100, Ottawa, Ontario, Canada, K1Y 4W7, astewart@ottawaheart.ca, tel: 613-751-5189, fax: 613-761-4647

This paper was first published as a clinical research article in the Journal of the American College of Cardiology (2013) Jan; 2013 Jan 15; 61(2):143-7.

Author contributions: NAMA and BLMC performed the experiments; HHC and RR provided essential reagents; MF analyzed the data, NAMA, HHC, and AFRS wrote the manuscript.

Key Words: 9p21.3; coronary artery disease; cyclin-dependent kinase inhibitor; interferon-γ; p15; p16.

See Appendix 1 for the permission to re-print from the Journal of the American College of Cardiology.

Abstract

Objective: The mechanism whereby the common variant at chromosome 9p21.3 confers risk for coronary artery disease (CAD) remains uncertain. A recent report proposed that 9p21.3 confers differential activation of adjacent genes in response to interferon-γ, but reported that mRNA levels of CDKN2B are reduced in response to interferon-γ. Since post-transcriptional mechanisms modulate levels of p16 (encoded by CDKN2A) and p15 (encoded by CDKN2B), I tested whether interferon-γ regulates the expression of these proteins and the effect of the 9p21 genotype.

Methods: Human umbilical vein endothelial cells (HUVECs), aortic smooth muscle cells, HeLa, HEK293 cells and 16 human lymphoblastoid cell lines, all genotyped for the 9p21.3 locus, were treated with interferon-γ and analyzed by immunoblot.

Results: In all cells tested, except HUVECs where expression was not modulated by interferon-γ, regardless of 9p21.3 genotype, interferon-γ increased the expression of p16 and p15. Northern blot analysis confirmed that interferon-γ has little effect on mRNA levels of CDKN2A and CDKN2B.

Conclusion: The 9p21.3 risk genotype does not affect the activation of cyclin-dependent kinase inhibitors p15 and p16 by interferon-γ. Thus, another mechanism is likely to account for the CAD risk associated with this locus.

Introduction

The common genetic variant located in the vicinity of the genes encoding the cyclin-dependent kinase inhibitors p15 (CDKN2B) and p16/ARF (CDKN2A) on the short arm of chromosome 9 at 9p21.3 contributes to the risk of CAD by an unknown mechanism that is independent of known risk factors (70,74,108). 9p21.3 associates with the severity of coronary atherosclerosis in a risk allele-dosage specific manner (109), recently confirmed by others (110). Among cases with CAD, 9p21.3 does not associate with myocardial infarction (109) suggesting that it promotes atherosclerosis rather than thrombosis.

The 9p21.3 risk locus consists of many tightly linked single nucleotide polymorphisms (SNPs) that cover an area of about 58,000 bp. Whether a single SNP at this locus is functional, or whether several SNPs have a functional effect remains controversial. We identified enhancer sequences within the 9p21.3 region, and in particular we found that the SNP rs1333045 conferred differential enhancer activity (80). A recent study that ablated the homologous sequences in the mouse genome observed markedly reduced expression of CDKN2A and CDKN2B mRNA (83), confirming the existence of regulatory sequences in this region. Another recent report provided evidence that the SNP rs10757278 at the 9p21.3 CAD risk locus disrupts a STAT1-responsive sequence and confers differential activation of adjacent genes in response to interferon-γ (78). Thus, these authors suggested that inability to upregulate p15 and p16 would promote cellular proliferation and atherosclerosis. However, the evidence they provided to support this suggestion appeared to contradict their hypothesis. For example, quantitative PCR measured reduced mRNA for CDKN2B in response to interferon-y in HeLa cells and HUVECs, both heterozygous for the rs10757278 SNP (78). However, the single STAT-1-responsive allele in heterozygous cells should have been

activated by interferon-y. Moreover, altered mRNA expression does not always translate to altered protein levels. For example, transforming growth factor-β markedly elevates p15 protein levels but barely increases mRNA levels (111), whereas the micro-RNA miR-24 suppresses translation of the p16 mRNA without affecting mRNA levels (112). In light of these post-transcriptional mechanisms, and to confirm whether or not an interferon-γ-dependent mechanism operates at the 9p21.3 risk locus, we re-examined the association of the 9p21.3 genotypes with the response of p15 and p16 to interferon-γ at the protein level.

Materials and Methods

Cell cultures

Human primary aortic smooth muscle cells (HAoSMCs) were purchased with culture medium from Cell Applications. (San Diego, CA), umbilical vein endothelial cells (HUVECs) were obtained from Lonza (Allendale, NJ), and cultured as recommended, lymphoblastoid cells (LCLs, n=16) were selected for their 9p21 genotype and purchased from the Coriell Institute for Medical Research (Camden, NJ), and cultured in RPMI Medium 1640 (Invitrogen, Burlington, Ontario). Recombinant human interferon-γ was purchased from R&D Systems (Minneapolis, MN).

Genotyping

DNA from HeLa, HUVECs, HEK293 cells were genotyped for the 9p21.3 risk locus by PCR and sequencing. A DNA fragment containing SNP rs1333048 was obtained using primers 5'-TGG CTA TAA ATG CCT TTG GC-3' and 5'-CCA TAT ATC TTG CTT ACC TCT GCG-3') and another fragment containing rs10757278 was obtained using primers 5'-TTG GAA CTG AAC TGA GGC CAG ACA-3' and 5'-TAG ACT CCA CGC TGT TCC

CAA GTA-3'. HAoSMCs were genotyped on Affymetrix Axiom arrays (Affymetrix Inc, Santa Clara, CA).

Processing of cells for immunoblotting

Cells were lysed in RIPA buffer (4.25 mM Tris, pH8.0, 135 mM NaCl, 1% IGEPAL CA-630, 1% SDS 0.5% deoxycholate) containing protease and phosphatase inhibitors (Roche Molecular Systems, Branchburg, NJ). Lysate protein concentrations were measured by Bradford assay before SDS-PAGE and immunoblot analysis.

Antibodies and immunoblot analyses

Mouse anti-p16 (sc-9968) and anti-p15 (sc-171798) antibodies were purchased from Santa Cruz Biotechnology (Santa Cruz, CA), antibody to p14 (clone 4C6/4) was from EMD Millipore (Temecula, CA), antibody to phosphorylated serine 727 (p-Ser 727) of Stat1 from Cell Signaling Technology (Danvers, MA), goat anti-mouse IgG (HAF007) from R&D Systems (Minneapolis, MN) and goat anti-rabbit IgG (#31460) from Piercenet (Rockford, IL). Immunoblots were quantified and normalized to GAPDH levels using ImageQuant TL V2005 software, expressed as means ± SD. The effect of 9p21.3 genotypes on the response to interferon-γ was determined by linear regression at $p<0.05$.

Northern blot analysis

RNA was isolated from HeLa and HUVECs treated with vehicle (PBS with 0.1% bovine serum albumin) or with 100 ng/ml interferon-γ using TRIzol® reagent (Life Technologies, Burlinton, ON), according to the manufacturer's instructions. Fifteen micrograms of RNA was size fractionated by polyacrylamide gel electrophoresis, transferred to nylon membrane and probed with CDKN2A (clone 3954155, Open Biosystems, Lafayette, CO) or CDKN2B (clone 4871014) radiolabelled with $dCT^{32}[P]$ using the random primers technique (Agilent Technologies, Lajolla, CA). Images were revealed using a phosphor-

storage screen and a Storm 860 molecular imager (GE Healthcare Life Sciences, Baie D'Urfe, QC).

Results

Interferon-γ markedly increases p16 and p15 protein levels

Lymphoblastoid cells (LCLs) are Epstein-Barr virus transformed B lymphocytes that remain in a proliferative state because $p16^{INK4A}$ (CDKN2A) expression is repressed by the Epstein-Barr virus nuclear antigens 3A and 3C (113,114). The ability to immortalize B lymphocytes from many individuals of different ancestry and to ascertain by high throughput the genotypes of common genetic variants has been a cornerstone of the International HapMap project (58). Since the genotype of common variants, including the rs10757278, are known or can be imputed for these cells lines, and since these cells maintain a low level of p16 expression, we tested whether interferon-γ can activate the expression of p16 and p15 and whether the 9p21.3 CAD risk genotype influences this response.

LCLs for each 9p21.3 genotype were selected from the HapMap database and purchased from the Coriell Institute for Medical Research. Where the genotype for the STAT1-responsive sequence disrupted by rs10757278 was not known, it was imputed using linked flanking SNPs (D'=1.0, r^2>0.8, see Table 1). All cell lines were also genotyped for the rs10757278 SNP by PCR amplification and direct sequencing and the genotypes agreed with the imputation. LCLs treated with interferon-γ markedly increased the levels of p15 and p16, as revealed by immunoblot (Figure 1A). We were unable to detect the alternative product of the CDKN2A gene $p14^{ARF}$ (data not shown). Importantly, of the 16 LCLs tested (5 homozygous non-risk, 5 heterozygotes and 6 homozygote risk for the 9p21.3 genotype),

Figure 1. Interferon-γ activates p16 and p15 expression regardless of 9p21.3 genotype. (A) LCLs homozygous non-risk (n=5), heterozygote (n=5) or homozygote risk (n=6) for the 9p21.3 genotypes were treated with vehicle or 100 ng/ml recombinant human interferon-γ for 24 hours and then harvested for immunoblot analysis (representative results). Antibody to phosphorylated serine 727 (p-Ser 727) of Stat1 confirmed activation by interferon-γ. Numbers below lanes are unique identifiers for the LCLs. (B) Quantification of the response to interferon-γ showed no significant difference between genotypes for p15 (n=5 per genotype) or p16 (n=3 per genotype). Fold induction is expressed as mean ± SD.

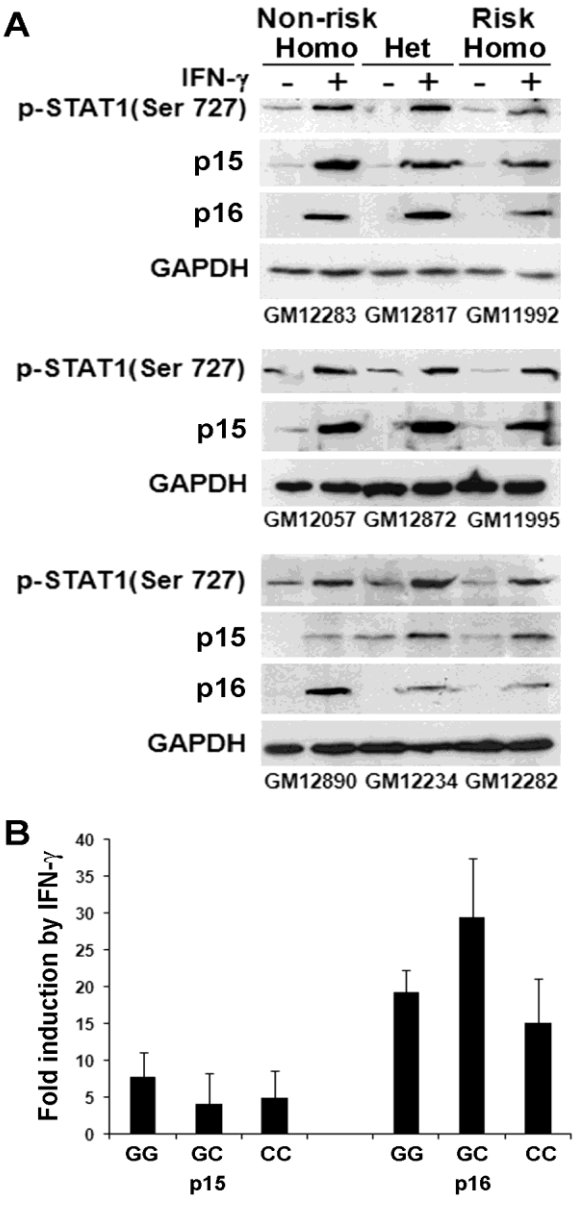
A
Non-risk
Risk
Homo
Het
Homo
IFN-γ
- + - + - +
p-STAT1(Ser 727)
p15
p16
GAPDH
GM12283 GM12817 GM11992
p-STAT1(Ser 727)
p15
GAPDH
GM12057 GM12872 GM11995
p-STAT1(Ser 727)
p15
p16
GAPDH
GM12890 GM12234 GM12282
B
Fold induction by IFN-γ
40
35
30
25
20
15
10
5
0
GG GC CC
p15
GG GC CC
p16

interferon-γ increased p15 (n=16) and p16 (n=12) to a similar degree regardless of 9p21.3 CAD genotype (Figure 1B).

The response to interferon-γ was also tested in other cell types (Figure 2A). In HAoSMCs heterozygous for the rs10757278 genotype (as well as for rs1333045, rs1333048, and rs133049), a robust elevation of p15 and p16 was observed. In contrast, p15 and 16 levels were not affected by interferon-γ treatment in HUVECs homozygous for the non-risk genotype of 9p21.3 (rs1333048), despite a clear activation of pSTAT1. Similar to the LCLs, the cell lines HEK293 (homozygous for the 9p21.3 rs1333048 risk allele) and HeLa (heterozygous for rs1333048) also increased p16 and p15 levels in response to interferon-γ. To determine whether interferon-γ treatment affects CDKN2A and CDKN2B mRNA levels, we performed northern blot analysis of HUVECs and HeLa cells (Figure 2B). Interferon-γ did not significantly elevate CDKN2A levels in HeLa cells and CDKN2A mRNA was not detected in HUVECs. On the other hand, a slight increase in CDKN2B was detected in HeLa cells treated with interferon-γ, whereas there was no change in CDKN2B mRNA in HUVECS.

Discussion

A recent study claimed that the mechanism whereby the 9p21.3 risk locus operates is by impairing the response to interferon-γ (78). These authors reported that interferon-γ markedly reduced the mRNA levels of the cyclin dependent kinase inhibitor p15 (encoded by CDKN2B) in HeLa and HUVECs (their cells that are heterozygous for the 9p21.3 risk locus) (78). However, using the same dose of interferon-γ (100 ng/ml), we observed increased increased expression of p15 in all cell types examined except HUVECs, where the levels

Figure 2. Effect of interferon-γ on p15 and p16 levels in different cell types.
(A) Results of immunoblot analysis of protein extracts from primary HAoSMCs (9p21 heterozygote) and HUVECs (9p21 homozygote non-risk), as well as from HEK293 (homozygote risk) and HeLa (heterozygote) cells are shown. GAPDH was not affected by interferon-γ and was used as a loading control. (B) Northern blot analysis shows no or only modest increases in CDKN2A and 2B levels in HUVECs and HeLa cells. 28S and 18S RNA signal confirmed equal loading of 15 µg RNA per lane.

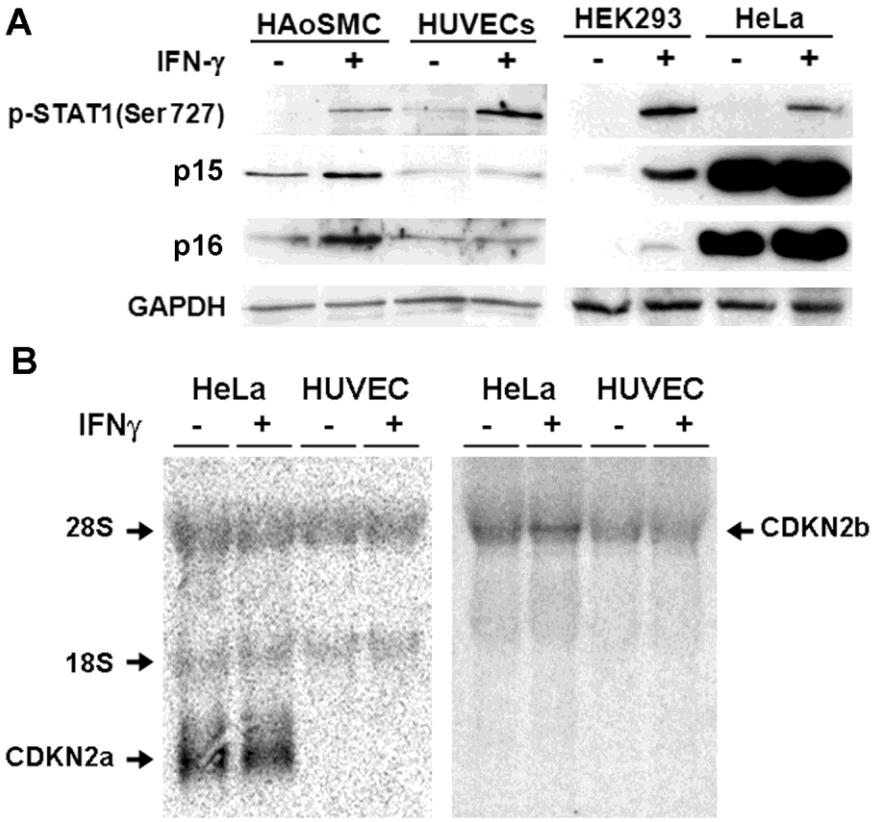
A
HAoSMC
HUVECs
HEK293
HeLa
IFN-γ
- + - + - + - +
p-STAT1(Ser727)
p15
p16
GAPDH
B
HeLa HUVEC HeLa HUVEC
IFNγ
- + - + - + - +
28S
18S
CDKN2a
CDKN2b

were unchanged. Importantly, when tested in 16 different LCLs, the 9p21.3 risk locus did not affect the response of p15 and p16 to interferon-y. Thus, it seems unlikely that the rs10757278 SNP that disrupts a STAT1-responsive element in the 9p21.3 risk locus is sufficient to affect the activation of p15 and p16 in response to interferon-y. It is worthwhile pointing out that whereas *Harismendy et al*. (2011) measured CDKN2B mRNA by RT-PCR (78), we measured protein levels of p15 and p16 by immunoblot. Furthermore, Northern blot analysis of mRNA from HeLa cells (heterozygote for 9p21.3) showed no change in CDKN2A mRNA and a slight increase in CDKN2B mRNAIn addition, our HUVECs were homozygous for the non-risk allele of 9p21.3, thus should have responded robustly to interferon-γ, but showed no change in CDKN2B mRNA levels. Both results contrast to the reduced expression reported by *Harismendy et al*. (2011). Our study is consistent with a previous report that also found that p16, but not $p14^{ARF}$, is upregulated by interferon-γ in human cells (115). Furthermore, interferon-γ was reported to increase the translation of the ICAM1 protein by a STAT1-dependent mechanism that suppresses miR-221 expression (116). Thus, in some instances interferon-γ can increase protein translation, and in the case of p16, this effect appears to be independent of the mRNA levels. Our study indicates that the mechanism whereby the 9p21.3 risk allele contributes to coronary artery disease is not by blocking the activation of p15 or p16 by interferon-γ.

Multiple enhancer-like sequences are present within the 9p21.3 risk locus that could influence the expression of flanking genes (78,80,83). Under basal conditions, in non-transformed cells, there may be differences in the levels of p15 and/or p16 conferred by the enhancer sequences at the 9p21.3 locus. However, these basal differences may be masked by the repression of the CDKN2A locus by the Epstein-Barr virus nuclear antigens 3A and 3C (113,114). Our choice of LCLs was not to test basal differences in p15 and p16 expression

but rather to test whether the 9p21.3 genotype influences the response of these genes to interferon-γ.

The hypothesis that the 9p21.3 locus confers a differential response to interferon-γ is clearly not supported by our data, because we observed increased p15 and p16 expression regardless of genotype. The disease process itself may influence the activity of the enhancer sequences at 9p21.3. Many other growth factors and cytokines are produced at atherosclerotic lesions (117) and could have differential effects at other enhancer elements that contain functional single nucleotide polymorphisms, like the one we identified at rs1333045 (80). In addition, many SNPs at the 9p21.3 locus could be the functional culprits and may act together to modulate gene expression. For example, the linked polymorphism rs10811656 located only 4 base pairs from the putative STAT1 binding sequence (rs10757278) disrupts a putative TEAD factor binding site (CATTCCG>CATTCTG) (118), but it is not known whether this element is functional or influences enhancer activity. Of the more than 100 SNPs linked to the 9p21.3 locus, exhaustive functional characterization would be required and is beyond the scope of the present report. Thus, the precise mechanism whereby the 9p21.3 locus contributes to the risk of CAD remains to be elucidated.

Sources of Funding

Supported by grants from the Canadian Institutes of Health Research, CIHR #MOP82810 (RR), CIHR #MOP77682 (AFRS), the Canada Foundation for Innovation, CFI #11966 (R.R.), and a student scholarship from Taibah University, Saudi Arabia (NAMA).

Table 1 Imputation of rs10757278 using flanking SNPs in high linkage disequilibrium.

LCL ID	rs944797	rs2383207	rs1537375	rs10757278	rs1333048	rs1333049
GM10835	CC	GG	CC	GG	CC	CC
GM11992	CC	GG	CC	GG	CC	CC
GM11995	CC	GG	CC	GG	CC	CC
GM12282	CC	GG	CC	GG*	CC	CC
GM11840	CT	AG	CT	AG	AC	CG
GM12234	CT	AG	CT	AG	AC	CG
GM12817	CT	AG	CT	AG*	AC	CG
GM12864	CT	AG	CT	AG	AC	CG
GM12872	CT	AG	CT	AG	AC	CG
GM12873	CT	AG	CT	AG	AC	CG
GM12003	TT	AA	TT	AA*	AA	GG
GM12057	TT	AA	TT	AA	AA	GG
GM12283	TT	AA	TT	AA*	AA	GG
GM12336	TT	AA	TT	AA*	AA	GG
GM12775	TT	AA	TT	AA*	AA	GG
GM12890	TT	AA	TT	AA*	AA	GG

*imputed genotypes using flanking SNPs, sorted by relative position on chromosome 9, with a D'=1 and an r^2>0.8.

CHAPTER 3

9p21.3 coronary artery disease risk variants disrupt TEAD transcription factor binding and TEAD-dependent TGFβ regulation of p16 expression in human aortic smooth muscle cells

Naif A. M. Almontashiri, MSc, Xun Zhou, MSc, Darlene Antoine, BSc, Ragnar O. Vilmundarson, MSc, Sean X. Zhang, Kennedy N. Hao, Hsiao-Huei Chen, PhD, Alexandre F. R. Stewart, PhD .

From the Ruddy Canadian Cardiovascular Genetics Centre, University of Ottawa Heart Institute, Ottawa, Ontario, Canada (NAMA, DA, ROV, SXZ, KNH, AFRS), the Department of Biochemistry, Microbiology and Immunology, University of Ottawa, Ottawa, Ontario, Canada (NAMA, DA, ROV, AFRS), the Center for Genetics and Inherited Diseases, Taibah University, Almadina, Saudi Arabia (NAMA), the Ottawa Hospital Research Institute (XZ, HHC), and the Department of Medicine, University of Ottawa, Ottawa, Ontario, Canada (HHC, AFRS).

¶Correspondence: Alexandre Stewart, University of Ottawa Heart Institute, 40 Ruskin St, Rm H3100, Ottawa, Ontario, Canada, K1Y 4W7. E-mail: astewart@ottawaheart.ca, tel: (613) 761-5189, fax: (613) 761-4647.

This paper is under review as a research article in Circulation (2015) April.

Author contributions: NAMA designed, performed and analysed most of the expriments, DA contributed figure 3B-E; XZ performed the Q-PCR ; ROV performed the statistical analysis; SZ and KH helped in generating some of the expression constructs, HHC provided essential reagents; NAMA, HHC, and AFRS wrote the manuscript.

Key word: coronary disease, atherosclerosis, genetics, molecular biology, smooth muscle cells

Abstract

Background: The mechanism whereby the 9p21.3 locus confers risk for coronary artery disease (CAD) remains incompletely understood. Risk alleles are associated with reduced expression of the cell cycle suppressor genes CDKN2A (p16 and p14) and CDKN2B (p15) and increased vascular smooth muscle cell proliferation. We asked whether risk alleles disrupt transcription factor binding to account for this effect.

Methods and Results: A bioinformatic screen was used to predict which of 59 single nucleotide polymorphisms (SNPs) at the 9p21.3 locus disrupt (or create) transcription factor binding sites. Electrophoretic mobility shift (EMSA) and luciferase reporter assays examined the binding and functionality of the predicted regulatory sequences. Primary human aortic smooth muscle cells (HAoSMCs) were genotyped for 9p21.3 and HAoSMCs homozygous for the risk allele showed reduced p15 and p16 levels and increased proliferation. rs10811656 and rs4977757 disrupted functional TEAD transcription factor binding sites. TEAD3 and TEAD4 over-expression induced p16 in HAoSMCs homozygous for the non-risk allele, but not for the risk allele. TGFβ, known to activate p16 and also to interact with TEAD factors, failed to induce p16 or to inhibit proliferation of HAoSMCs homozygous for the risk allele. Knockdown of TEAD3 blocked TGFβ-induced p16 expression and dual knockdown of TEAD3 and TEAD4 markedly reduced p16 expression in heterozygous HAoSMCs.

Conclusion: Here, we identify a novel mechanism whereby sequences at the 9p21.3 risk locus disrupt TEAD factor binding and TEAD3-dependent TGFβ induction of p16 in HAoSMCs. This mechanism accounts, in part, for the 9p21.3 CAD risk.

Introduction

Atherosclerosis of coronary arteries is an inflammatory disease whereby cholesterol and other lipids accumulate in macrophages and smooth muscle cells in the vessel wall (119). Genetic variants on chromosome 9 at 9p21.3 confer risk for coronary artery disease (CAD) (70,74,75,120). The 9p21 risk alleles predict the severity of CAD as measured by the burden of atherosclerosis (121,122). These same variants also contribute to abdominal aortic aneurism (AAA) (72), pointing to a predominantly vascular phenotype.

Given that macrophages and smooth muscle cells are the predominant cellular components of atherosclerotic lesions, 9p21.3 risk alleles likely affect one or the other cell type. Gene expression profiling of monocyte-derived macrophages failed to tie the 9p21.3 genotype to differential expression of genes in the vicinity of the locus (79). Although global deletion of the 9.21.3 orthologous sequences in the mouse genome did not worsen the phenotype of atherosclerosis in susceptible mice, the deletion was associated with worsened outcomes in an experimental model of AAA (123). It is also noteworthy that bone marrow-specific ablation (including macrophages) had no effect on this phenotype, whereas the aneurysm was prevented by treatment with a CDK inhibitor that arrests cell cycle progression (123). Thus, deletion of the 9p21.3 homologous locus in mice replicates part of the vascular phenotype (aortic aneurysm) seen in humans. Furthermore, these results argue that smooth muscle cells rather than macrophages are the primary site of 9p21.3 risk.

The 9p21.3 risk locus comprises 59 linked single nucleotide polymorphisms (SNPs) within a gene desert 100,000 base pairs upstream of the genes encoding the cyclin-dependent kinase inhibitors CDKN2A (p16 and p14) and CDKN2B (p15). Smooth muscle cells homozygous for the 9p21.3 risk alleles showed reduced expression of p16 and p15, increased

proliferation and failure to enter senescence in several studies (82,83). *Motterle et al.* (2012) found an association between SNP rs1333049 and smooth muscle cell content in the intima: atherosclerotic plaques of the C/C genotype having the highest VSMC content (82). Moreover, they found an inverse correlation between human smooth muscle cells proliferation and p15 and p16 expression in the atherosclerotic plaques. p15 and p16 are known tumor suppressors that control cell cycle and cellular senescence(34,36). Migration and proliferation of smooth muscle cells contributes to the pathogenesis of atherosclerosis, restenosis after angioplasty and abdominal aortic aneurysms (11,124). Deletion of the 9p21.3-orthologous sequences in the mouse genome markedly reduces p15 and p16 expression in aortic tissues (83) confirming the presence of regulatory sequences in this region. Functional characterization of the 9p21.3 locus has identified regulatory sequences (80), but the identity and tissue-specificity of the cognate transcription factors was not known.

Chromatin conformation capture identified long-range interactions between enhancers within the 9p21.3 locus with chromatin in the vicinity of genes encoding p16, p15, MTAP and the interferon family of proteins (78), although specific differences in the expression of these proteins was not reported. It was claimed that a polymorphism at the 9p21.3 locus (rs10757278) affects the response to interferon-γ signaling by disrupting a putative STAT1 consensus binding site and thereby affecting the expression of p16 and p15 (78). However, we showed that carriers of the risk alleles respond to interferon-γ by inducing p15 and p16 just as well as the carriers of the non-risk alleles (125). Therefore, the mechanism by which the 9p21.3 CAD risk locus affects the expression of p16 and p15 has remained elusive (76).

Here, we performed a bioinformatics scan of each of the 59 SNPs within the 9p21.3 CAD risk locus to find variants that could disrupt or create binding sites for transcription factors.

Using EMSA and luciferase reporter assays, we found that rs10811656 and rs4977757 disrupted functional binding sites for TEAD transcription factors, known for regulating gene expression in muscle (126-129) and to control cell proliferation (130,131). Using HAoSMCs, we found that TEAD3 or TEAD4 over-expression increased p16 expression whereas dual knockdown decreased it. Importantly, HAoSMCs homozygous for the risk allele failed to respond to TEAD3 or TEAD4 overexpression. In addition, p16 expression is known to be induced by TGFβ by a Smad-dependent mechanism (53). Of interest, TEAD factors have been reported to mediate TGFβ-dependent gene activation (54,132,133). We found that TGFβ was unable to induce p16 expression in HAoSMCs homozygous for the 9p21.3 risk allele or in heterozygote cells in which TEAD3 was knocked down. Thus, our studies reveal a novel TEAD-dependent mechanism disrupted by the 9p21.3 CAD risk locus in HAoSMCs.

Methods

Expanded information on Methods is available in the online-only Data Supplement.

Bioinformatics scan

The 59 linked SNPs at the 9p21.3 locus were examined to identify genetic variants that would disrupt or create transcription factor binding sites using the publically available databases ENCODE chromatin immunoprecipitation (http://encodeproject.org/ENCODE/) and the JASPAR CORE (http://jaspar.genereg.net/) databases. The sequence was scanned for binding sites using position weight matrix (PWM) models of transcription factor (TF) binding specificity from the JASPAR CORE database, with a stringent minimum relative score of 85%. Both risk and non-risk allele-containing sequences were tested by this approach to identify putative

transcription factor binding sites disrupted or created by the risk variants. Putative targets are listed in Table 2 in the online-only Data Supplement.

EMSA

EMSA was carried out as described previously (134), using radiolabeled oligonucleotides corresponding to different SNPs (Table 3 in the online-only Data Supplement). Details are provided in the Supplemental methods.

Constructs, Luciferase Reporter Assays and lentiviral transductions

TEAD expression plasmids, transient transfections and luciferase assays were carried out as described previously(135). For each of the SNPs that passed EMSA (Table 5 in the online-only Data Supplement), oligonuleotides flanked with KpnI and XhoI sites were sub-cloned into the pGL3 promoter luciferase vector (Invitrogen, Carlsbad, CA) and sequenced. Details are provided in the Supplemental methods.

Immunoblotting

Cell proteins were analyzed by immunoblot as described previously(125). Detailed reagents and antibodies are provided in the Supplemental methods.

Results

The effect of the 9p21.3 locus on cultured primary HAoSMC proliferation and senescence

In primary HAoSMCs homozygous for the 9p21 risk locus, we observed reduced expression of p16 and p15 as compared to cells heterozygous and homozygous for the non-risk allele (Figure 1A), consistent with a previous report (82). Also, in line with our previous study(125), we were unable to detect p14 in HAoSMC extracts (data not shown). Lower expression of p16 and p15 by the risk allele would be expected to increase cell proliferation.

Indeed, HAoSMCs heterozygous and homozygous for the risk alleles showed increased BrdU labeling, consistent with increased cellular proliferation compared to cells homozygous for the non-risk alleles (Figure 1B). HAoSMCs homozygous for the risk allele failed to reach senescence even after 18 passages whereas cells homozygous for the non-risk allele could not be passaged more than 6 times (Table 1 in the online-only Data Supplement). Given that the 9p21.3 risk locus affects p15 and p16 expression as well as cellular proliferation, we sought to determine which of the 59 SNPs might be responsible for this effect. Transcription factors bind to cognate DNA sequences to regulate gene expression from regulatory sequences. Following the scheme outlined in Figure 1C, bioinformatics identified 14 SNPs potentially disrupting transcription factor binding (Table 2 in the online-only Data Supplement). EMSA was used to exclude SNPs that showed no differential binding between the genotypes (risk vs. non-risk). SNPs that showed differential binding by EMSA were then subjected to a luciferase reporter assay to further determine whether the sites were functional.

TEAD transcription factor binding is disrupted at the 9p21.3 locus

Ten of the 14 SNPs were negative for transcription factor binding by EMSA (data not shown and Figure 1 – Figure 4 in the online-only Data Supplement). SNPs that were predicted previously to disrupt a STAT1 (rs10757278)(78) or a Smad3 (rs1333045)(80) consensus did not show differential binding by EMSA (Figure 1 and Figure 2 in the online-only Data Supplement) or an effect on luciferase reporter activity (data not shown).

Interestingly, four of the 14 SNPs showed differential binding for TEAD (TEA-domain) (rs10811656 and rs4977757) and GATA (rs9632885 and rs10757269) transcription factors by EMSA. TEAD transcription factors (TEAD1-TEAD4) bind to a consensus 5’-CATTCC-3’

Figure 1. The 9p21 coronary artery disease risk allele is associated with reduced p16 and p15 protein expression and increased cellular proliferation in HAoSMCs.
(A) p16 and p15 levels are negatively correlated with the 9p21risk allele, in a representative blot. HNR, homozygous for the non-risk allele; HET, heterozygous; and HR, homozygous for the risk allele. Individual primary HAoSMC cultures from different donors are indicated with unique identifiers. Right panel, quantification of the protein levels by densitometry, normalized to GAPDH. * = $p<0.05$, data were normally distributed and ANOVA was done to compare the 3 groups and post-hoc pair wise comparisons to correct for multiple testing, (n=13 independent primary cultures, in triplicates). Relative protein level is expressed as mean ± SEM. (B) Cellular proliferation was significantly increased as shown by the increased BrdU labeling in cells homozygous for the risk allele (HR) compared to cells to cells homozygous for the non-risk allele (HNR) or heterozygous (HET). * = $p<0.05$ (data were normally distributed and ANOVA compared the 3 groups and post-hoc pair-wise comparisons corrected for multiple testing), n=13 independent primary cultures, 3 HNR, 5 HET and 5 HR (experiments performed in triplicates). (C) Schematic chart of the study workflow to test the 59 SNPs at the 9p21.3 risk locus for their effect on transcription factor binding.

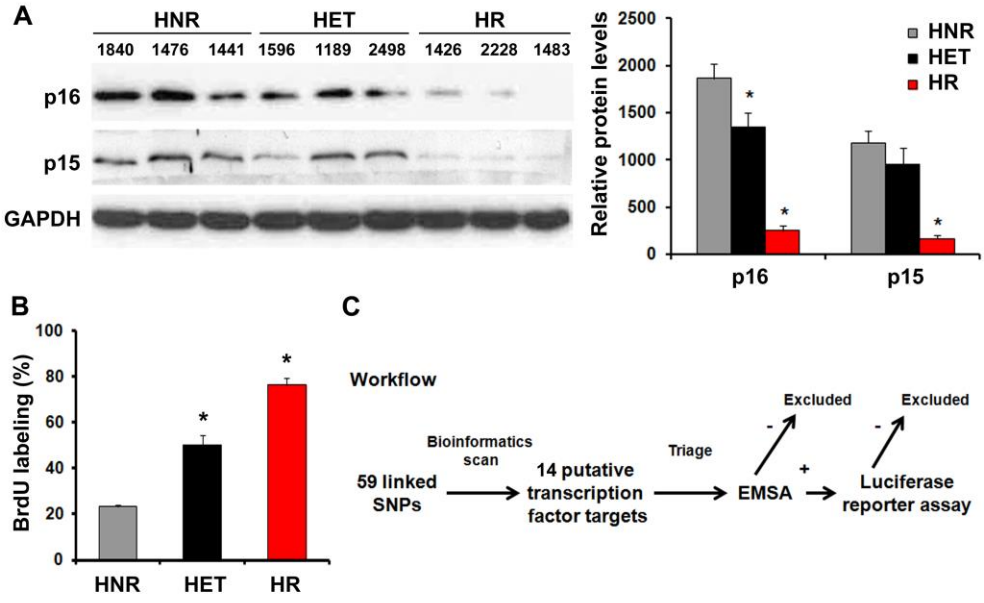
A
HNR
HET
HR
1840 1476 1441 1596 1189 2498 1426 2228 1483
p16
p15
GAPDH
Relative protein levels
2500
2000
1500
1000
500
0
HNR
HET
HR
p16
p15
B
BrdU labeling (%)
100
80
60
40
20
0
HNR
HET
HR
C
Workflow
59 linked SNPs
Bioinformatics scan
14 putative transcription factor targets
Triage
EMSA
Excluded
Luciferase reporter assay
Excluded

sequence (134). Gel shift analysis demonstrated that the TEAD sequences at rs10811656 and rs4977757 are functional. Using HAoSMCs nuclear extracts, TEAD complex formation with the non-risk sequences of rs10811656 or rs4977757 were more robust compared to the sequence containing the risk alleles (Figure 4 in the online-only Data Supplement). Nuclear extracts from HeLa cells over-expressing TEAD3 or TEAD4 showed robust binding to the non-risk sequences of rs10811656 or rs4977757 compared to the risk allele-containing sequences (Figure 2A and 2B). It is important to be aware that not all antibodies produce a "supershited" complex. Some antibodies interfere with DNA binding. Antibody binding to the protein complex in EMSA can be observed as supershifted complex ((as in Figure 2B) or reduced signal of the protein complex upon incubation with the antibody (as in Figure 2A and Figure 1 in the online-only Data Supplement) compared to lanes that have no IgG added(136). This is likely due to the fact that the flanking sequence surrounding different DNA elements (rs10811656 or rs4977757) can result in different complex binding and different affinity for the antibody. However, the specific interaction of the individual TEAD factors with these elements was confirmed in luciferase reporters (Figure 3D and 3E). TEAD1 and TEAD2 showed no binding to either allele (data not shown). As for the putative GATA sites, rs10757269 was predicted to disrupt, whereas rs9632885 to create, a binding site for GATA transcription factors. Indeed, EMSA showed allele-specific binding, consistent with the predicted effects of the SNPs (Figure 3A in the online-only Data Supplement). HAoSMCs nuclear extracts were used to perform the EMSAs, and additional cell line-specific nuclear extracts were also used for several transcription factors, including THP1 cells to test for IRF4, HeLa cells for Meis1 and TEAD factors, and HEK293 cells for PRC1 (see table S2). Based on the EMSA results, the functionality of these four SNPs

Figure 2. The rs10811656 and rs4977757 polymorphisms disrupt a functional TEAD factor binding site.

Nuclear extracts from HeLa cells transiently transfected with TEAD3 (left panel) or TEAD4 (right panel) expression plasmids reveal that an oligonucleotide probes containing the non-risk allele of rs10811656 (A) and rs4977757 (B) are functional TEAD factor binding sites, whereas the risk allele disrupts TEAD binding to about 1/10th the level seen for the non-risk allele (compare lanes 5 to 12 and 19 to 26). Free, unbound radiolabelled probe; NS, a non-specific shift; and SS, super-shifted complex (n= 3 experiments).

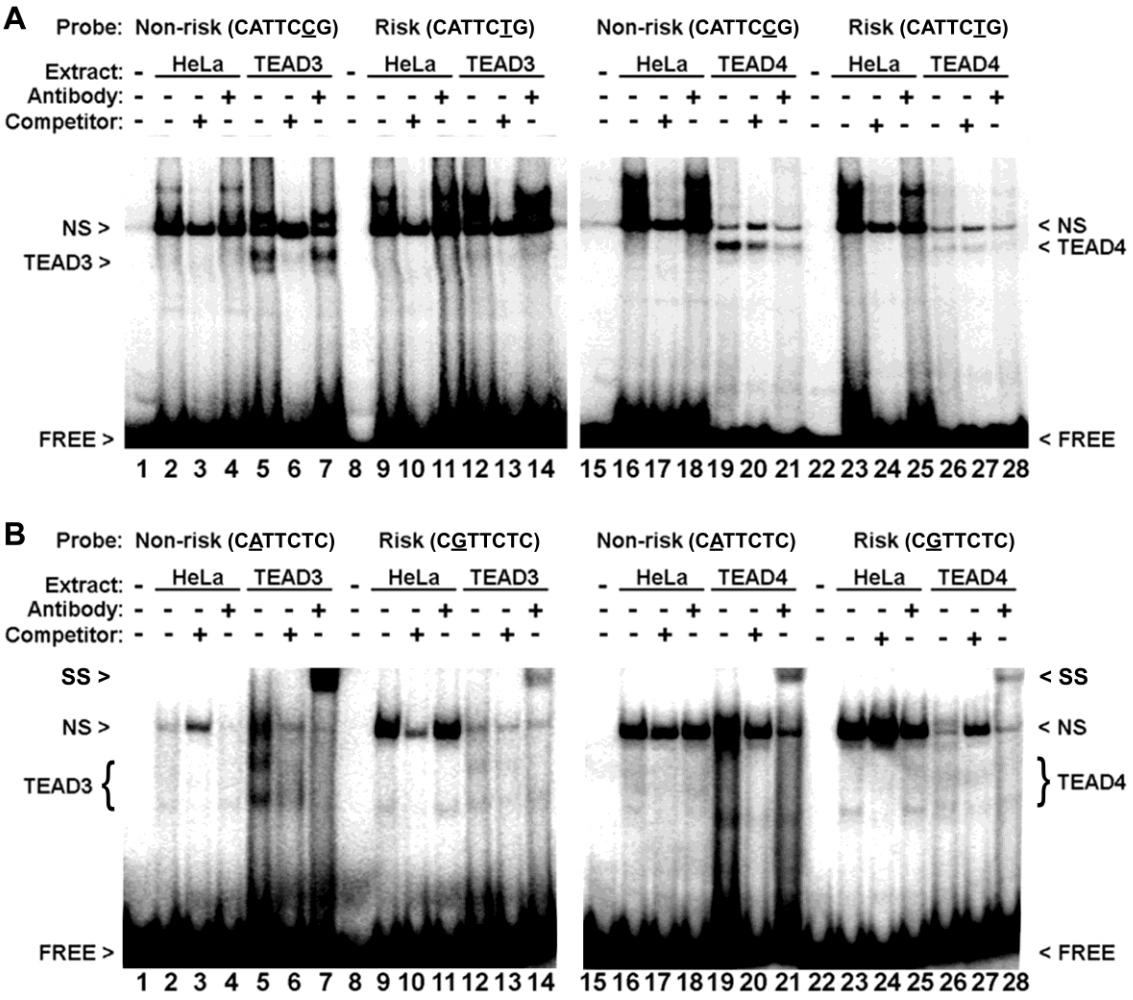
A
Probe: Non-risk (CATTCCG) Risk (CATTCTG) Non-risk (CATTCCG) Risk (CATTCTG)
Extract: - HeLa TEAD3 - HeLa TEAD3 - HeLa TEAD4 - HeLa TEAD4
Antibody:
Competitor:
NS >
TEAD3 >
FREE >
< NS
< TEAD4
< FREE
1 2 3 4 5 6 7 8 9 10 11 12 13 14 15 16 17 18 19 20 21 22 23 24 25 26 27 28
B
Probe: Non-risk (CATTCTC) Risk (CGTTCTC) Non-risk (CATTCTC) Risk (CGTTCTC)
Extract: - HeLa TEAD3 - HeLa TEAD3 - HeLa TEAD4 - HeLa TEAD4
Antibody:
Competitor:
SS >
NS >
TEAD3
FREE >
< SS
< NS
TEAD4
< FREE
1 2 3 4 5 6 7 8 9 10 11 12 13 14 15 16 17 18 19 20 21 22 23 24 25 26 27 28

Figure 3. The rs4977757 and rs10811656 risk alleles disrupt functional binding sites for TEAD3 and TEAD4 at the 9p21.3 CAD risk locus.

The rs4977757 and rs10811656 risk alleles disrupt functional binding sites for TEAD3 and TEAD4 at the 9p21.3 CAD risk locus. (A) ChIP confirmed that rs4977757 and rs10811656 are binding sites for TEAD3 and TEAD4. NoAb, ChIP was done without antibody; IgG, ChIP was done with normal mouse IgG antibody (GAPDH); Input, Total chromatin from HAoSMCs transfected with empty vector; T3, Chromatin immunoprecipitated using anti-HA tag antibody from HAoSMCs (heterozygote) transfected with HA tagged TEAD3, and T4, Chromatin immunoprecipitated using anti-HA tag antibody from HAoSMCs (heterozygote) transfected with HA tagged TEAD4 (n= 3 experiments). A luciferase reporter assay was used to examine the transcriptional activity of rs4977757 and rs10811656 upon the binding of endogenous TEADs in HAoSMCs (B and C) or over-expression of TEAD factors in HEK293 cells (D and E). Control, empty pGL3 promoter vector is co-expressed with the different pXJ-40 vectors (TEAD-containing and empty pXJ-40 vectors); Vector, TEADs are not expressed and only empty PXJ-40 is co-expressed with the different PGL3 promoter constructs (D and E). For normalization, the luciferase activity was expressed as fold change relative to empty PGL3 promoter vector (control) of each group. ANOVA and post-hoc pair wise comparisons were used, correcting for multiple testing. *, $p<0.05$. , n=6 experiments in triplicate (B-E). Fold is expressed as mean ± SEM.

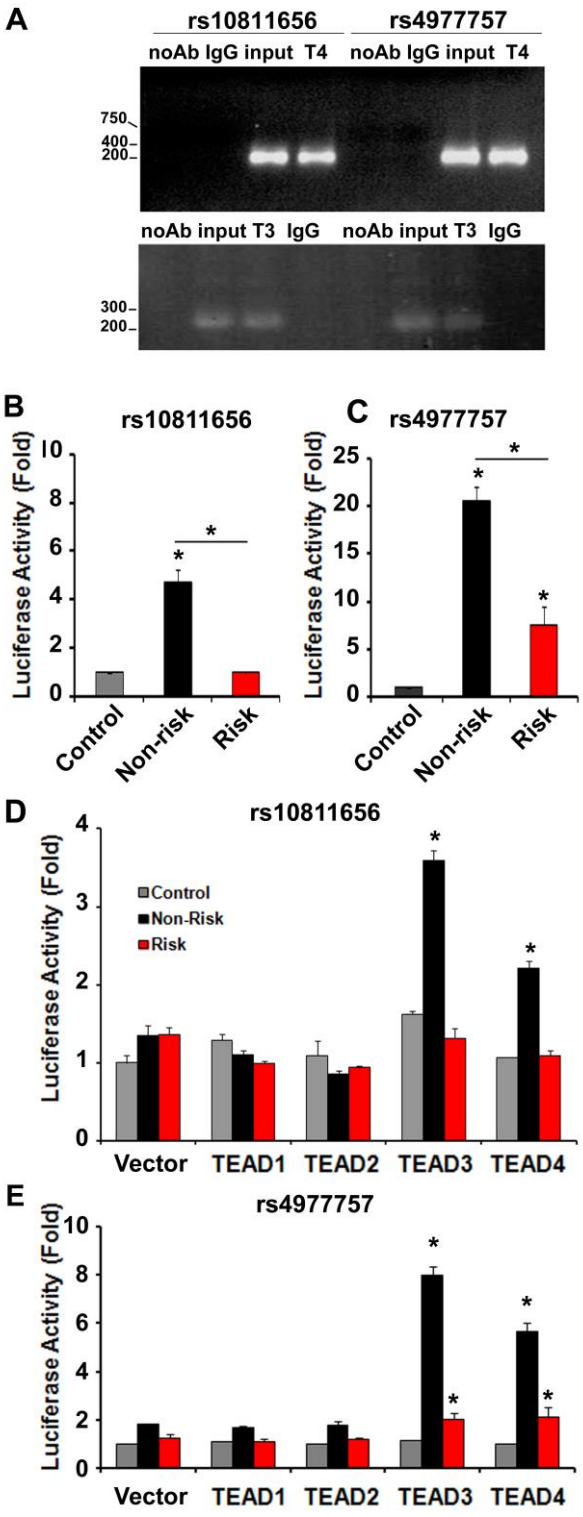
A
rs10811656
rs4977757
noAb IgG input T4
noAb IgG input T4
750
400
200
noAb input T3 IgG
noAb input T3 IgG
300
200
B
rs10811656
Luciferase Activity (Fold)
Control
Non-risk
Risk
C
rs4977757
Luciferase Activity (Fold)
Control
Non-risk
Risk
D
rs10811656
Luciferase Activity (Fold)
Control
Non-Risk
Risk
Vector
TEAD1
TEAD2
TEAD3
TEAD4
E
rs4977757
Luciferase Activity (Fold)
Vector
TEAD1
TEAD2
TEAD3
TEAD4

(rs10811656 and rs4977757 for TEAD factors and rs10757269 and rs9632885 for GATA factors) was further tested in luciferase reporter assays.

TEAD sites disrupted by 9p21.3 risk alleles are functional

Chromatin immunoprecipitation (ChIP) confirmed that both the non-risk alleles for rs10811656 and rs4977757 bind to TEAD factors in HAoSMCs (Figure 3A). Consistent with the EMSA demonstrating binding *in vitro* and the ChIP assay demonstrating binding *in vivo*, endogenous TEAD factors in HAoSMCs activated luciferase reporters bearing the non-risk alleles of rs10811656 and rs4977757 three to four-fold more robustly than reporters bearing the risk alleles (Figure 3B and 3C). We next tested the effect of each of the four TEAD transcription factors on the response of these luciferase reporters in HEK293 cells by transient transfection. TEAD1 or TEAD2 over-expression produced no significant difference in the luciferase activity between the risk and non-risk alleles. In contrast, TEAD3 and TEAD4 activated the reporters bearing the non-risk alleles (Figure 3D and 3E). In contrast, reporters bearing the risk alleles were not (rs10811656) or only weakly (rs4977757) activated by TEAD3 and TEAD4.

Disruption of TEAD regulation of p16 at the 9p21.3 risk locus

TEAD transcription factors are required for many developmental processes including cardiogenesis (137) and development of neural crest, the precursor of arterial smooth muscle(138). TEADs also regulate cell cycle progression (130,131). In our studies, only TEAD3 and TEAD4 showed differential binding (Figure 2) and activation (Figure 3C and 3D) of rs10811656 and rs4977757.

To test whether p15 and p16 expression is affected by TEAD3 or TEAD4, we over-expressed HA-tagged TEAD3 and TEAD4 in 13 primary HAoSMCs genotyped for the 9p21.3

risk locus. We found that over-expression of TEAD3 (Figure 4A and 4B) or TEAD4 (Figure 4C and 4D) could induce endogenous p16 (CDKN2A) mRNA and protein expression in cells heterozygous or homozygous for the non-risk allele, whereas these TEAD factors failed to induce p16 in cells homozygous for the risk allele. In contrast, TEAD3 only weakly activated p15 mRNA (Figure 4A), but this was not reflected at the protein level (Figure 4B) and TEAD4 had no effect on either p15 mRNA or protein expression (Figure 4C and 4D).

9p21.3 risk locus impairs TGFβ induction of p16

TGFβ has been reported to directly induce the expression of p16 and p15 through Smad proteins like Smad2 and Smad3, to control cell cycle and induce cellular senescence (28,52,53). Deletion of the 9p21.3 homologous sequence in the mouse is associated with an impaired Smad-dependent response to TGFβ (53,123,139) indicating that this region contains DNA sequences targeted by SMAD proteins. However, by gel shift, the 2 putative SMAD target sequences disrupted by rs10757275 (data not shown) and rs1333045 (Figure 2 in the online-only Data Supplement) did not show differential binding by gel shift assay in response to TGFβ stimulation. This result argued that TGFβ works indirectly at the 9p21.3 region to regulate p15 and p16 expression. Since TEAD3 and TEAD4 transcription factors have been reported to interact with Smad3 and to mediate TGFβ-dependent gene activation (54,133,140), we asked if polymorphisms that disrupt TEAD factor binding could also disrupt the response to TGFβ signaling. Indeed, HAoSMCs homozygous for the risk allele failed to induce p16 expression after TGFβ1 treatment as opposed to the homozygous non-risk or heterozygote cells (Figure 5A). In contrast, TGFβ induced p15 regardless of 9p21.3 genotype in HAoSMCs. TGFβ reduced proliferation of HAoSMCs heterozygous for the 9p21.3 risk locus, but not those homozygous for

Figure 4. TEAD3 and TEAD4 regulate the expression of p16 but not p15 at the 9p21.3 locus.

(A,C) Q-PCR showed that primary HAoSMCs homozygote for 9p21.3 risk locus failed to induce p16 expression in response to TEAD3 or TEAD4 overexpression. GAPDH was used for normalization as an internal control. Data were presented as fold induction relative to the untreated group of each genotype, * = $p<0.05$. Relative mRNA level is expressed as mean ± SEM.(B,D) Representative immunoblots of HAoSMCs that were transiently transfected with empty CMV expression plasmid or plasmids expressing HA tagged TEAD3 or TEAD4. Overexpression of TEAD3 or TEAD4 in primary HAoSMCs homozygote for 9p21.3 risk locus failed to induce p16 expression in a representative blots. Antibody to GAPDH was used to confirm equal loading. n= 13 independent primary cultures of HAoSMCs.

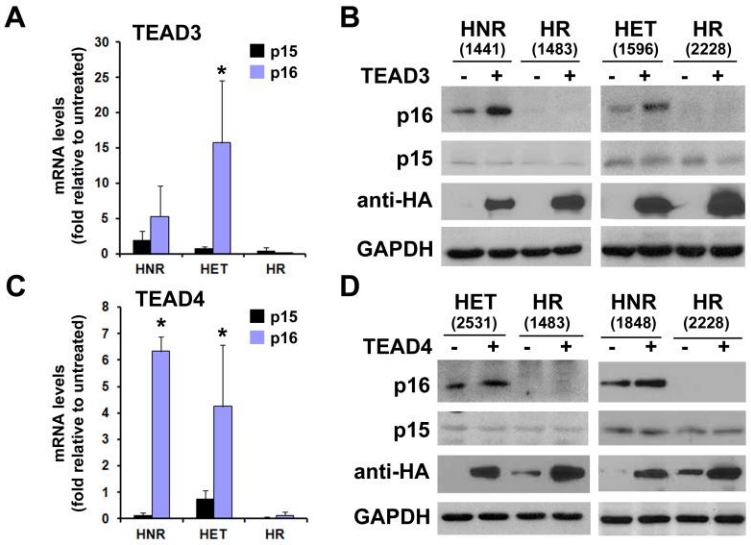
A
TEAD3
p15
p16
mRNA levels
(fold relative to untreated)
HNR
HET
HR
B
HNR
(1441)
HR
(1483)
HET
(1596)
HR
(2228)
TEAD3
p16
p15
anti-HA
GAPDH
C
TEAD4
p15
p16
mRNA levels
(fold relative to untreated)
HNR
HET
HR
D
HET
(2531)
HR
(1483)
HNR
(1848)
HR
(2228)
TEAD4
p16
p15
anti-HA
GAPDH

Figure 5. TGFβ induced p16 expression is TEAD-dependent and disrupted by the 9p21.3 risk allele.

(A) Representative immunoblot reveals that primary HAoSMCs treated with TGFβ (2ng/ml for 8 hours) increased p16 levels in cells heterozygote for the risk allele but not in cells homozygote for the risk allele. Induction of p15 was not impaired by the 9p21.3 risk locus. GAPDH was used as a loading control. p-Smad3 (Ser423/425) was used to monitor the TGFβ response. Right panel, quantification of TGFβ response (n=12 independent primary cultures, 2 HNR, 5 HET and 5 HR). (B) TGFβ reduces BrdU incorporation in HAoSMCs heterozygote for the 9p21.3 locus. *, $p<0.05$, (n=10 independent primary cultures, 5 HET and 5 HR). Knock-down of TEAD3 blocks TGFβ-induced p16 expression and knock-down of both TEAD3 and TEAD4 lowers p16 mRNA (C) or protein (D) expression in HAoSMCs.n=3 independent experiments performed in triplicates. GAPDH was used as a loading control. (E) Over-expression of mouse Tead3 and Tead3 in HAoSMCs transduced with lentivirus expression shRNA to TEAD3 and TEAD4 rescues p16 expression. n=3 independent experiments performed in triplicates. (F) rs10811656 and rs4977757 mediate TEAD3-dependent response to TGFβ. HEK293 cells were transfected in 3 separate experiments in triplicate. ANOVA compared the 3 groups (risk/non-risk, vector/TEAD3, vehicle/TGFβ) and post-hoc pairwise comparisons were used, correcting for multiple testing. *, $p<0.05$.

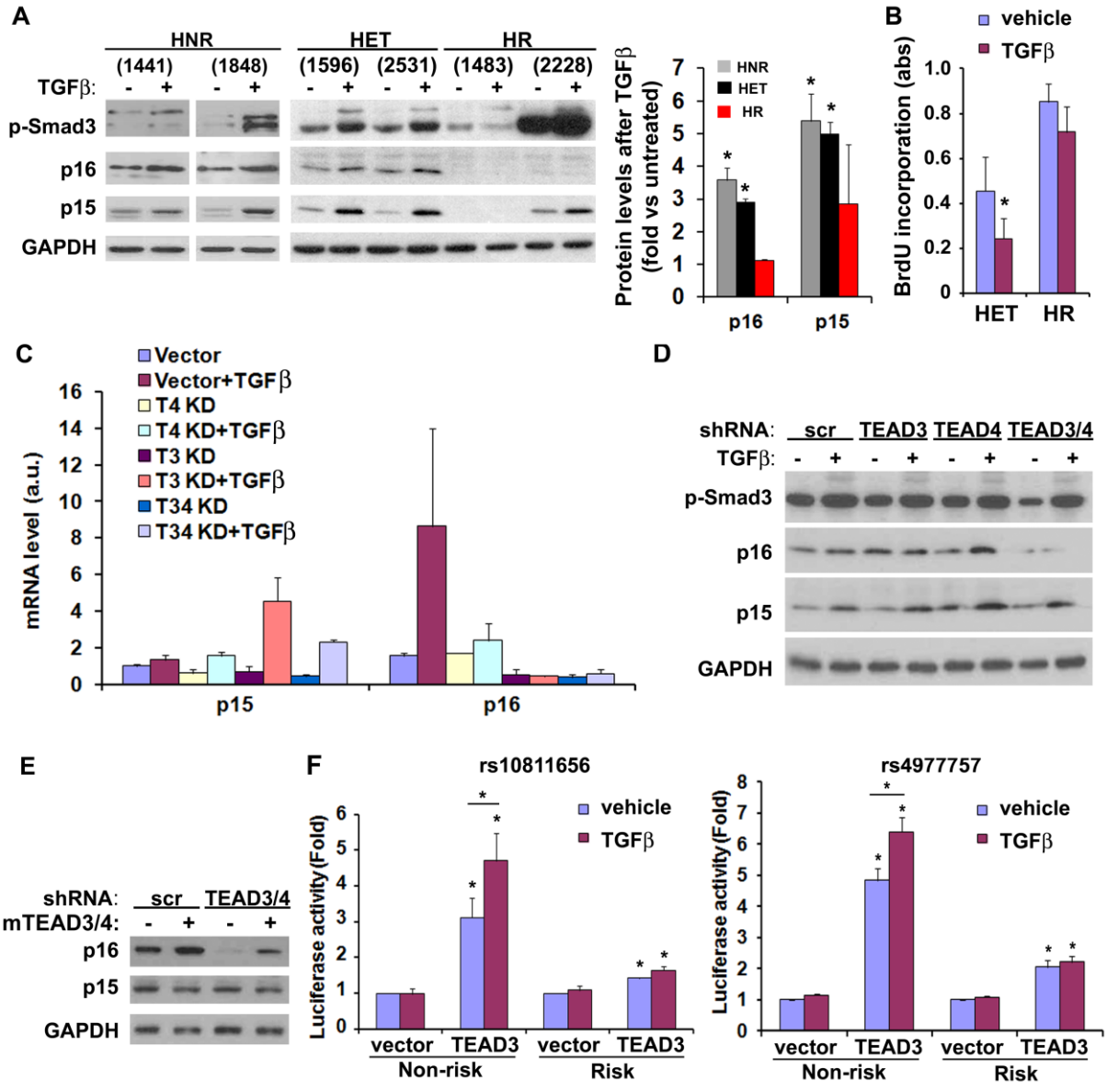
A
HNR
HET
HR
(1441)
(1848)
(1596)
(2531)
(1483)
(2228)
TGFβ:
p-Smad3
p16
p15
GAPDH
Protein levels after TGFβ (fold vs untreated)
HNR
HET
HR
p16
p15
B
vehicle
TGFβ
BrdU incorporation (abs)
HET
HR
C
Vector
Vector+TGFβ
T4 KD
T4 KD+TGFβ
T3 KD
T3 KD+TGFβ
T34 KD
T34 KD+TGFβ
mRNA level (a.u.)
p15
p16
D
shRNA:
scr
TEAD3
TEAD4
TEAD3/4
TGFβ:
p-Smad3
p16
p15
GAPDH
E
shRNA:
scr
TEAD3/4
mTEAD3/4:
p16
p15
GAPDH
F
rs10811656
Luciferase activity (Fold)
vehicle
TGFβ
vector
TEAD3
Non-risk
Risk
rs4977757
Luciferase activity (Fold)
vehicle
TGFβ
vector
TEAD3
Non-risk
Risk

the risk allele (Figure 5B). The homozygote non risk cells were lost to senescence; therefore our analysis was limited to HAoSMCs heterozygote or homozygous for the risk allele.

To determine whether TGFβ-induced p16 expression is mediated through TEAD3 or TEAD4, we used lentiviral shRNA vectors to knockdown TEAD3 or TEAD4 either separately or at the same time in HAoSMCs (Figure 5C and 5D). These cells were then treated with TGFβ1 and p15 and p16 protein levels were examined by immunoblot. Knock-down of either TEAD3 or TEAD4 did not affect the basal levels of p15 or p16 mRNA or protein levels (Figure 5C and 5D). However, the dual knockdown of TEAD3 and TEAD4 resulted in reduced expression of p16 but not p15, suggesting a redundant role of TEAD3 and TEAD4 in p16 induction. This also indicates that p15 expression is independent of TEAD3 and TEAD4. TEAD3 and TEAD4 were both detected in nuclear protein extracts of HAoSMCs (Figure 6 in the online-only Data Supplement). Given that mouse Tead3 and Tead4 are 97% and 94% identical to the human protein sequences, we used mouse Tead3 and Tead4 expression plasmids that are not affected by the human-specific shRNAs (Table 6 in the online-only supplement) to rescue the endogenous expression of p16 in HAoSMCs after knockdown of TEAD3 and TEAD4 (Figure 5E), further confirming the regulation of p16 by these factors.

Interestingly, TEAD3 knockdown resulted in impaired p16 mRNA and protein induction after TGFβ treatment, whereas TEAD4 knockdown did not (Figure 5C and 5D). We further confirmed that the TEAD elements at rs4977757 and rs10811656 are sufficient to mediate the TEAD3-dependent TGFβ response, in a luciferase reporter assay (Figure 5F). In contrast, no effect of TEAD4 was observed on the TGFβ response (Figure 5 in the online-only supplement). In HEK293 cells that do not express TEAD3, TGFβ did not induce the non-risk allele luciferase reporters unless TEAD3 was over-expressed, indicating that this response requires TEAD3. On

the other hand, the risk allele luciferase reporters were not TGFβ-responsive even with TEAD3 over-expression. Taken together, our results suggest that TGFβ regulation of p16 at the 9p21.3 locus is mediated by TEAD3 and that 9p21.3 risk alleles disrupt this regulation by interfering with TEAD3 binding (see model, Figure 6).

Discussion

Our study has identified two functional SNPs (rs10811656 and rs4977757) at the 9p21.3 locus that disrupt binding of TEAD3 and TEAD4 transcription factors *in vitro* (by EMSA) and *in vivo* (by ChIP and luciferase assays) in primary HAoSMCs. In addition, we found that TGFβ induced expression of p16 required TEAD3 and that this was impaired in HAoSMCs homozygous for the 9p21.3 risk allele.

TEAD transcription factors regulate gene expression in smooth muscle (132) and control cell proliferation (128,130,131). In addition, TEAD3 interacts with Smad3 to regulate TGFβ-dependent gene activation (54,132,133,140). TEAD3 and TEAD4 have both been implicated in regulating the expression of the smooth muscle alpha actin gene (55). Moreover, the expression of TEAD3 and TEAD4 are both suppressed in the wall of the aorta of aortic aneurysm patients compared to healthy controls (141). Thus, these TEAD factors were strong candidates for mediating TGFβ-dependent gene expression at the 9p21.3 locus in HAoSMCs. TGFβ is known to induce p16 and p15 expression to mediate cellular senescence and control cellular proliferation (28,52,53). Importantly, TGFβ inhibits smooth muscle cell proliferation (45) and reduces atherosclerosis (142) and the levels of TGFβ are reduced at sites of lesion development in the intima of the coronary arteries and human aorta (48). In myocardial and aortic tissues, genes whose expression was most affected by the 9p21.3 risk locus were found to involve the TGFβ signaling pathway (143).

Figure 6. TGFβ regulation of p16 expression is dependent on TEAD3 transcription factor and disrupted by 9p21.3 risk alleles rs4977757 and rs10811656.
TEAD3 or TEAD4 are sufficient for p16 expression, but TEAD3 is required for the TGFβ response.

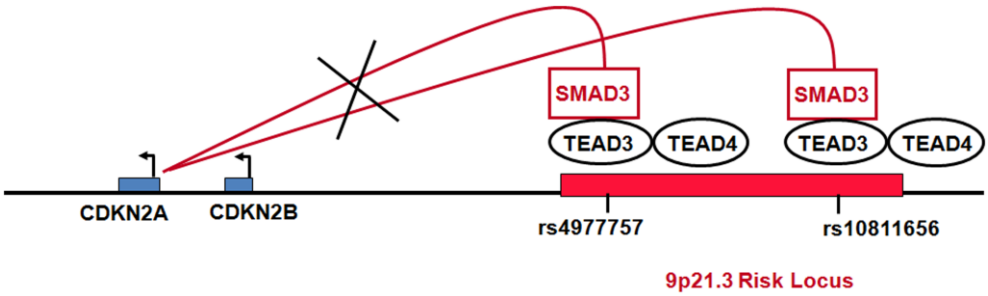
SMAD3
SMAD3
TEAD3
TEAD4
TEAD3
TEAD4
CDKN2A
CDKN2B
rs4977757
rs10811656
9p21.3 Risk Locus

We examined all the 59 SNPs within 9p21.3 locus for functional SNPs that could affect Smad binding and although we found two SNPs that matched a Smad consensus, these were not functional Smad binding sites by EMSA analysis using primary HAoSMCs. Instead, we found that TGFβ signaling at the risk locus is indirectly impaired through the disruption of the binding of the Smad3 partner TEAD3, but not TEAD4, by the risk alleles of rs10811656 and rs4977757. This mechanism accounts for the effect of the 9p21.3 risk genotype on blocking the TGFβ induction of p16 expression.

TEAD factors and TGFβ could be involved in other pathological effects other than cell proliferation such as smooth muscle cell migration, apoptosis or matrix accumulation (56,144). However, there is no evidence that supports an *a priori* hypothesis to tie the 9p21.3 locus to these phenotypes. Therefore, our hypothesis was evidence-based to explain the link between the disruption of TEAD binding with the known effect of the 9p21.3 risk locus on p15 and p16 levels and their associated phenotypes of proliferation and senescence (80,82,83,123)

Deletion of the 9p21.3 homologous sequence in the mouse is associated with an impaired Smad-dependent response to TGFβ (53,123,139) and with failure of cells to enter senescence (83). A recent study reported that mice with a deletion of the 9p21.3 homologous region (chr4$^{\Delta 70kb/\Delta 70kb}$ mice) have reduced p15 transcripts in the aorta, with undetectable levels of p16 (123). Our data are not entirely consistent with this finding, but this could reflect a species-specific difference. In addition, it should be pointed out that deletion of the entire region is not the same as having the sequence bearing the risk alleles. CAD-linked SNPS are not associated with increased risk of cancer, unlike the deletion of this region in mice and humans. Although p15^{ink4b} contributes to limiting cell proliferation (28), p16^{ink4a} also plays an essential part since deletion of p16^{ink4a} in mice is sufficient to promote tumorigenesis (145). Elevated expression of

$p16^{ink4a}$ inhibits vascular smooth muscle cell proliferation and reduces intimal hyperplasia in response to vascular injury (146). Another intriguing observation is that the two SNPs characterized here, rs10811656 and rs4977757, do not associate with altered gene expression in public eQTL databases (e.g., http://www.gtexportal.org/). This may reflect the phenotypic heterogeneity of different cell types in different tissues isolated from humans exposed to various environmental factors (e.g., age, diet, smoking, disease, etc)(38). Our findings in primary HAoSMCs under controlled culture conditions would be expected to enhance genetic associations.

Our study cannot account for reduced expression of p15 in HAoSMCs homozygous for the risk allele, and this mechanism will require further study. Another potential limitation of our study is the relatively small sample size of primary HAoSMC cultures (13 individual donors in total). However, these cells are relatively difficult to acquire from different individuals and the limited proliferation of cells homozygous for the non-risk allele limits their utility in functional studies. Several studies with larger sample sizes have consistently established the reduced expression of p15 and p16 and increased cellular smooth muscle proliferation as biological phenotypes linked to 9p21.3 risk locus (80,82,83,123). Therefore, our finding of increased cellular proliferation with the 9p21.3 risk allele confirms previous reports. Another limitation is that the number of passages to senescence was not adjusted for age, race, and gender due to the small sample size. However, all HAoSMCs homozygotes for the risk allele failed to enter senescence and cells homozygous for the non-risk allele reached senescence after a maximum of 6 passages. Heterozygote cells entered senescence after maximum of 14 passages. Therefore, the effect of the 9p21.3 on the senescence is genotype specific and appears to be much more important than age, race, and gender (see Table S1). Our stringent approach to test SNPs for their

effect on transcription factor binding used nuclear extracts from relevant cell types, where the putative transcription factors are known to be expressed. For example, the human myeloid cell line THP1 was used to test for PU.1 and IRF4 binding. Additional cell types that could affect atherosclerosis burden (e.g., lymphocytes, primary macrophages) might have revealed additional transcription factors not present in HAoSMCs. However, given the known effect of 9p21.3 risk alleles on smooth muscle cells (82,83,123), we sought to identify transcription factors relevant to these cells. In addition, the EMSA has its own limitations. Although we observed a difference in gel shift patterns between the risk and non-risk alleles at GATA sites, these differences were not reflected in luciferase promoter activities. Single GATA sites may not be sufficient to confer differences in promoter activity *in vivo* if GATA factors require association with other transcription factors.

Conclusions

Our study provides a novel mechanism whereby the 9p21.3 locus confers risk for coronary atherosclerosis. Emerging therapies using selective peptide competitors to activate TEAD factors have been developed that limit cell proliferation and tumor growth in gastric cancer (147). A similar strategy may be applicable to atherosclerosis, but this approach may require knowledge of the 9p21.3 genotype to be effective.

Acknowledgements

We thank Dr. Ruth McPherson for providing 2 of the 13 primary cultures of HAoSMCs.

Source of funding

This work is supported by operating grants from the Canadian Institute of Health Research (Chen, Stewart) and Natural Sciences and Engineering Research Council of Canada (Chen, Stewart). Chen was supported by a New Investigator Award from the HSFC and a Mid-career Investigator Award from the HSFO. Almontashiri was supported by a graduate scholarship from Taibah University, Saudi Arabia and a University of Ottawa Endowed Graduate Award at the Heart Institute. There are no relationships to industry.

Disclosures

None.

Clinical perspective

Among individuals of non-black African ancestry, 75% of the population carries one or two copies of the 9p21.3 risk locus for coronary artery disease. Genetic testing for the 9p21.3 locus identifies individuals at increased risk for coronary atherosclerosis and abdominal aortic aneurysm. Impaired binding of TEAD transcription factors and loss of TGFβ-dependent activation of the cell cycle suppressor p16 in smooth muscle cells accounts for part of the elevated risk from the 9p21.3 locus. Emerging cancer therapies that activate TEAD factors to inhibit cellular proliferation may also be useful to limit atherosclerosis progression in individuals heterozygous or homozygous for the non-risk allele of 9p21.3.

Supplemental information

Expanded methods

Cell cultures and Genotyping

HeLa and HEK293 cells were cultured in DMEM medium (Corning Cellgro, Manassas, VA) supplemented with 10% FBS. THP1 cells were cultured in RPMI Medium 1640 (Invitrogen). HAoSMCs were purchased from Cell Applications (San Diego, CA) and Lonza (Walkersville, MD) (Table 1) and cultured in Lonza SmGM-2 BulletKit medium (Cat# CC-3182). The datasheets stated that the HAoSMCs were isolated from the tunica media of healthy and fibrous plaque-free aorta and were cryopreserved at second passage prior to shipping. HAoSMCs were purchased and genotyped for the 9p21.3 risk locus, as described previously (125) and details are presented in Table 1, below. For all experiments, cells with different genotypes were maintained under identical growth conditions, were plated at equal densities and were re-plated when they reached 80% confluence. Cells were counted using a haemocytometer. Human recombinant TGFβ1 was purchased from Cell Signaling (8915LC).

Immunoblotting Analyses, Antibodies and Reagents

After 4 passages, HAoSMCs were suspended and cultured in Lonza SmGM-2 BulletKit smooth muscle medium (10% FBS) (Cat# CC-3182) plated in 100 mm plates at 250,000 cells and grown for 48 hours at 37°C. Cells with different genotypes were maintained under identical growth conditions, were plated at equal densities and were re-plated when they reached 80% confluence. Mouse anti-HA antibody used in EMSA and western blot was purchased from Millipore (05-904, Temecula, CA). Rabbit anti-Tead4 was reported previously (148). Rabbit anti-TEAD3 antibody (215-304) was from Abnova (H00007005-A01, Taipei, Taiwan). Phospho-Smad3 (Ser423/425) rabbit monoclonal antibody (#9520) was from Cell Signaling (Danvers, MA). Mouse anti-CDKN2A (sc-9968), anti-CDKN2B (sc-171798), anti-MTAP (sc-100782) antibodies were from Santa Cruz Biotechnology (Santa Cruz, CA) and diluted 1:1,000 in blocking solution. Goat anti-mouse

IgG (HAF007, R&D Systems, MN) and goat anti-rabbit IgG (31460, Piercenet, Rockford, IL) were diluted in 1:15,000. Quantification of protein levels, normalized to GAPDH, was performed using ImageQuant TL V2005 software. Relative protein levels were expressed as mean ± SEM.

Constructs, Luciferase Reporter Assays and lentiviral transductions

Luciferase activities presented in Figure 3 were expressed as a fold change relative to empty pGL3 promoter vector (control) of each group. We did not normalize to a co-transfected Renilla luciferase reporter, as many do who use a kit, because we have extensively documented that this reporter is affected by TEAD transcription factors and does not control for transfection efficiency (149). As for the reproter activity after TGFβ treatment (Figure 5E), luciferase activity was expressed as fold change relative to the activity of the vector (vehicle) groups for normalization.

Lipofectamine 200 was used to transfect HAoSMCs (after 4 passages) with HA-tagged TEADs or empty PXJ-40 plasmids, pGL3 luciferase constructs for 6 hours in serum and antibiotic free smooth muscle medium. After 6 hours, the medium was replaced by regular smooth muscle growth medium for 48 hours.

For knockdown experiments in Heterozygotes HAoSMCs (after 4 passages), lentiviral particles were purchased from Santa Cruz biotechnology (Santa Cruz, CA): scrambled shRNA (sc-108080) as a control, a pool of two different shRNA lentiviral vectors against human TEAD3 (sc-95636-V), and a pool of three different shRNA lentiviral vectors against human TEAD4 (sc-96187-V) (see Table S6 for shRNAs sequences). The infection was done as instructed by the company. For rescue experiments, mouse Tead3 and Tead4 expression plasmids (135,150) were

used to transfect lentiviral-transduced HAoSMCs expressing either the scrambled or human-specific shRNAs for TEAD3 and TEAD4.

Chromatin immunoprecipitation (ChIP) analysis

HAoSMC cells homozygote for the non-risk allele were transfected with HA tagged TEED3 and TEAD4 pXJ40 vector for 48 hours. The Antibody-chromatin cross-linking was done for 10 minutes with 1% formaldehyde and then quenched with 125 mM glycine. Cells were washed with ice-cold PBS and then lysed with cell lysis buffer and then the chromatin was extracted by lysing the nuclei in the nuclear lysis buffer. The chromatin immunoprecipitation using anti-HA antibody (cat #11815016001, Roche) and PCR amplification were performed using Chromatin Immunoprecipitation Kit from Upstate (Catalog # 17-371, cell signaling solutions) as described by the manufacturer. Primers used to sequence verify and amplify TEAD3 and TEAD4 binding elements are: 5` TTGGAACTGAACTGAGGCCAGACA 3` (sense), 5` TAGACTCCACGCTGTTCCCAAGTA 3` (anti-sense) for rs10811656; and 5` GATCAGCTGTTAGTCTGATGGG 3` (sense), 5` CTGAAAGTGACGGGCAGAA 3` (anti-sense) for rs4977757.

Quantitative real-time RT-PCR (Q-PCR)

Total RNA was extracted from cultured HAoSMCs using RNeasy Micro kit (cat # 74004, Qiagen). Concentration and quality of isolated RNA was measured using NanoDrop 2000 (Thermo Scientific). 2ug of total RNA from each sample was reverse transcribed to make cDNA using M-MLV reverse transcriptase (Life Technologies) with random primers according to manufacturer's protocol. Quantitative real time- PCR was performed with the gene specific forward and reverse primers using DyNAmo HS SYBR Green qPCR Kit (Life Technologies) on the Rotor-Gene Q(Qiagen). The primers for real-time PCR are: GGTGGCTACGAATCTTCCG, CCTAAGTTGTGGGTTCACCA (CDKN2B);ACTCTGGAGGACGAAGTTTG,

CTTCCTTGGCTTCCCAAGC (CDKN2A);GATTTGGTCGTATTGGG, TCCACGACGTACTCAGC (GAPDH). The PCR protocol included polymerase activation (95°C for 15min) and cycling step [40 cycles of: denaturation at 95°C for 10s, annealing at 55°C for 20s, extension at 72°C for 30s]. The $2^{-\Delta\Delta CT}$ method was used for the relative quantification of gene expression normalized against GAPDH.

Electrophoretic mobility shift assay (EMSA).

Nuclear protein extracts from cultured HAoSMCs and other cell types used in EMSA, were prepared as described by *Farrance et al*. (1992) (134). Nuclear protein concentrations were determined by Bradford assay. EMSA using SNPs specific oligonucleotide (Table S3) is performed as described previously (151), using radiolabeled oligonucleotides corresponding to different SNPs (Table S3) in the presence of 13 ug of the nuclear extracts form different cells depending on the transcription factor (see Table S2). Some of the gel shift performed in this study lack the use of antibody due to the fact that. Some antibodies to transcription factors do not produce a supershift. Where available, we have used commercial antibodies known to supershift transcription complexes. Some gel shift experiments did not include antibodies either because these do not give satisfactory supershifts or we did not observe a shifting complex, and this precluded the need for an antibody. To help overcome this problem, we used control oligonucleotides that are known to specifically bind the transcription factor in question (Table S4).

Bromodeoxyuridine (BrdU) staining and Cell Counts

HAoSMCs were cultured in Lonza SmGM-2 BulletKit smooth muscle medium (10% FBS) (Cat# CC-3182) plated in 100 mm plates at 250,000 cells and grown for 48 hours at 37°C. Cells were used on the 4^{th} passage. Because we observed increased cell death when we labeled

cultured HAoSMCs for more than 45 minutes, we found that pulse-labeling with 10 μM bromodeoxyuridine (BrdU) for 45 minutes was the optimal condition for measuring the actively dividing HAoSMCs and harvested for fluorescence-activated cell sorting (FACS) analysis as described previously (152). For TGFβ effects on cell proliferation, cells were grown in 96 well plates and BrdU incorporation was measured using the Cell Proliferation ELISA kit (Roche, Indianapolis, IN).

Statistics

Data were normally distributed and were evaluated by ANOVA with the Bonferroni's post hoc test. $P < 0.05$ was considered statistically significant.

Figure S1. Gel mobility shift assay reveals that the STAT1 does not bind to rs10757278.
Using nuclear extracts from untreated (HeLa) or IFN-γ treated (HeLa IFNG) HeLa cells and a positive control IFN-γ response element (IRE) (Table S4), we observed a clear shifted complex in IFN-γ treated (100ng/ml for 24 hours) nuclear extract (compare lanes 2 and 4). A 200-fold molar excess of the IRE-probe self-competed. By comparison, a similar 200 fold molar excess of the non-risk allele of rs10757278 competed weakly (30% reduced binding) and not at all for the risk allele of rs10757278 (compare lanes 5 to 7 and 8). However, STAT1 activation did not result in a shifted complex for either the risk or non-risk probes. These results do not support a robust STAT1 interaction with sequences at rs10757278. Note: the complexes seen with the risk probe are non-specific since they do not compete with the cold risk oligonucleotide (lane 13). Free, unbound radio-labeled probe; NS, a non-specific shift (n= 3 experiments).

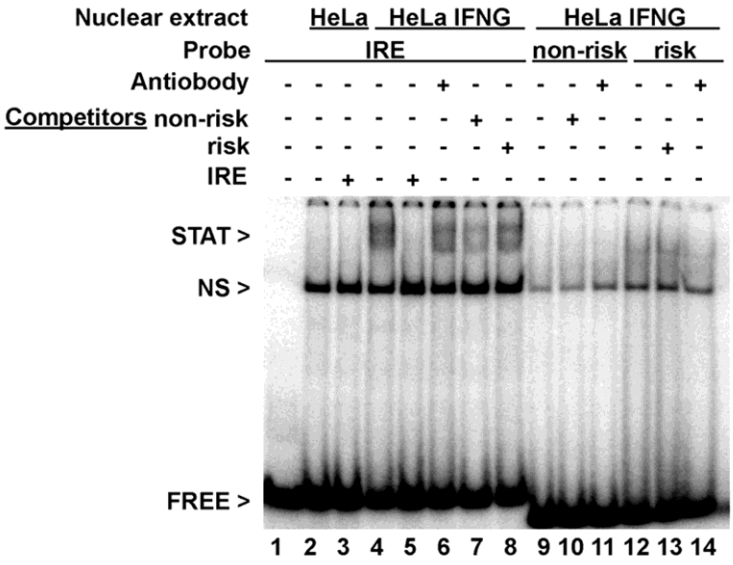
Nuclear extract
HeLa
HeLa IFNG
HeLa IFNG
Probe
IRE
non-risk
risk
Antiobody
Competitors non-risk
risk
IRE
STAT >
NS >
FREE >
1 2 3 4 5 6 7 8 9 10 11 12 13 14

Figure S2. EMSA analysis shows that rs1333045 dose not contain a functional Smad3 binding site.
Oligonucleotide containing Smad3 binding consensus (Table S4) was used as a positive control for Smad3 binding after TGF□ treatment (2ng/ml for 8 hours), (n=3 experiments).

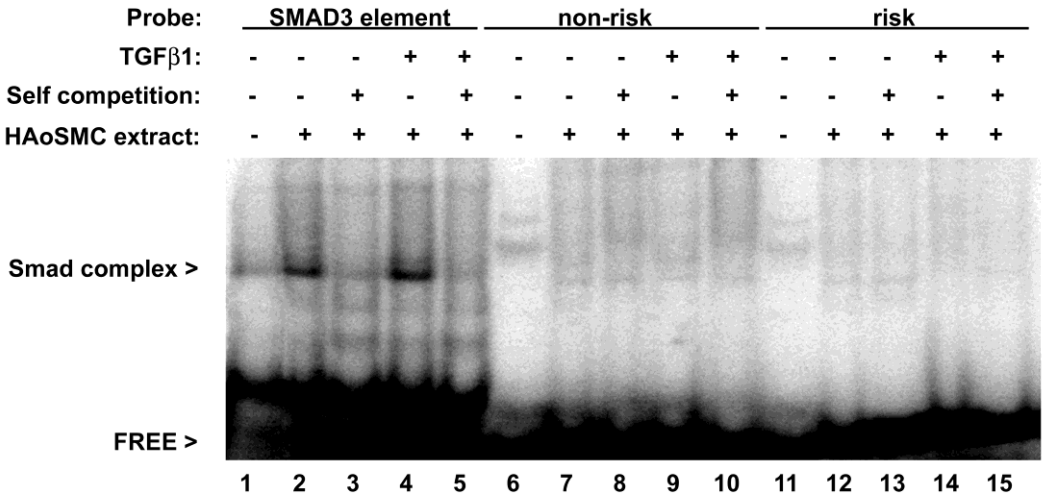
Probe:
SMAD3 element
non-risk
risk
TGFβ1:
- - - + + - - - + + - - - + +
Self competition:
- - + - + - - + - + - - + - +
HAoSMC extract:
- + + + + - + + + + - + + + +
Smad complex >
FREE >
1 2 3 4 5 6 7 8 9 10 11 12 13 14 15

Figure S3
(A) EMSA analysis confirmed that rs10757269 and rs9632885 contain GATA binding sites and the risk alleles conferred differential binding compared to the non-risk alleles, (n=3). (B) Luciferase reporter assay is performed to examine the transcriptional activity of rs10757269 and rs9632885 upon the binding of endogenous GATAs in HAoSMCs. Both SNPs are functional and showed no difference between the risk and the non-risk alleles. Luciferase activity was expressed as fold change and normalized to empty pGL3 promoter vector (control), (n=6 experiments, in triplicates). Fold is expressed as mean ± SEM.

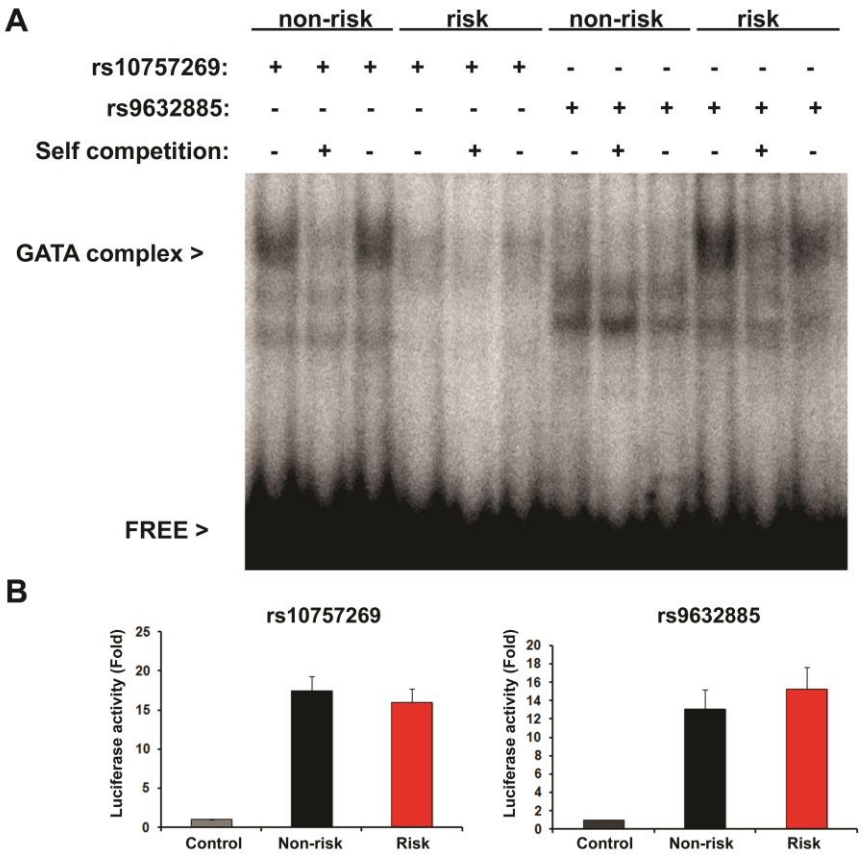
A
non-risk
risk
non-risk
risk
rs10757269: + + + + + + - - - - - -
rs9632885: - - - - - - + + + + + +
Self competition: - + - - + - - + - - + -
GATA complex >
FREE >
B
rs10757269
Luciferase activity (Fold)
25
20
15
10
5
0
Control
Non-risk
Risk
rs9632885
Luciferase activity (Fold)
20
18
16
14
12
10
8
6
4
2
0
Control
Non-risk
Risk

Figure S4. EMSA analysis shows that rs10811656 and rs4977757 polymorphisms disrupt the binding the endogenous TEADs factors to its binding sites.
Oligonucleotides containing TEAD binding consensus from the promoter of the skeletal alpha actin (SKA) gene was used as a positive control for endogenous TEADs complex binding from HAoSMCs nuclear extracts. Note the formation of the non-specific complex (third lane from the left) compared to the specific complex in the non-risk lanes, because the self competition with cold probe did not compete for complex binding and therefore the disappearance of the complex (n=3).

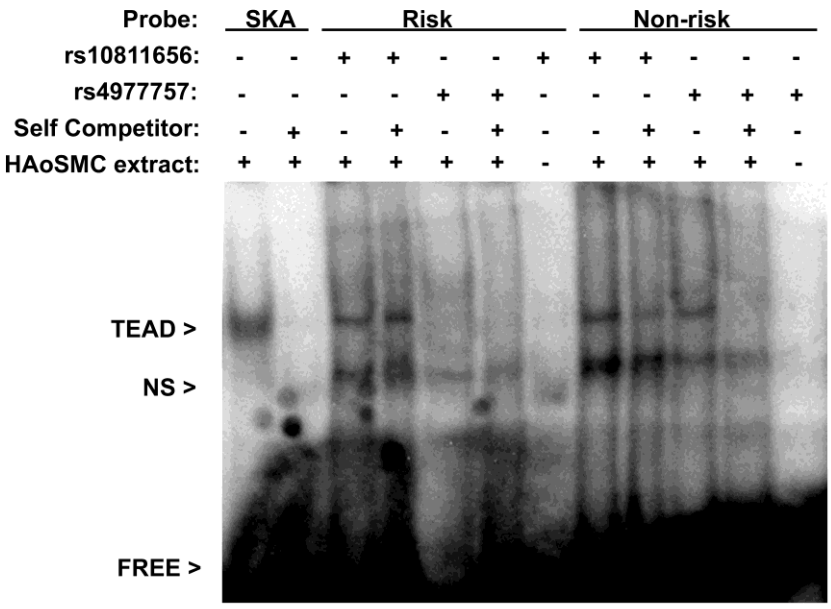
Probe: SKA Risk Non-risk
rs10811656: - - + + - - + + + - - -
rs4977757: - - - - + + - - - + + +
Self Competitor: - + - + - + - - + - + -
HAoSMC extract: + + + + + + - + + + + -
TEAD >
NS >
FREE >

Figure S5. TEAD4 does not affect the response to TGFβ of luciferase reporters bearing rs10811656 and rs4977757.
HEK293 cells were transfected in 3 separate experiments in triplicate. ANOVA compared the 3 groups (risk/non-risk, vector/TEAD3, vehicle/TGFβ) and post-hoc pairwise comparisons were used, correcting for multiple testing. *$p<0.05$.

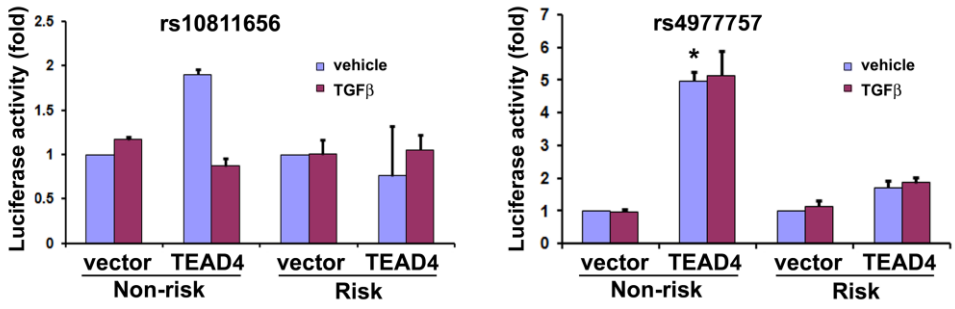
rs10811656
Luciferase activity (fold)
2.5
2
1.5
1
0.5
0
vehicle
TGFβ
vector
TEAD4
vector
TEAD4
Non-risk
Risk
rs4977757
*
Luciferase activity (fold)
7
6
5
4
3
2
1
0
vehicle
TGFβ
vector
TEAD4
vector
TEAD4
Non-risk
Risk

Figure S6.
Immunoblot of TEAD3 and TEAD4 from nuclear extracts confirmed their knock-down in primary HAoSMCs using Lentiviral vectors. Histone-H1 was used as loading control for nuclear protein. Scr, scrambled shRNA particles (n=3 experiments).

Table S1 Characteristics of the primary HAoSMCs used in this study.

Vendor	Lot #	Race	Age	Gender	9p21.3 genotype	# passages to senescence
Cell Applications, Inc	1596	Caucasian	53	male	heterozygote	15
Cell Applications, Inc	1441	African American	54	male	homozygote non-risk	6
Cell Applications, Inc	1401	Hispanic	39	male	homozygote risk	>18*
Cell Applications, Inc	2228	Caucasian	21	female	homozygote risk	>25*
Cell Applications, Inc	1483	Caucasian	44	female	homozygote risk	>25*
Cell Applications, Inc	2531	Caucasian	20	male	heterozygote	13
Cell Applications, Inc	1189	Caucasian	17	female	heterozygote	11
Cell Applications, Inc	2498	Caucasian	55	male	heterozygote	10
Cell Applications, Inc	1848	Caucasian	48	male	homozygote non-risk	7
Lonza Walkersville Inc	287836	Caucasian	30	male	heterozygote	11
Lonza Walkersville Inc	6F3972	Caucasian	14	male	homozygote risk	>18*
Cell Applications, Inc	1476	Caucasian	42	male	homozygote non-risk	6
Cell Applications, Inc	1426	Caucasian	50	female	homozygote risk	>17*

*Maximum number of passages attempted.

Table S2 Summary of the bioinformatics scan and functional validation of SNPs with possibly disruptive effect.

SNP	Binding element (non-risk)	Binding element (risk)	Transcription factor	Source of nuclear extracts	Predicted risk allele effect	Testing method	
rs1333045	CTGTGTCTGGC	CTGTGCCTGGC	Smad3	TGFβ treated HAoSMCs	Disrupted binding	EMSA (-)	NA
rs10757278	GGTAAGCAG	GGTAGGCAG	STAT1	Interferon gamma treated HAoSMCs	Disrupted binding	EMSA (-)	Reporter assay (-)
rs10811656	GGTCATTCCGG	GGTCATTCTGG	TEAD4 and TEAD3	HAoSMCs and Hela cells	Disrupted binding	EMSA (+)	Reporter assay (+)
rs10738610	GACAGAAAT	GACCGAAAT	IRF4	THP1 cells and HAoSMCs	De novo binding	EMSA (-)	NA
rs10757275	ACAGACAC	ACAGGCAC	Smad3	TGFβ treated HAoSMCs	Disrupted binding	EMSA (-)	NA
rs6475609	AAGATAGG	AAGATGGG	GATA	HAoSMCs	Disrupted binding	EMSA (-)	NA
rs9632885	TAGATAATAT	TAGATGATAT	GATA	HAoSMCs	De novo binding	EMSA (+)	Reporter assay (-)
rs10757269	TAGATAA	TAGGTAA	GATA	HAoSMCs	Disrupted binding	EMSA (+)	Reporter assay (-)
rs1537376	ATGATATG	ATGACATG	GATA	HAoSMCs	Disrupted binding	EMSA (-)	NA
rs10757271	CAAGCAATCCT	CAAGCGATCCT	TEAD4 and TEAD 3	HAoSMCs and Hela cells	Disrupted binding	EMSA (-)	NA
rs785972	GAATGACAGG	GAATGATAGG	Meis1	HAoSMCs and Hela cells	Disrupted binding	EMSA (-)	NA
rs10757274	TGAGAC	TGGGAC	PRC1	HAoSMCs and HEK293 cells	Disrupted binding	EMSA (-)	NA
rs4977757	TGTGGCATTCT	TGTGGCGTTCT	TEAD4 and TEAD 3	HAoSMCs and Hela cells	Disrupted binding	EMSA (+)	Reporter assay (+)
rs1333043	TGGGAATGCTT	TGGGAAAGCTT	TEAD4 and TEAD3	HAoSMCs and Hela cells	Disrupted binding	EMSA (-)	NA

EMSA (-), absence or EMSA (+), presence of a difference in nuclear protein binding according to genotypes. Reporter assay (-) signifies absence and reporter assay (+), presence of a difference in luciferase reporter activity observed between genotypes.

Table S3 The oligonucleotides used for EMSA to test transcription factors binding to different SNPs.

SNP	Non-Risk oligonucleotides	Risk oligonucleotides
rs1333045	5′ GTACACTGTGTCTGGCATCTAG 3′ 5′ CTAGATGCCAGACACAGTGTAC 3′	5′ GTACACTGTGCCTGGCATCTAG 3′ 5′ CTAGATGCCAGGCACAGTGTAC 3′
rs10757278	5′ GGTGTGGTCATTCCGGTAAGCAGCG 3′ 5′ CGCTGCTTACCGGAATGACCACACC 3′	5′ GGTGTGGTCATTCTGGTAGGCAGCG 3′ 5′ CGCTGCCTACCAGAATGACCACACC 3′
rs10811656	5′ GGTGTGGTCATTCCGGTAAGCAGCG 3′ 5′ CGCTGCTTACCGGAATGACCACACC 3′	5′ GGTGTGGTCATTCTGGTAGGCAGCG 3′ 5′ CGCTGCCTACCAGAATGACCACACC 3′
rs10757271	5′ CCAGGCTCAAGCAATCCTCTCACCT 3′ 5′ AGGTGAGAGGATTGCTTGAGCCTGG 3′	5′ CCAGGCTCAAGCGATCCTCTCACCT 3′ 5′ AGGTGAGAGGATCGCTTGAGCCTGG 3′
rs4977757	5′ GAGTATCTTTGTGGCATTCTCTGTATTTCCT 3′ 5′ AGGAAATACAGAGAATGCCACAAAGATACTC 3′	5′ GAGTATCTTTGTGGCGTTCTCTGTATTTCCT 3′ 5′ AGGAAATACAGAGAACGCCACAAAGATACTC 3′
rs10757274	5′ AGCTGAGTGTTGAGACATAATTGAA 3′ 5′ TTCAATTATGTCTCAACACTCAGCT 3′	5′ AGCTGAGTGTTGGGACATAATTGAA 3′ 5′ TTCAATTATGTCCCAACACTCAGCT 3′
rs785972	5′ GCATCTGAATGACAGGCATTCCTTTGAAT 3′ 5′ GCAATTCAAAGGAATGCCTGTCATTCAG 3′	5′ GCATCTGAATGATAGGCATTCCTTTGAAT 3′ 5′ GCAATTCAAAGGAATGCCTATCATTCAG 3′
rs10738610	5′ TCCAGGGGACAGAAATAGGAC 3′ 5′ GTCCTATTTCTGTCCCCTGGA 3′	5′ TCCAGGGGACCGAAATAGGAC 3′ 5′ GTCCTATTTCGGTCCCCTGGA 3
rs1333048	5′ AGGAGATGTTTAAATGTCGAAT 3′ 5′ ATTCGACATTTAAACATCTCCT 3′	5′ AGGAGATGTTTCAATGTCGAAT 3′ 5′ ATTCGACATTGAAACATCTCCT 3′
rs10757275	5′ GCTGGGAGTACAGACACACGCCACC 3′ 5′ GGTGGCGTGTGTCTGTACTCCCAGC 3′	5′ GCTGGGAGTACAGGCACACGCCACC 3′ 5′ GGTGGCGTGTGCCTGTACTCCCAGC 3′
rs6475609	5′ CTTAGTAAAGATAGGGTTTCAGCAT 3′ 5′ ATGCTGAAACCCTATCTTTACTAAG 3′	5′ CTTAGTAAAGATGGGGTTTCAGCAT 3′ 5′ ATGCTGAAACCCCATCTTTACTAAG 3′
rs9632885	5′ ATGTTATTAGATAATATAGTCTCAG 3′ 5′ CTGAGACTATATTATCTAATAACAT 3′	5′ ATGTTATTAGATGATATAGTCTCAG 3′ 5′ CTGAGACTATATCATCTAATAACAT 3′
rs10757269	5′ AGGTTCTTTTAGATAATTTTTTTAT 3′ 5′ ATAAAAAAATTATCTAAAAGAACCT 3′	5′ AGGTTCTTTTAGGTAATTTTTTTAT 3′ 5′ ATAAAAAAATTACCTAAAAGAACCT 3′
rs1537376	5′ TACTCCCCATGACATGTATATCTGT 3′ 5′ ACAGATATACATGTCATGGGGAGTA 3′	5′ TACTCCCCATGATATGTATATCTGT 3′ 5′ ACAGATATACATATCATGGGGAGTA 3′
rs1333043	5′ CAGTTTGTGGGAAAGCTTTTTTAGTTA 3′ 5′ TAACTAAAAAAGCTTTCCCACAAACTG 3′	5′ CAGTTTGTGGGAATGCTTTTTTAGTTA 3′ 5′ TAACTAAAAAAGCATTCCCACAAACTG 3′

Table S4 Control oligonucleotides used as competitors in EMSA for different transcription factors.

Binding element	**Control oligonucleotides**
STAT1 binding site (153)	5′ GCATGTTTCAAGGATTTGAGATGTATTTCCCAGAAAAGG 3′ 5′ CCTTTTCTGGGAAATACATCTCAAATCCTTGAAAGATGC 3′
Smad 3 binding site (154)	5′ TCGAGAGCCAGACAAAAAGCCAGACATTTAGCCAGACAC 3′ 5′ GTGTCTGGCTAAATGTCTGGCTTTTTGTCTGGCTCTCGA 3′
GATA binding site (155)	5′ CACTTGATAACAGAAAGTGATAACTCT 3′ 5′ AGAGTTATCACTTTCTGTTATCAAGTG 3′
IRF4 binding site (156)	5′ CTGACACCCGAAACCAC 3′ 5′ GTGGTTTCGGGTGTCAG 3′
TEAD binding site (157)	5′ GCAGCAACATTCTTCGGGGC 3′ 5′ GCCCCGAAGAATGTTGCTGC 3′
Meis1 binding site (158)	5′ TGACAGCTGCTGACAGCTG 3′ 5′ CAGCTGTCAGCAGCTGTCA 3′
PRC1 binding site (159)	5′ AAAGAGAGCCCGGGAGAGAGAAA 3′ 5′ TTTCTCTCTCCCGGGCTCTCTTT 3′
PU-1 binding site (160)	5′ CTTCTTCTAACTTCCTCTCCTGTGAC 3′ 5′ GTCACAGGAGAGGAAGTTAGAAGAAG 3′

Table S5 Oligonucleotides used to generate different reporter constructs carrying the risk and non risk variants that are shown.

SNP	Non-Risk	Risk
rs10811656	5′ CGGTGTGGTCATTCCGGTAAGCAGCGC 3′ 5′ TCGAGCGCTGCTTACCGGAATGACCACACCGGTAC 3	5′ CGGTGTGGTCATTCTGGTAGGCAGCGC 3′ 5‘ TCGAGCGCTGCCTACCAGAATGACCACACCGGTAC 3′
rs4977757	5′ CTATCTTTGTGGCATTCTCTGTATTTC 3′ 5′ TCGAGGAAATACAGAGAATGCCACAAAGATACGGTAC 3′	5 CTATCTTTGTGGCGTTCTCTGTATTTC 3′ 5′TCGAG GAAATACAGAGAACGCCACAAAGATACGGTAC 3′
rs9632885	5 CATGTTATTAGATAATATAGTCTCAGC 3 5 TCGAGCTGAGACTATATTATCTAATAACATGGTAC 3′	5′ CATGTTATTAGATGATATAGTCTCAGC 3′ 5′ TCGAGCTGAGACTATATCATCTAATAACATGGTAC 3′
rs10757269	5′ CAGGTTCTTTTAGATAATTTTTTTATC 3′ 5′ TCGAGATAAAAAAATTATCTAAAAGAACCTGGTAC 3′	5′ CAGGTTCTTTTAGGTAATTTTTTTATC 3′ 5′ TCGAGATAAAAAAATTACCTAAAAGAACCTGGTAC 3′

Table S6 Sequences of the lentiviral shRNAs used to knock down human TEAD3 and TEAD4

TEAD3 shRNA	**Sequence**	**Orthologous sequence in mouse**
Pool 1 (sense)	CACCTGUGGGTATTTATGA	CACCTG_GG_TATTTATGA
Pool 2 (sense)	CTGUGATGGGTTATATCAT	CTGTGATGGGCTACATCAT
TEAD4 shRNA	**Sequence**	**Orthologous sequence in mouse**
Pool 1 (sense)	CCCATGATGTGAAGCCTTT	CCCACGATGTGAAACCTTT
Pool 2 (sense)	GTATGCTCGCTATGAGAAT	GTATGCCCGCTATGAGAAT
Pool 3 (sense)	GCATTGCCTATGTCTTTGA	GCATTGTGGTGATGCTACAGA

Underlined sequences indicate divergence in the mouse sequence from the targeted human sequence. All sequences are provided in the 5′ → 3′ orientation.

CHAPTER4

SPG7 variant escapes phosphorylation-regulated processing by AFG3L2, elevates mitochondrial ROS and associates with multiple clinical phenotypes

Naif A. M. Almontashiri[1,2,3], Hsiao-Huei Chen[4], Ryan J. Mailloux[2], Takashi Tatsuta[9], Allen C. T. Teng[1,2], Ahmad B. Mahmoud[2,3], Tiffany Ho[1], Nicolas A. S. Stewart[5], Peter Rippstein[1], Mary Ellen Harper[2], Robert Roberts[1], Christina Willenborg[6] and Jeanette Erdmann[6] for the CARDIoGRAM consortium, Annalisa Pastore[7], Heidi McBride[8], Thomas Langer[9], Alexandre F. R. Stewart[1,2*].

[1]University of Ottawa Heart Institute, Ottawa, Canada; [2]Department of Biochemistry, Microbiology and Immunology, University of Ottawa; [3]Department of Applied Medical Sciences, Taibah University, Almedinah, Saudi Arabia; [4]Ottawa Hospital Research Institute, Ottawa, Canada; [5]Center for Clinical Pharmacology, Department of Medicine, University of Pittsburgh, Pittsburgh, USA; [6]University of Lübeck, Germany; [7]National Institute for Medical Research, The Ridgeway, Mill Hill, London, UK; [8]McGill University, Montreal, Canada; [9]Institute for Genetics, University of Cologne, Germany.

*correspondence: astewart@ottawaheart.ca

This paper was first published as a research article in Cell Reports (2014), May; 8;7(3):834-47.

Figure 1 (A and D-F), Figure 3 (B, C and F) and Figure 5 (B, G, H and I) were part of my Master Dissertation.

Author contributions: NAMA (all the experimnets and figures unless otherwise mentioned), RJM (figure 4A-F and figure S3 and 4) , TT (figure 2B), ACTT maintained tissue cultures, ABM (FACS analysis in figure 5G), JA and CW (figure 1B), AP (figure 2C), PR (figure 3C), TH (helped in tissue culture), NASS (mass specterometry) performed the experiments; MEH, JE, AP, HM, TL provided essential data and analysis; NAMA, HHC, RJM, AP, TL, HM, RR, and AFRS wrote the manuscript.

Key words: AFG3L2; mitochondrial bioenergetics; reactive oxygen species; SPG7; tyrosine phosphorylation

Abstract

Mitochondrial production of reactive oxygen species (ROS) affects many processes in health and disease. SPG7 assembles with AFG3L2 into the mAAA protease at the inner membrane of mitochondria, degrades damaged proteins and regulates the synthesis of mitochondrial ribosomes. SPG7 is cleaved and activated by AFG3L2 upon assembly. Here, we characterized a variant in SPG7 that replaces arginine 688 with glutamine and associates with several phenotypes, including toxicity of chemotherapeutic agents, type 2 diabetes mellitus and now with coronary artery disease. We demonstrate a novel mechanism whereby SPG7 processing is regulated by tyrosine phosphorylation of AFG3L2. Carriers of the risk variant of SPG7 (Q688) bypass this regulation and constitutively process and activate the SPG7-containing protease. Cells expressing Q688 produced higher ATP levels and ROS, promoting cell proliferation. Our results thus reveal an unexpected link between the phosphorylation-dependent regulation of the mitochondrial mAAA protease affecting ROS production and several clinical phenotypes.

Highlights

- **SPG7 Q688 variant associates with multiple clinical phenotypes**
- **SPG7 Q688 variant escapes regulated processing by its partner AFG3L2**
- **SPG7 Q688 variant increases mitochondrial ROS production**
- **AFG3L2 tyrosine phosphorylation regulates SPG7 proteolytic processing**

Introduction

Chronic diseases, like type 2 diabetes mellitus (T2DM) or coronary artery disease (CAD), are associated with altered mitochondrial function and elevated reactive oxygen species (ROS) production (161,162). Mitochondria provide energy (ATP) to the cell through oxidative metabolism at the electron transport chain (ETC). During this process, mitochondria also produce ROS as a byproduct. ROS oxidize and damage mitochondrial proteins and DNA. For this reason, mitochondria contain enzymes that eliminate ROS, including superoxide dismutase (SOD2) and peroxiredoxin 3 (Prdx3), to actively maintain a reduced state and the mitochondrial electrochemical potential required for ATP production (91).

Mitochondrial matrix proteins that are damaged from oxidation by ROS are degraded by the Lon protease (97). In addition, the mAAA (matrix ATPase Associated with diverse cellular Activities) protease also participates in this process, because oxidized mitochondrial proteins accumulate in brain extracts from mice carrying a missense mutation in the core AAA domain of AFG3L2 or in mice deficient in AFG3L2 (98). By sensing and destroying damaged matrix proteins, including the components of the ETC, the mAAA protease performs an essential quality control function (163,164). The mAAA protease also regulates the assembly of mitochondrial ribosomes and the synthesis of respiratory chain subunits within mitochondria (99,100). Thus, by controlling the integrity and assembly of the ETC, the mAAA protease may be uniquely positioned to regulate ROS production. Recent evidence indicates that mitochondrial ROS (mROS) production is actively regulated (165) and controls diverse mechanisms such as cell proliferation (166) and the bactericidal activity of macrophages (167).

The mAAA protease is assembled as a homohexamer of AFG3L2 or as a heterohexamer between SPG7 and AFG3L2 (168). AFG3L2 is a self-processing protease that is active upon assembly at the mitochondrial inner membrane. In contrast, cleavage and processing of SPG7 to a mature active protease requires co-assembly with AFG3L2 (102). Loss-of-function mutations in AFG3L2 cause spinocerebellar and spastic ataxia (105,169). Mutations in SPG7 (also called paraplegin) cause hereditary spastic paraplegia (HSP), a neurodegenerative disorder characterized by progressive weakness and spasticity of the lower limbs due to degeneration of corticospinal axons (103,170). Of note, vascular lesions in the frontal cortex have been detected by functional MRI in some forms of HSP linked to the SPG7 locus (104).

A protein coding variant that changes an arginine (R688) to glutamine (Q688) in the highly conserved protease domain of SPG7 was recently associated with resistance to the toxic effects of anticancer drugs (171). This same variant has also been reported to nominally associate with the risk of T2DM (172). Here, we report an association of this variant with risk of CAD. Our study revealed that unlike the common form of SPG7 whose cleavage is regulated, the Q688 variant is constitutively cleaved and activated. The Q688 variant rescued a dominant negative form of AFG3L2. Moreover, the Q688 SPG7 variant increased ROS production, promoting cell proliferation and lowering endothelial nitric oxide bioactivity. Our study provides a novel regulatory mechanism linking mitochondrial matrix quality control to mROS production.

Experimental procedures

Genome-wide association studies

All participants gave written informed consent according to study protocols approved for each of the 12 GWAS as described extensively in the CARDIoGRAM study (173). GWAS and all other experimental procedures are provided in detail in the Supplemental Experimental Procedures.

Cell culture, Plasmid constructs, and Transfection

Details are provided in the Supplemental Experimental Procedures.

Yeast complementation assay

Studies in S. cerevisiae were carried out as described previously by Bonn et al. (2010) and Koppen et al. (2007) and as detailed in Supplemental Experimental Procedures.

Determination of mitochondrial H+-ATPase activity

Mitochondria and cytosol were isolated as described by Schauss et al. (2010). Mitochondrial H+-ATPase activity was measured by fluorescence bioluminescence (A22066; Molecular Probes), as described by Qian et al. (2004) and as detailed in the Supplemental Experimental Procedures.

In situ measurement of cellular bioenergetics

Mitochondrial bioenergetics and glycolytic flux were tested in intact cells using the Seahorse XF24 Extracellular Flux Analyzer (Seahorse Bioscience, North Billerica), as described previously (Mailloux et al., 2011) and as detailed in the Supplemental Experimental Procedures.

Immunoblot and Immunoprecipitation

Immunoblot and immunoprecipitation protocols and antibodies are described in detail in the Supplemental Experimental Procedures.

Structural Modeling of AFG3L2 and SPG7, Q688, Heterohexamer

Molecular models of AFG3L2 and SPG7 were built as described previously by Di Bella et al. (2010) and in detail in the Supplemental Experimental Procedures.

Intracellular ROS measurement

The OxiSelect ROS Assay Kit (STA-342; Cell Biolabs) was used to assay ROS activity in HEK293 cells. This is a cell-based assay for measuring activity of ROS using a cell-permeable fluorogenic probe 20, 70-dichlorodihydrofluorescein (DCFH) diacetate (DCFH-DA) that is deacetylated by cellular esterases to nonfluorescent DCFH once in the cells. DCFH is rapidly oxidized to highly fluorescent 20, 70-dichlorodihydrofluorescein (DCF) by ROS, and fluorescence intensity is proportional to the ROS levels within the cytosol. Confocal live imaging details are provided in the Supplemental Experimental Procedures.

Electron micrography

Cells were cultured on plastic coverslips, washed in PBS, fixed in 1.6% glutaraldehyde, and were embedded in LR white (Marivac). Thin sections were cut with a Leica Ultracut E ultramicrotome and counterstained with lead citrate and uranyl acetate. Digital images were taken using a JEOL 1230 transmission electron microscope at 60 kV adapted with a 2 3 2 K bottom-mount CCD digital camera (Hamamatsu) and AMT software.

BrdU staining and Fluorescence-activated cell sorting analysis

Details are provided in the Supplemental Experimental Procedures.

Mass spectrometry

Details are provided in the Supplemental Experimental Procedures.

Measurement of mitochondrial membrane potential

The fluorescent probe TMRE (Abcam; ab-113852) was used to measure mitochondrial membrane potential in cells expressing R688 or Q688, as described previously by McClintock et al. (2002).

Cytochrome oxidase assay

The determination of COX activity in isolated mitochondria was carried out using the Cytochrome c Oxidase Assay Kit according to the manufacturer's protocol (Sigma-Aldrich).

Oleate loading assay

HEK293 cells were cultured in modified Eagle's medium containing 10% fetal bovine serum supplemented with 100 mM oleate for 24 hr. Cells were stained with Nile red (Greenspan et al., 1985), and lipid droplets were visualized by fluorescence using a Zeiss AxioImager.Z1 fluorescence microscope.

Supplemental Information

Supplemental information includes Supplemental Experimental Procedures, 6 additional figures.

Results

A variant of SPG7 (Q688) associates with CAD risk

In a search for protein coding variants that associate with the risk of CAD, we identified one variant rs12960 in SPG7 in the Ottawa Heart Genomics Study (OHGS) GWAS (1542 cases and 1455 controls, $p=2.34x10^{-3}$, odds ratio (95% confidence interval) = 1.235 (1.078-1.415)). Carrying this allele forward by meta-analysis of 12 GWAS in the CARDIoGRAM consortium comprising 22,233 CAD cases and 64,764 controls, a consistent suggestive association with CAD was found with a combined association of $p=3.74x10^{-5}$, OR(95%CI)=1.076 (1.039-1.114)(Figure 1A and 1B). This variant replaces a positively charged arginine at position 688 with a neutral glutamine residue (Figure 1C) and occurs at an allele frequency of 13-15% in the European population. It is noteworthy that R688 is invariant among vertebrates and is not polymorphic in the mouse. Although the Q688 allele did not reach genome-wide significant association with CAD in our study, a survery of the literature showed that this allele associates with other clinically important phenotypes including resistance to the chemotherapeutic agent docetaxel (171) and T2DM (172). Given the pleiotropic effects of this allele, we pursued its functional characterization.

SPG7 protein processing and maturation is enhanced in individuals who carry the Q688 allele

SPG7, like AFG3L2, undergoes 2 maturation steps. Upon import into the mitochondrial matrix, the N-terminal signal peptide is cleaved by the mitochondrial processing peptidase (MPP) (102). A second proteolytic cleavage removes an additional N-terminal fragment upon assembly of SPG7 into the SPG7/AFG3L2 heterohexamer (102).

Figure 1. Q688 variant of SPG7 associates with risk of CAD and alters proteolytic processing of SPG7.

(A) Cluster of linked SNPs at the SPG7 gene genotyped in CARDIoGRAM (173). (B) Meta-analysis of 12 GWAS combining genotype and imputed SNP data from over 22,000 CAD cases and 60,000 controls suggest the SPG7 locus is associated with CAD ($p=3.74x10^{-5}$, heterogeneity, $I^2=0$).

(C) SNP rs12960 replaces the conserved arginine 688 (R688) with glutamine.

(D) PBMCs from CAD patients genotyped for rs12960 reveal increased proteolytic processing of SPG7 in Q688 homozygotes (QQ) compared to R688 homozygotes (RR) in whole cell extracts. Note the increased processing from the precursor (p) and intermediate (i) forms to the mature form (m) in a representative blot.

(E) Quantification of immunoblots, normalized to GAPDH levels, reveal an allele dosage association with the processing of SPG7. RR, (n=14), RQ, heterozygotes (n=4) and QQ, homozygotes for the Q688 allele (n=9).

(F) HAoSMCs genotyped for rs12960 also reveal increased processing to mature SPG7 in heterozygotes (RQ) compared to homozygotes for the common allele (RR) in whole cell extracts. The identifier for each donor is simplified to the last 2 digits (see Procedures for details).

(G) Mitochondria from stably transformed HEK293 cells expressing the Q688 variant show increased processing to mature SPG7 compared to cells stably expressing the common allele (R688) or non-transfected cells (NT)(n=4). AFG3L2 levels are increased in cells expressing the variant, as were the levels of PRDX3. TOM20 was used as mitochondrial loading control protein marker. Over-expression of SPG7 (mature and precursor) was not different for the Q688 and R688 isoforms (Figure S1).

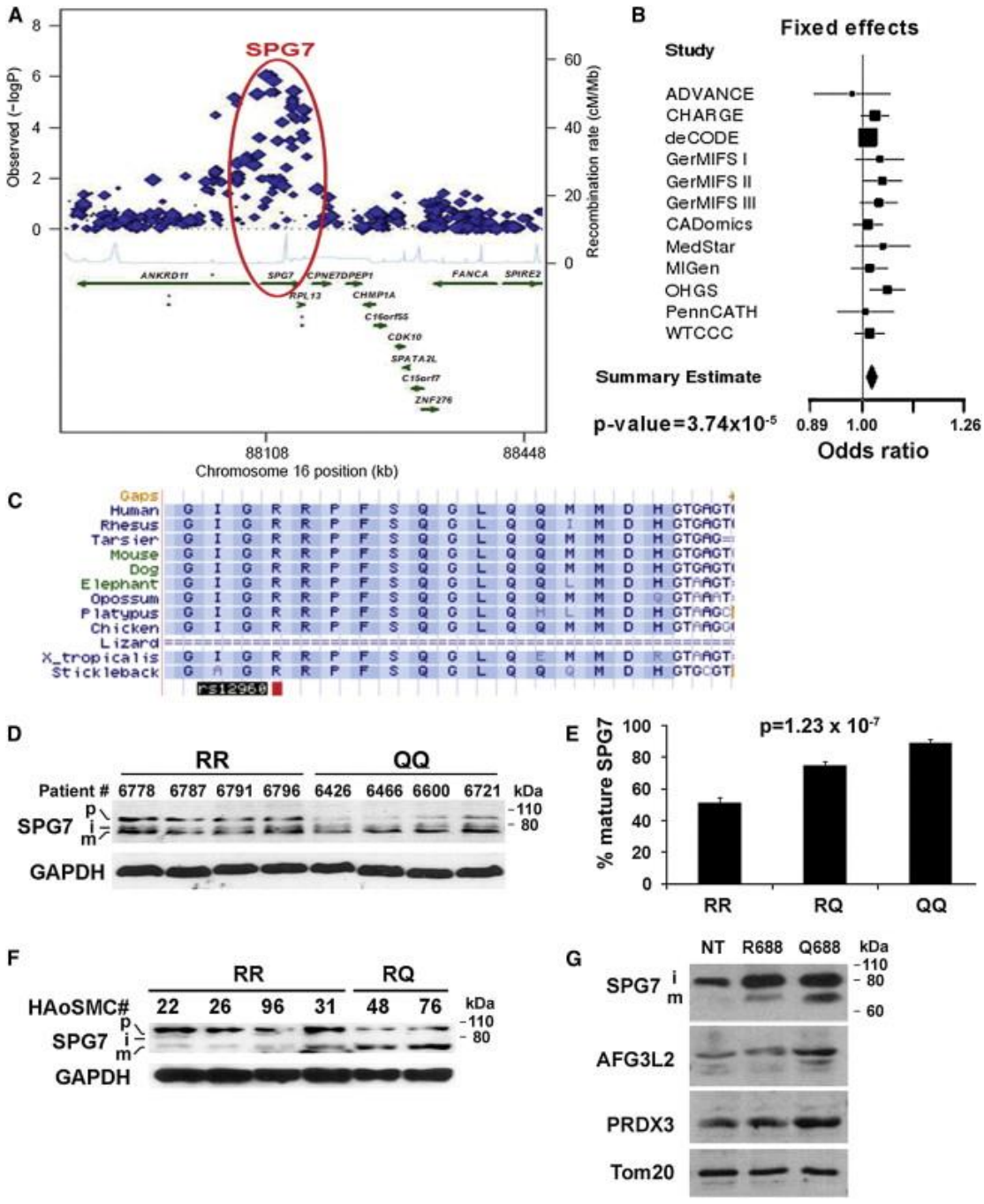
A
SPG7
Observed (−logP)
Recombination rate (cM/Mb)
ANKRD11
SPG7
CPNE7
DPEP1
RPL13
CHMP1A
FANCA
SPIRE2
C16orf55
CDK10
SPATA2L
C15orf7
ZNF276
88108
88448
Chromosome 16 position (kb)
B
Fixed effects
Study
ADVANCE
CHARGE
deCODE
GerMIFS I
GerMIFS II
GerMIFS III
CADomics
MedStar
MIGen
OHGS
PennCATH
WTCCC
Summary Estimate
p-value=3.74x10-5
0.89
1.00
1.26
Odds ratio
C
Gaps
Human
Rhesus
Tarsier
Mouse
Dog
Elephant
Opossum
Platypus
Chicken
Lizard
X_tropicalis
Stickleback
rs12959
D
RR
QQ
Patient #
6778
6787
6791
6796
6426
6466
6600
6721
kDa
SPG7
p
i
m
110
80
GAPDH
E
p=1.23 x 10-7
% mature SPG7
RR
RQ
QQ
F
RR
RQ
HAoSMC#
22
26
96
31
48
76
kDa
SPG7
GAPDH
G
NT
R688
Q688
kDa
SPG7
i
m
110
80
60
AFG3L2
PRDX3
Tom20

Whereas AFG3L2 is autocatalytic, removing its own N-terminal intermediate peptide, SPG7 is dependent on AFG3L2 to be processed to its mature form. Since SPG7 processing is necessary to activate its protease activity, we examined the pattern of SPG7 processing by immunoblot analysis of peripheral blood mononuclear cells (PBMCs) from genotyped CAD patients. Processing of the SPG7 protein to its shorter mature and proteolytically active form was highly correlated ($p=1.23x10^{-7}$ by trend test) with the gene dosage of the Q688 variant; with nearly 90% of SPG7 being fully processed in PBMCs of patients homozygous for Q688 (Figure 1D and 1E). In addition to being readily accessible from our GWAS banked blood samples, PBMCs are relevant for CAD studies since they give rise to macrophages, the inflammatory cells that accumulate cholesterol to become the foam cells of atherosclerotic lesions (39). In addition, several studies have validated changes in PBMC gene expression as sensitive indicators of CAD progression or myocardial infarction (174,175). Although the precise location of the N-terminal cleavage sites have been determined for mouse SPG7 (102), they have not been identified in human SPG7 whose N-terminal sequence is divergent from the mouse. Thus, we assigned the names precursor, intermediate and mature based on the molecular weights of the bands in the immunoblot.

Migration and proliferation of arterial smooth-muscle cells enlarge the atherosclerotic lesion (39). We obtained primary cultures of human aortic smooth muscle cells (HAoSMCs) from different individuals and found the same correlation with increased processing of SPG7 in the 2 samples heterozygote for the Q688 variant (Figure 1F). These results show that the Q688 variant is associated with increased processing of SPG7 to its proteolytically active form.

Stable HEK293 cells expressing the Q688 SPG7 variant also show increased SPG7 maturation

To verify that processing of the Q688 variant is intrinsic to this isoform and to further functionally characterize the Q688 variant, HEK293 cells were stably transfected with lentiviral vectors expressing equal levels of the common R688 allele of SPG7 or the CAD risk variant Q688 (Figure 1G and Figure S1). We chose HEK293 cells because they are easily transfected human cells homozygous for the common allele of SPG7. Isolated mitochondria showed that over-expression of the common form of SPG7 did not affect its processing whereas over-expression of the Q688 variant markedly increased processing to the mature SPG7. shRNA knockdown of SPG7 confirmed the identity of the bands as SPG7 (Figure S2). That SPG7 is largely unprocessed in untransfected HEK293 cells was noted (Figure 1G). We cannot exclude the possibility that the intermediate band is a partially processed fragment and that further N-terminal cleavage occurs. Nonetheless, these cells replicate the phenotype (i.e., increased SPG7 processing) observed in PBMCs and HAoSMCs that carry the Q688 allele. This result indicates that increased processing of Q688 SPG7 variant is not due to over-expression or to an extrinsic factor. It is noteworthy that AFG3L2 levels were elevated in cells expressing the Q688 variant but not the common form of SPG7, compared to other loading controls, suggesting that the Q688 variant might stabilize AFG3L2 in the heterohexameric complex. Also of note, Q688 cells had elevated levels of PRDX3, a mitochondrial antioxidant protein that scavenges ROS (93).

The Q688 form of SPG7 is a gain-of-function variant

Processing of SPG7 to its mature form requires AFG3L2. Therefore, we asked what effect silencing AFG3L2 would have on processing of the common and variant of SPG7.

HEK293 cells expressing the common form of SPG7 accumulated unprocessed protein with AFG3L2 silencing, as expected (Figure 2A). Surprisingly, Q688 was more efficiently processed even when AFG3L2 was knocked down.

Because the SPG7 Q688 variant is more readily processed to its proteolytically active mature form, we used a yeast complementation assay to test whether the Q688 variant could rescue a functionally inactive mutant of AFG3L2. A dominant negative mutant of AFG3L2 (E691K) that causes spinocerebellar ataxia 28 (SCA28) does not allow mAAA-deficient yeast (lacking both the SPG7 and AFG3L2 homologues) to grow on a non-fermentable carbon source (glycerol) that requires mitochondrial function (105). This mutant was not rescued by the common form of SPG7 (105), and also see Figure 2B. Strikingly, growth arrest caused by the AFG3L2 (E691K) mutation was fully rescued by the Q688 SPG7 variant (Figure 2B). Thus, the Q688 variant behaves as a gain-of-function.

Molecular modeling suggests a stabilizing influence of the Q688 variant

We built a 3D model to analyze the impact of the Q688 variant on the structure of the SPG7/AFG3L2 heterohexamer (Figure 2C). Salt bridge formation between residues at the central pore of the heterohexamer could stabilize the complex. The R688 residue in the common form of SPG7 directly faces K415 in AFG3L2 and positive charge repulsion between these two residues is likely attenuated by the spatially proximal E691 of AFG3L2 forming a salt bridge with K415. In contrast, Q688 of the variant forms a salt bridge both with K415 and E691 presumably stabilizing the heterohexamer could alter the mechanism by

Figure 2. The SPG7 Q688 variant rescues loss of function AFG3L2 mutants in yeast.
(A) Silencing of AFG3L2 prevents processing of the common form of SPG7, but not the Q688 variant, in whole-cell extracts. Quantification is shown of mature SPG7 as a percentage of total SPG7 (n = 2 experiments).
(B) Complementation studies in *S. cerevisiae* tested for the ability of the Q688 variant (R688Q) to rescue mutant forms of AFG3L2. Serial dilutions of exponentially growing yeast cultures spotted on plates show oxidative growth phenotype of *yta10*Δ*yta12*Δ cells (□□) expressing normal and mutant human AFG3L2. Respiratory competence is deduced by the ability to grow on 2% glycerol (YPG), a non-fermentable carbon source. The protease deficient variant of AFG3L2 (E575Q) was partially rescued by the Q688 variant but the inactivating variant (E691K) was restored to the same extent as cells over-expressing the wild type AFG3L2. In contrast, the common form of SPG7 did not rescue the inactivating variant of AFG3L2 (n=2 experiments, in duplicate).
(C) Model of an SPG7 Q688 and AFG3L2 heterohexamer suggests increased stability. Using the structure of the *Thermus thermophilus* AAA protease FtsH as a template (176), we modeled the effect of the Q688 variant on a heterohexameric complex with AFG3L2. An enlarged view of the surface representation of the protease face of the AFG3L2/SPG7 heterohexamer (dashed white circle) shows an enlarged wire-frame model of the protease pore. In the common form of SPG7, R688 phases directly K415, a conserved positively charged residue present in AFG3L2 whereas the Q688 residue of the variant SPG7 can form a salt bridge directly with K415.
(D) BN-PAGE immunoblot analysis of supramolecular assembly of SPG7. Blue native electrophoresis of whole cell extracts from HEK293 cells stably expressing R688 or Q688 showed higher levels of SPG7-containing complexes (~ 1 MDa) in cells expressing the Q688 variant compared to R688 expressing cells (n=4). Medium-chain acyl-CoA dehydrogenase (MCAD) was used as BN-PAGE loading control.

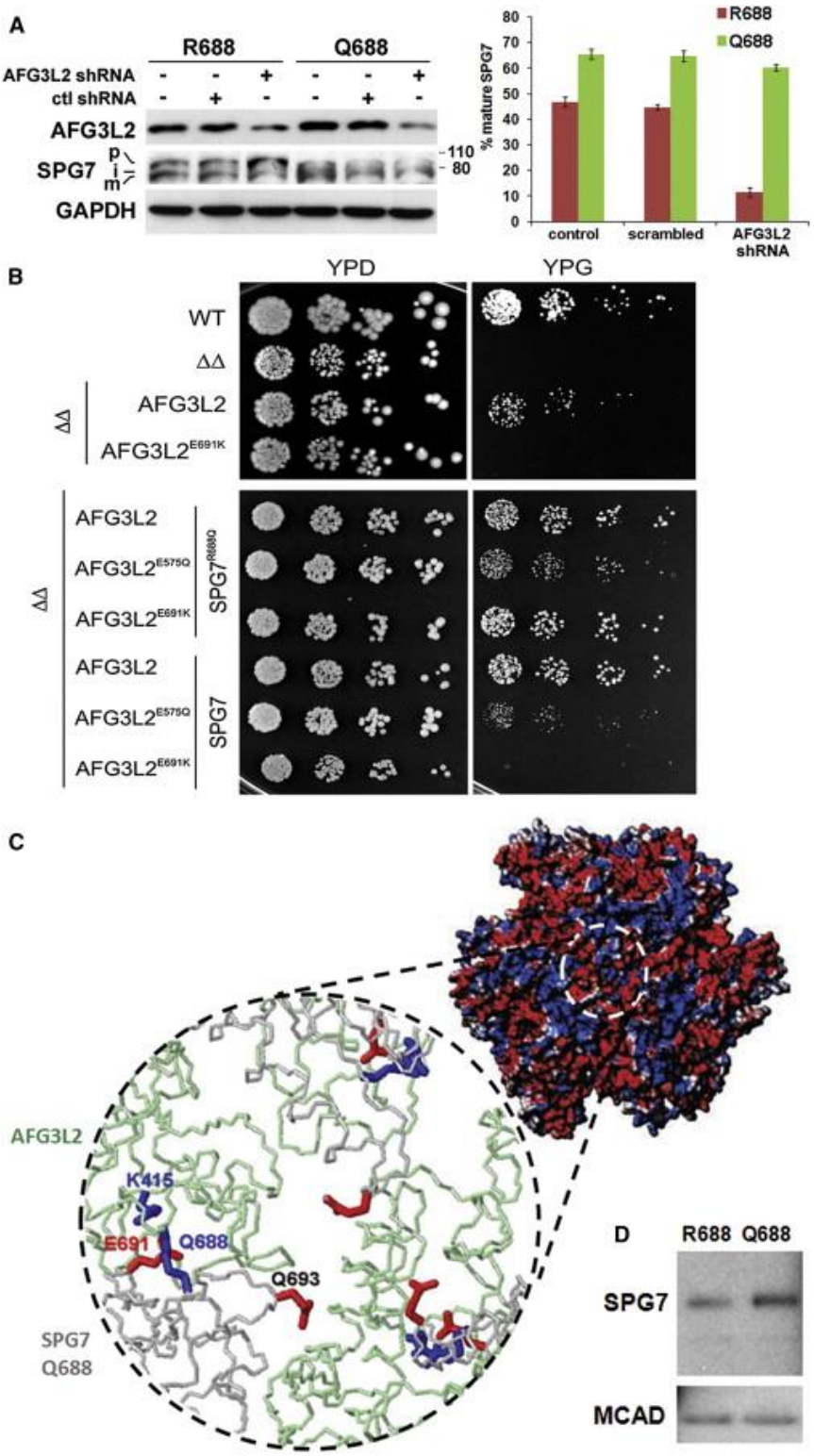
A
R688
Q688
AFG3L2 shRNA
ctl shRNA
AFG3L2
SPG7
p
i
m
GAPDH
110
80
% mature SPG7
R688
Q688
control
scrambled
AFG3L2 shRNA
B
YPD
YPG
WT
ΔΔ
AFG3L2
AFG3L2E691K
AFG3L2
AFG3L2E575Q
AFG3L2E691K
SPG7R688Q
AFG3L2
AFG3L2E575Q
AFG3L2E691K
SPG7
C
AFG3L2
K415
E691
Q688
Q693
SPG7
Q688
D
R688 Q688
SPG7
MCAD

which the protease pore functions. To test this hypothesis, we performed native gel electrophoresis (BN-PAGE) and found that cells expressing the Q688 variant had higher levels of SPG7-containing mAAA protease complexes, consistent with increased heterohexamer stabilization (Figure 2D).

The Q688 SPG7 variant increases ATP production

Since the SPG7/AFG3L2 mAAA protease requires ATP for its activity (177,178) and participates in mitochondrial ribosome assembly (99,100) and the degradation of inner membrane proteins (98), we asked whether increased processing and production of the active form of SPG7 by the Q688 variant would increase energy demands and affect ATP production. We performed immunoblot analysis of phospho-AMPK from the mitochondrial extracts of genotyped PBCMs that were used in Figure 1D as well as whole cell extracts of stably transfected cells. AMPK is a cellular energy sensor that is phosphorylated when ATP levels are inadequate and the ratio of ATP to ADP is low (179). We observed markedly reduced levels of phosphorylated AMPK in PBMCs from homozygous carriers of the Q688 variant (Figure 3A). Similarly, cells over-expressing both the common and the variant Q688 forms of SPG7 (Figure 3A) had reduced levels of phosphorylated AMPK, indicating that these cells have increased ATP production. Although we could not measure ATP production in the frozen banked PBMCs, consistent with the phospho-AMPK results, we found elevated ATP synthesis in mitochondria isolated from stable HEK293 cells over-expressing the common form of SPG7, and even more so the Q688 variant, suggesting increased respiratory activity (Figure 3C). Similarly, mitochondria from primary HUVECs transduced with lentiviral vector expressing the Q688 SPG7 variant also had elevated ATP production

Figure 3. The SPG7 Q688 variant alters mitochondrial bioenergetics.
(A and B) Immunoblot analysis showed that phospho-AMPK levels are markedly lower in whole cell extracts of PBMCs from CAD patients homozygous for the Q688 variant (A) and in HEK293 cells stably expressing the Q688 variant (B) (n=3).
(C and D) ATP synthesis was elevated in stably transfected HEK293 cells (C) and in lentiviral-transduced HUVECs (D) expressing Q688. ATP synthesis was measured by a luciferase assay using isolated mitochondria (n=6). *$p<0.001$ compared to control; **$p<0.001$ compared to R688.
(E and F) Stoichiometry of complex IV subunits is altered in mitochondrial extracts of PBMCs homozygous for the Q688 variant (E) or in whole cell extracts of HEK293 cells over-expressing Q688 (F). Levels of Mrpl32 were increased in cells expressing the Q688 variant, indicated increased processing of this ribosomal subunit of mitochondria. However, expression of COX2 was not coordinately upregulated with COX1, COX3, and COX4 in cells expressing the Q688 variant. GAPDH was used as a loading control. Proteins were quantified by densitometry, (n=3), *$p<0.05$.
(G) Cytochrome c oxidase (COX) activity was elevated in isolated mitochondria of HEK293 cells over-expressing the Q688 variant. (n=3 experiments).
(H) Electron micrographs revealed increased numbers of mitochondria in cells expressing the Q688 variant compared to NT cells or cells expressing the common form of SPG7. Scale bar = 2 μm. Quantification of mitochondrial density (mitochondria/ μm^2 of cytoplasm) was obtained by counting mitochondria (white arrows) from ten individual cells per genotype. Means ± SEM. *$p<0.001$.

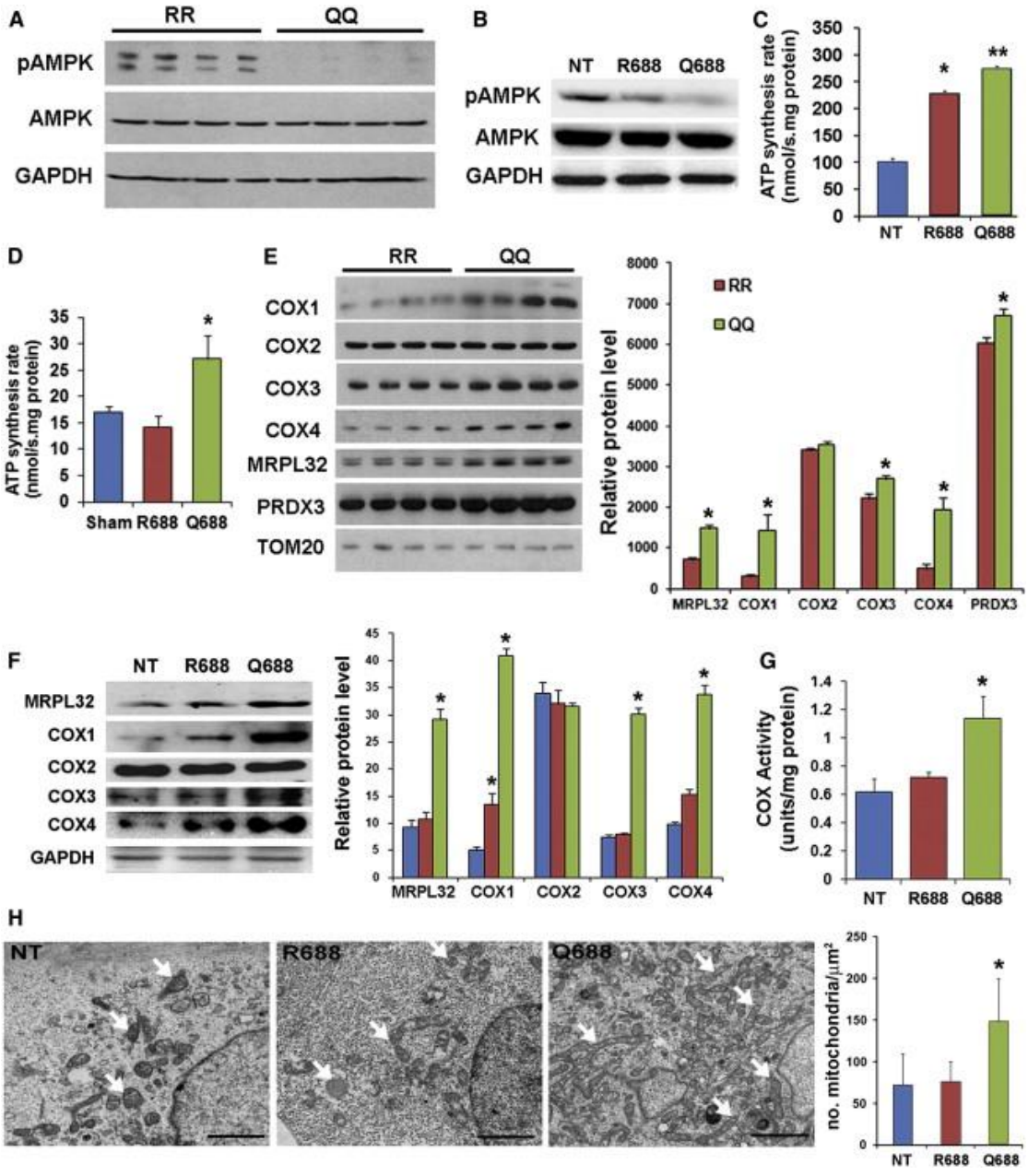
A
RR
QQ
pAMPK
AMPK
GAPDH
B
NT
R688
Q688
pAMPK
AMPK
GAPDH
C
ATP synthesis rate (nmol/s.mg protein)
NT
R688
Q688
D
ATP synthesis rate (nmol/s.mg protein)
Sham
R688
Q688
E
RR
QQ
COX1
COX2
COX3
COX4
MRPL32
PRDX3
TOM20
Relative protein level
MRPL32
COX1
COX2
COX3
COX4
PRDX3
F
NT
R688
Q688
MRPL32
COX1
COX2
COX3
COX4
GAPDH
Relative protein level
G
COX Activity (units/mg protein)
H
NT
R688
Q688
no. mitochondria/μm²

(Figure 3D), although HUVECs transduced with the common form (R688) did not have increased ATP production, despite expressing similar levels of SPG7 (data not shown). Uninfected HUVECs were homozygous for the common allele.

The Q688 SPG7 variant Alters the stoichiometry of components of the electron transport chain and proton leak from fatty acid oxidation

The mitochondrial ribosome protein Mrpl32 is required for the de novo synthesis of mitochondrially encoded respiratory chain subunits and is a natural target of the mAAA protease (99,100). Upon expression in yeast, loss-of-function mutations in AFG3L2 impair processing of the Mrpl32 precursor leading to of respiratory chain deficiencies (60,105).

Almajan et al. (2012) observed decreased levels of mature Mrpl32 in the absence of the m-AAA protease in AFG3L2-deficient cells (99). The increased production of the active form of SPG7 by the Q688 variant was expected to have the opposite effect. Indeed, we found that Mrpl32 processing is enhanced in PBMCs homozygous for the Q688 allele (Figure 3E) as well as in cells expressing the Q688 variant (Figure 3F), indicating increased activity of the m-AAA protease. Surprisingly, although the mitochondrially encoded COX1 and COX3, as well as the nuclear encoded COX4 subunits of complex IV were elevated in cells over-expressing the Q688 variant, COX2 levels were not affected (Figure 3E and F). Furthermore, despite COX2 levels not being increased, cytochrome c oxidase activity was elevated in isolated mitochondria expressing the Q688 variant but not the common form of SPG7 (Figure 3G). Electron microscopy revealed an increased number of mitochondria in cells expressing the Q688 variant (Figure 3H), providing an explanation for elevated ATP production in these cells.

The effect of over-expressing the common and Q688 variant of SPG7 on bioenergetics was further assessed in living cells using a SeaHorse analyzer. Cells were fed with glutamine and pyruvate, substrates of the Krebs cycle that generates nicotinamide adenine dinucleotide required for oxidative phosphorylation and ATP production. Cells overexpressing either the common or variant Q688 SPG7 had an increased resting oxygen consumption rate (OCR) in comparison to nontransfected cells (Figure 4A) and increased carbonilcyanide p triflouromethoxyphenylhydrazone (FCCP)-stimulated OCR (Figure S3B). Of note, subtracting the proton leak-dependent respiration from resting respiration reveals that cellular respiration associated with ATP synthesis is higher in Q688-expressing cells (Figure S3C). These results agree with the increased ATP synthesis measured in isolated mitochondria. We next determined the contribution of resting respiration towards aerobic ATP synthesis, as an index of energy efficiency and found that a higher proportion of resting respiration was used to support aerobic ATP synthesis in cells expressing the Q688 variant (Figure 4B). No difference in proton leak-dependent OCR or glycolytic rate was observed between non-transfected, and stably transfected cells expressing either the common or Q688 form of SPG7 (Figure 4C). Also, it is important to note that no difference in resting, proton leak-dependent or maximal respiration was observed in these cells provided with the standard Seahorse glucose-supplemented incubation medium (data not shown). These results indicate that over-expression of the common or the Q688 variant SPG7 does not cause cell stress (180).

Next, we measured the bioenergetics of cells supplied with oleate, a non-fermentable carbon source that requires oxidative metabolism (Figure 4D-4F). Intriguingly, no difference in resting respiration was observed between non-transfected cells and cells

Figure 4. Effect of SPG7 Q688 variant on cellular bioenergetics measured in living cells.
Cells were either fed pyruvate (A and C) or oleate (D and E) as substrates.
(A) Resting OCR, is elevated in cells expressing the common and variant (Q688) form of SPG7 when fed the TCA cycle substrate pyruvate (n=4)
(B) Cells expressing the Q688 variant fed pyruvate show an elevated contribution of resting respiration to the aerobic synthesis of ATP (n=4) (see **Figure S1** for details).
(C) Proton leak dependent OCR was not affected by over-expression of the SPG7 common or variant forms.
(D) A higher percent contribution of resting OCR to ATP synthesis was observed in cells expressing the Q688 variant when fed oleate (n=4).
(E) The contribution of resting respiration to aerobic synthesis of ATP was suppressed by over-expression of the R688 form of SPG7 but was elevated by over-expression of the Q688 variant. (F) Proton leak-dependent OCR in cells expressing the Q688 variant was suppressed. (n=4) (see **Figure S1** for details).
In (A)-(F), mean±SEM.
(G) Cells expressing the Q688 variant accumulate less fatty acid, as indicated by Nile red fluorescence, after 24 hr loading with 100 mM oleate. Scale bar, 50 μm.
*$p < 0.05$; **$p < 0.01$.

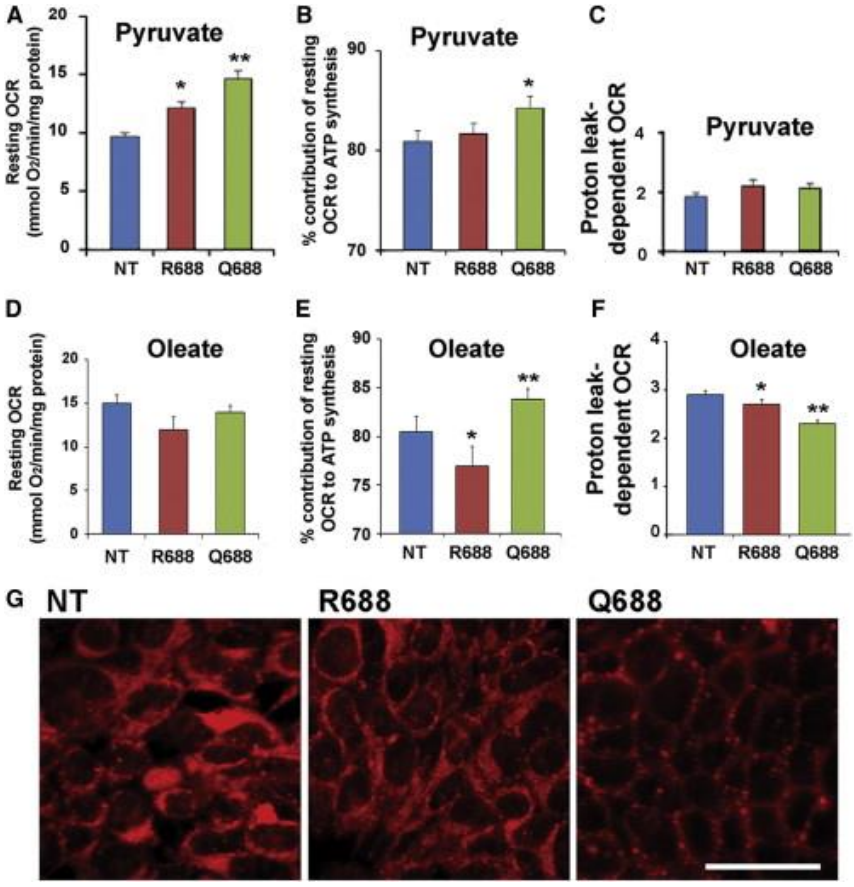
A
Pyruvate
Resting OCR (mmol O2/min/mg protein)
20
15
10
5
0
*
**
NT
R688
Q688
B
Pyruvate
% contribution of resting OCR to ATP synthesis
90
80
70
*
NT
R688
Q688
C
Pyruvate
Proton leak-dependent OCR
4
2
0
NT
R688
Q688
D
Oleate
Resting OCR (mmol O2/min/mg protein)
20
15
10
5
0
NT
R688
Q688
E
Oleate
% contribution of resting OCR to ATP synthesis
90
85
80
75
70
*
**
NT
R688
Q688
F
Oleate
Proton leak-dependent OCR
4
3
2
1
0
*
**
NT
R688
Q688
G
NT
R688
Q688

expressing either the R688 or Q688 variant (Figure 4D). FCCP- stimulated respiration was lower in cells expressing the R688 and the Q688 form of SPG7 (Figure S4B) whereas no difference in glycolytic rate was observed (Figure S4C). However, cells over-expressing the Q688 variant form of SPG7 contributed a larger proportion of oxygen consumption to produce ATP from oleate (Figure 4E). Consistent with this finding, proton leak-dependent respiration was markedly reduced for the Q688 expressing cells (Figure 4F). Because proton leak buffers cellular ROS (181), this suggest reduced ROS-buffering capacity with oleate. Next, we loaded cells with oleate and observed fewer fat droplets in cells expressing the Q688 variant (Figure 4G). Together, these results show higher fatty acid consumption by β-oxidation and reduced proton leak in cells expressing the Q688 variant, predicting higher ROS production in these cells.

The Q688 SPG7 variant increases mROS levels

Altered ETC protein stoichiometry has been associated with elevated ROS release from mitochondria (182). Furthermore, cells expressing the Q688 variant contributed a larger proportion of mitochondrial respiration to fatty acid oxidation, a known source of ROS (183). We then visualized mROS production using the vital dye MitoSox Red by fluorescence microscopy and found that HEK293 cells expressing the Q688 variant had markedly elevated ROS production compared to those expressing the common allele (Figure 5A). In addition, we also used the conversion of dihydroethidium to ethidium that accumulates in the nucleus of stable HEK293 cells actively producing ROS and confocal time-lapse fluorescent image reconstructions further confirmed that ROS production was mitochondrial by the colocalization of hydroethidium (Het; Figure 5A, red) with mitotracker

Figure 5. The SPG7 Q688 variant increases mROS production and cellular proliferation.
(A) Mitochondrial ROS was visualized using MitoSox (red) and mitochondria were visualized using Mitotracker (green). Scale bar, 20 μm.
(B and C) Intracellular ROS measured by DCF fluorescence were highly elevated in HEK293 cells (B) as well as in lentiviral vector-transduced HUVECs (C) expressing the Q688 variant (n = 3 experiments).
(D) Mitochondrial membrane potential measured using the TMRE fluorescent probe showed higher membrane potential in cells expressing the Q688 variant (n=4 experiments).
In (B)–(D), mean ± SEM.
(E) Immunoblot analysis of whole-cell extracts shows that PBMCs homozygous for the Q688 variant have activated eNOS, as revealed by dephosphorylation of threonine 495 (peNOS-Thr495), and increased levels of TFAM.
(F) Basal and hypoxia-induced (1.5% O2 for 4 hr) HIF1a levels are higher in cells expressing the Q688 variant (n = 4 experiments).
(G) FACS analysis of BrdU incorporation of synchronized stable HEK293 cells showed increased proliferation of cells expressing the Q688 variant (n = 2 experiments).
(H) Immunoblot analysis revealed elevated levels of cell proliferation markers (PCNA, CyclinE, Cyclin D, and p-RB) and reduced levels of cell-cycle suppressors (p27 and p21) in whole-cell extracts of HEK293 cells stably expressing the Q688 variant (n = 3 experiments). GAPDH verified protein loading..
(I) ROS scavengers NAC (10 mM) or Tiron (10 mM) restored PCNA and cyclin E levels (n = 3 experiments).

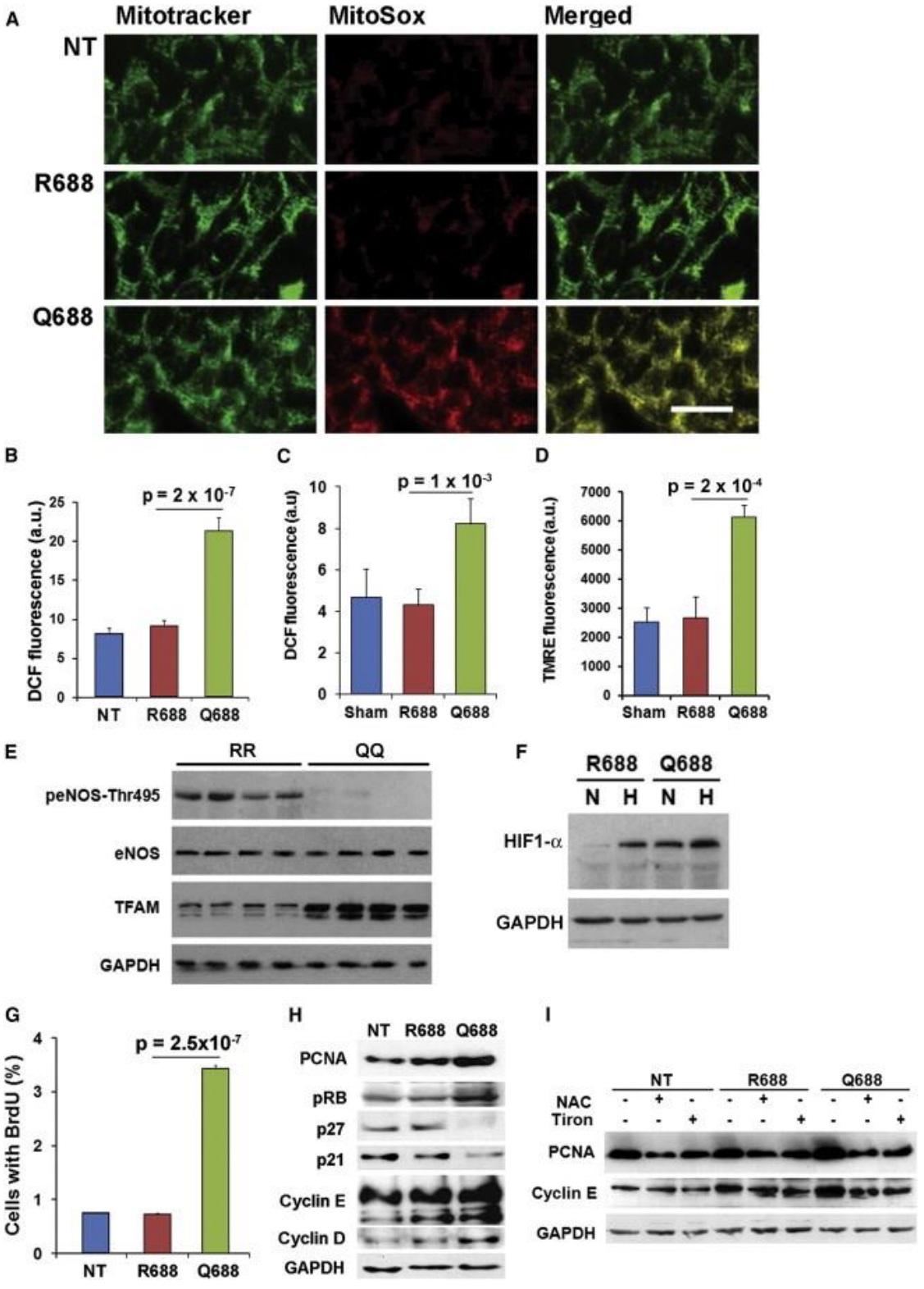
A
Mitotracker
MitoSox
Merged
NT
R688
Q688
B
DCF fluorescence (a.u.)
p = 2 x 10-7
NT
R688
Q688
C
DCF fluorescence (a.u)
p = 1 x 10-3
Sham
R688
Q688
D
TMRE fluorescence (a.u.)
p = 2 x 10-4
Sham
R688
Q688
E
RR
QQ
peNOS-Thr495
eNOS
TFAM
GAPDH
F
R688
Q688
N
H
N
H
HIF1-α
GAPDH
G
Cells with BrdU (%)
p = 2.5x10-7
NT
R688
Q688
H
NT
R688
Q688
PCNA
pRB
p27
p21
Cyclin E
Cyclin D
GAPDH
I
NT
R688
Q688
NAC
Tiron
PCNA
Cyclin E
GAPDH

(Figure 5A,green) . ROS levels were also quantified by a colorimetric assay and found to be elevated in stable HEK293 cells (Figure 5B) and in HUVECs transduced with lentiviral vector (Figure 5C) expressing the Q688 variant. Elevated levels of ROS scavenging enzyme PRDX3 in PBMCs from CAD patients homozogyous for the Q688 allele (Figure 3E) and in mitochondria from cells expressing the Q688 variant (Figure 1G) were consistent with increased mROS production. Because mitochondrial membrane potential drives mROS production (184), we measured mitochondrial membrane potential using the fluorescent dye tetramethylrhodamine ethyl ester (TMRE) and found that it was elevated in cells expressing the Q688 variant (Figure 5D). ROS production activates endothelial nitric oxide synthase (eNOS) activity, in part by the dephosphorylation of a constitutively phosphorylated inhibitory threonine at position 495 (peNOS-Thr495) (185). PBMCs homozygous for the Q688 variant had markedly reduced peNOS-Thr495 levels (Figure 5E). A similar result was observed in HUVECS transduced with lentiviral vector expressing the Q688 variant (Figure S5). eNOS activation promotes mitochondrial biogenesis (186), and the levels of the mitochondrial transcription factor A (TFAM) were elevated in PBMCs homozygous for the R688 SPG7 variant (Figure 5E), consistent with increased mitochondrial density observed by electron microscopy in cells over-expressing the R688 variant (Figure 3H). Consistent with the reported effects of mROS and TFAM to stabilize HIF1α (187), we found that cells expressing the Q688 variant had elevated basal HIF1α levels and increased activation of HIF1α in response to hypoxia (Figure 5F).

The Q688 SPG7 variant increases cell proliferation

Increased mROS production promotes cell proliferation (166); a hallmark of atherosclerotic lesions (188). Given that HEK293 cells expressing the Q688 variant had increased ROS production, we tested whether cell proliferation was also increased. Flow cytometry after BrdU incorporation showed that HEK293 cells expressing the Q688 variant had a 4 fold increase in cell proliferation (Figure 5G). Markers of cellular proliferation, like the Proliferating Cell Nuclear Antigen (PCNA), cyclin E and cyclin D and the level of phosphorylated retinoblastoma (pRB) were all elevated, whereas the cyclin-dependent kinase inhibitors p27 and p21 were suppressed in these cells (Figure 5H). Addition of the ROS scavengers N-acetyl cysteine (NAC) and Tiron blunted the elevation of PCNA and cyclin E levels (Figure 5I). Thus, these results are consistent with the notion that mROS production controls cellular proliferation (166).

Forskolin blocks processing of the R688 SPG7 but not the Q688 variant

Next, we asked whether the degree of SPG7 processing might be regulated by the metabolic state, like fasting, when PKA is activated (189). Activation of PKA by forskolin in vitro markedly inhibited processing of the common form of SPG7 but had little effect on processing of the Q688 variant (Figure 6A). This indicates that SPG7 processing is dynamically regulated. To identify a mechanism whereby PKA activation might control SPG7 processing by AFG3L2, we consulted the PhosphositePlus databases of curated tandem mass spectrometry sequences (http://www.phosphosite.org/). AFG3L2 contains 3 phosphorylated residues, Y179 (identified in 12 independent reports) in the Fts-

Figure 6. SPG7 processing is controlled by AFG3L2 phosphorylation.
(A) Forskolin (FSK) blocks processing of the R688 common form but not the Q688 variant of SPG7. Quantitation of immunoblots (10% acrylamide) showed a significant inhibition of R688 SPG7 processing (n = 3 experiments). Mean ± SEM.
(B) AFG3L2 is phosphorylated at three residues (Y179, T560, and S634), as reported by multiple mass spectrometry studies (http://www. phosphosite.org/).
(C) Forskolin increases tyrosine phosphorylation of AFG3L2. Immunoblots (10% acrylamide) of
immunoprecipitated AFG3L2 protein from wholecell extracts were probed with phosphotyrosine, phosphothreonine, and phosphoserine antibodies. GAPDH antibody confirmed specificity of AFG3L2 immunoprecipitation (Figure S6).
(D) Tyrosine 179 of AFG3L2 regulates SPG7 processing. Site-directed mutagenesis of c-mytagged WT AFG3L2 (WT) converted tyrosine 179 to a pseudophosphorylated aspartic acid (Y > D) or to a nonphosphorylatable phenylalanine (Y > F). Immunoblots (6% acrylamide) of whole-cell extracts were probed with antibodies to SPG7, c-myc (to detect overexpressed AFG3L2), and GAPDH to control for loading.

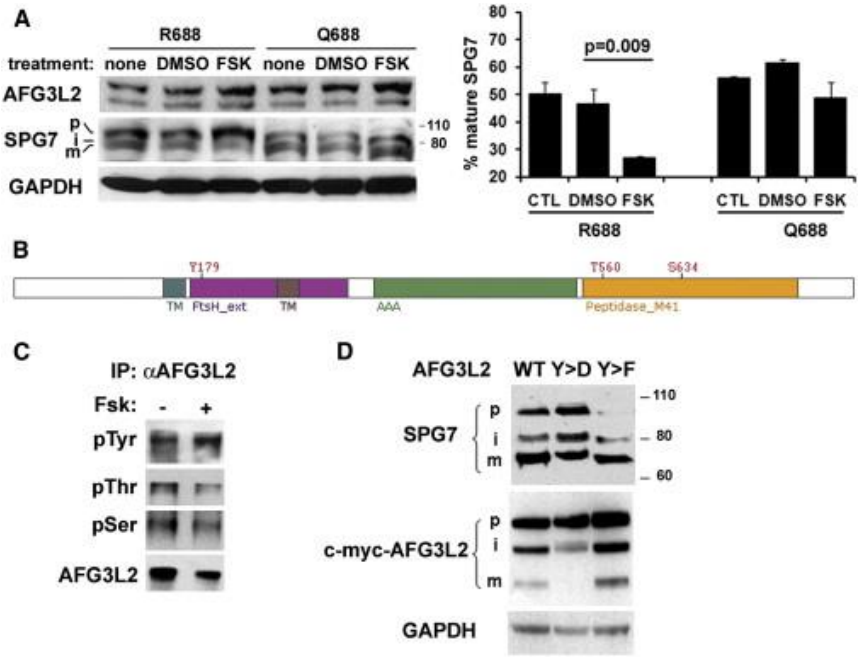
A
R688
Q688
treatment: none DMSO FSK none DMSO FSK
AFG3L2
SPG7
p
i
m
GAPDH
110
80
% mature SPG7
p=0.009
CTL DMSO FSK
CTL DMSO FSK
R688
Q688
B
Y179
T560
S634
TM
FtsH_ext
TM
AAA
Peptidase_M41
C
IP: αAFG3L2
Fsk: - +
pTyr
pThr
pSer
AFG3L2
D
AFG3L2 WT Y>D Y>F
SPG7
p
i
m
c-myc-AFG3L2
p
i
m
GAPDH
110
80
60

homology external (FtsH-ext) domain facing the mitochondrial inter-membrane space, and T560 (1 report) and S634 (2 reports) on the matrix side (Figure 6B).

PKA activates an unknown tyrosine kinase in the inter-membrane space (190,191). A phosphopeptide of SPG7 phosphorylated at Y195 has been deposited in the PhosphositePlus database but we were unable to confirm this finding by immunoprecipitation or mass spectrometry (data not shown). We therefore examined the possibility that phosphorylation of AFG3L2 regulates SPG7 processing. Immunoprecipitation of AFG3L2, followed by immunoblot analysis using phosphorylated residue-specific antibodies revealed that Forskolin markedly increased phosphorylation of tyrosine residues (Figure 6C). To test whether Y179 of AFG3L2 affects processing of SPG7, we used site-directed mutagenesis to convert this residue to aspartic acid (Y>D, a mutation bearing a negative charge that mimics phosphorylation) or to phenylalanine (Y>F, a residue that cannot be phosphorylated) and tested the effect of over-expression of wild type and mutant c-myc-tagged AFG3L2 proteins on endogenous SPG7 processing (Figure 6D). The AFG3L2 Y179D mutation caused accumulation of the intermediate form of SPG7 compared to the wild type form of AFG3L2. In contrast, the phosphorylation dead AFG3L2 mutant Y179F, stimulated SPG7 processing. Processing of AFG3L2 was also affected similarly by these mutations, suggesting that phosphorylation of Y179 affects processing of both AFG3L2 and SPG7.

In Figure 7 we propose a model whereby Tyr179 phosphorylation of AFG3L2 controls processing of the common form of SPG7 (as well as AFG3L2) to regulate mitochondrial bioenergetics and mROS production. The Q866 variant appears to escapes the AFG3L2-dependent control mechanism because it is efficiently processed independently of

Figure 7. Model of SPG7 processing.
SPG7 preprotein is imported from the cytosol through the intermembrane (IM) space to the mitochondrial matrix, where the signal peptide is cleaved by the mitochondrial matrix peptidase (MPP). SPG7, like its partner AFG3L2, is somehow anchored through 2 transmembrane (TM) domains to the inner mitochondrial membrane, with the protease domain facing the matrix. Upon co-assembly, tyrosine phosphorylation of AFG3L2 prevents processing of SPG7. Mature SPG7 protein is processed when AFG3L2 is not phosphorylated. The Q688 variant escapes this regulatory process.

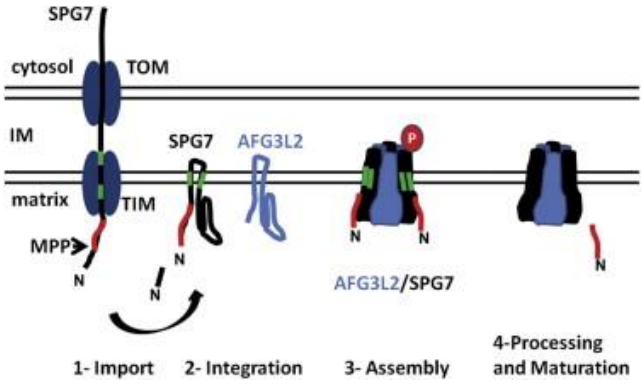
SPG7
cytosol
TOM
IM
matrix
TIM
MPP
N
N
SPG7
AFG3L2
N
N
P
N
N
AFG3L2/SPG7
N
1- Import
2- Integration
3- Assembly
4-Processing
and Maturation

AFG3L2 phosphorylation at Y179 and maintains mitochondria in an energetically activated state.

Discussion

We have characterized Q866 as gain-of-function variant of SPG7 that causes an increased activity of SPG7-containing mAAA proteases. The SPG7 Q866 variant is efficiently processed independent of phosphorylation of AFG3L2 at Y179, which inhibits processing of SPG7. This increases m ROS production, mitochondrial biogenesis and cellular proliferation. Our data showed that the Q688 mutant of SPG7 is a gain-of-function variant that rescues a dominant negative form (E691K) of AFG3L2 associated with SCA28. It will be interesting to determine whether individuals who carry the SCA28 mutation of AFG3L2 (E691K) (105) and also carry the Q688 variant have an attenuated phenotype relative to individuals homozygous for the common form of SPG7. This could account for the variable penetrance reported for this dominant form of hereditary ataxia (192).

The association of the Q688 allele with CAD risk at a level that does not reach genome-wide significance ($p=3.74x10^{-5}$) is indicative of the pleiotropic effects of this allele. Indeed, a similar association was reported with the risk of type 2 diabetes in the DIAGRAM consortium (Stage 2, OR=1.05 (1.02-1.08), p=0.003), n=75,063) (172). Mitochondrial dysfunction and mROS production have been implicated in T2DM (162). A limitation of our study is the lack of data on T2DM in the CARDIoGRAM cohorts. However, because diabetes was an exclusion criterion in the OHGS, the association with CAD and T2DM are likely to be independent.

A recent pharmacogenetic study found that prostate cancer patients with the Q688 variant are more resistant to the toxic effects of anticancer drugs (171). It is likely that the increased ability to detoxify xenobiotic compounds is a direct effect of the Q688 variant. This could explain how this allele has become fixed in the human population. Genes involved in detoxifying xenobiotics evolve more rapidly (193), presumably because they offer a strong selective advantage. The Q688 allele shows a similar fequency in Asians as in Europeans (11-16%), but is rare in black Africans. Although a variant that protects against toxic xenobiotic compounds would confer immediate advantage, the long term consequence of this gain of protease function may be to increase susceptibility to diseases of ageing like CAD and T2DM.

A key finding of our study is that cleavage and activation of SPG7 is a regulated process that can be inhibited by a PKA-like activity. The ability to inhibit the mAAA protease by blocking the cleavage and activation of SPG7 allows cells to regulate mitochondrial protein synthesis and degradation to meet their metabolic needs. Because PKA is a serine/threonine kinase, our data suggest that PKA indirectly inhibits SPG7 processing by activating a tyrosine kinase in the inter-membrane space that phosphorylates AFG3L2 at tyrosine 179. Tyrosine kinase activity in mitochondria is located in the inter-membrane space (194) and several studies have shown that mitochondrial tyrosine kinase activity modulates cellular metabolism (190,191,195). Although the PhosphoSite repository documents phosphorylation of Y195 in SPG7, we were unable to confirm this finding, suggesting that regulation of SPG7 processing takes place largely through its interaction with AFG3L2. Consistent with this notion, we found that over-expression of a mutant form of AFG3L2 that cannot be phosphorylated at Y179 (Y179F) promoted SPG7 (and AFG3L2) processing. It

will be important in future studies to identify the tyrosine kinase and phosphatase that regulate AFG3L2 Tyr179 phosphorylation and SPG7 processing. The Q688 variant is insensitive to AFG3L2-mediated regulation; this could result for its stabilized interaction with AFG3L2 at the protease pore complex, or if this variant of SPG7 is independent of AFG3L2 (i.e., autocatalytic).

The presence of a constitutively activated mAAA protease in cells expressing the Q688 variant of SPG7 likely leads to an altered stoichiometry of ETC complexes and increased mROS production. Complex IV stoichiometry was similarly altered in PBMCs from patients with CAD homozygous for the Q688 allele as in HEK293 cells over-expression the Q688 variant, indicating that this is a natural and direct consequence of the Q688 allele. Cellular bioenergetics were affected differently by over-expression of the R688 and Q688 variant of SPG7, in particular in the presence of oleate as a substrate of β-oxidation, a known source of mROS (183). We observed that cells expressing the Q688 variant required a larger proportion of oxygen consumption to produce ATP from oleate and accumulated less oleate in lipid droplets, consistent with increased fatty acid utilization. In addition, these cells displayed reduced proton leak when fed oleate, consistent with reduced ROS buffering capacity accounting for elevated mROS levels.

Mitochondrial biogenesis was increased in cells expressing the Q688 variant. The mitochondrial count was elevated in electron micrographs and expression of TFAM was also elevated in these cells. We observed that expression of Tom20, the mitochondrial translocase of the outer membrane, was not changed despite increased mitochondrial biogenesis. Of note, during muscle differentiation when mitochondrial biogenesis is activated, Tom20 levels

remain relatively unchanged (196). Thus, increased mitochondrial biogenesis is not necessarily accompanied by increased Tom20 expression.

Increased mROS production increases cell proliferation (166) and depletion of ROS by NAC induces cell cycle arrest (197). We observed increased proliferation of cells expressing the Q688 variant and the upregulation of cyclin E and PCNA were reversed by NAC or Tiron, providing direct evidence that mROS drives proliferation in these cells. The altered bioenergetics of mitochondria expressing Q688, in particular the reduced proton efflux when utilizing oleate as a substrate of fatty acid oxidation, is consistent with a reduced ability to buffer ROS leading to elevated ROS production. Furthermore, elevated mROS production associated with fatty acid oxidation (198), increased HIF1α and its associated effect on inflammation (199), and increased cell proliferation are all conditions that would promote coronary atherosclerosis.

The innate immune response is also tied to mROS production. Importantly, the bactericidal activity of macrophages is activated by Toll-like receptors 1, 2 and 4 through elevated mROS production (167). CAD has long been suspected of being linked to bacterial infections and inflammation (200). The Q688 variant, through its effect on elevating mROS production, may promote innate immunity, but at the cost of increased inflammation that contributes to CAD. That PBMCs from CAD patients homozygous for the Q688 variant showed similar elevations in PRDX3 as seen in cells over-expressing the Q688 variant is consistent with the notion that this allele might augment the inflammatory response.

To date, GWAS have identified more than 40 genetic variants contributing to the risk of CAD (201), but account for only 10% of the CAD heritability. This is due in part to the limited power of GWAS to discover CAD genetic risk variants that are pleiotropic (63).

Pleiotropy occurs when a genetic factor influences more than one physiological trait. Thus, if individuals who have these traits are included in the control group this would prevent pleiotropic genetic variants that contribute to CAD risk from reaching a level of stringent genome-wide significance ($p<5x10^{-8}$). Our discovery and functional characterization of the Q688 SPG7 variant as a potential risk factor for CAD and its pleiotropic effects supports the notion that much of the missing heritability contributing to the risk of CAD is carried by similar functionally important but pleiotropic alleles.

Acknowledgments

We thank Florian Bonn for his contribution to yeast complementation studies,Vincent Soubannier for help with confocal microscopy, and Thomas Lagace for providing oleate and Nile Red. This research was supported by a graduate scholarship from Taibah University, Saudi Arabia and a University of Ottawa Endowed Graduate Award at the Heart Institute (to N.A.M.A.), grants MOP77682 (to A.F.R.S.), MOP179197 (to H.-H.C.), and MOP82810 (to R.R.) from the Canadian Institutes of Health Research, Deutsche Forschungsgemeinschaft SFB635, C4 (to T.L.), the European Research Council AdG No. 233078 (to T.L.), and the Medical Research Council, UK U117584256 (to A.P.). This project used the UPCI Cancer Biomarkers Facility/Mass Spectrometry Platform Laboratory and was supported in part by award P30CA047904 from the National Cancer Institute, USA.

Conflict of Interest

The authors declare that there is no conflict of interest.

Supplemental experimental procedures

Genome-wide association studies

DNA samples were genotyped on single nucleotide polymorphism (SNP) microarrays covering the human genome. Our study followed the STREGA guidelines in reporting on genetic association (202). Within each study, quality control of the data was performed. This includes a check of consistency of the given alleles across all studies, deviation for Hardy-Weinberg equilibrium in the controls, the minor allele frequency, and the SNP call rate. Population stratification was evaluated using either the genomic control or a principal components analysis approach. The association between CAD (MI) and genotypes was carried out under an additive model adjusted for age and sex. Meta-analysis was performed using fixed-effect models with inverse-variance weighting. The Cochrane's Q and I^2 statistics were also calculated to test the heterogeneity across studies. Heterogeneity was assumed if I^2>50%. Random-effect models were used for the SNPs with evidence of heterogeneity. Genotyping of the imputed rs12960 polymorphism was confirmed by PCR and sequencing using forward primer, 5'-AGT GCT GAG GAT GCT CTG TCT CG-3' and reverse primer, 5'-TTG TGT GGT AGA CCC AGG GAC TCC-3'.

Cell Culture, Plasmid constructs and Transfection

Primary HAoSMCs were obtained and cultured in smooth muscle growth medium (cat.311-500) from Cell Applications, Inc. (San Diego, CA). HAoSMCs from 6 Caucasian donors were genotyped for the SPG7 rs12960 polymorphism by PCR. Two were heterozygous for Q688 risk allele of SPG7 (#1848, #1576) and 4 homozygous (#8222, #1426, #1596, #2531) for R688 non-risk allele. Human Embryonic Kidney cells (HEK 293) were obtained from American Type Culture Collection (ATCC, Manassas, VA) and found to be

homozygous for the R688 common form of SPG7. Cells were maintained in high glucose DMEM with 20% fetal bovine serum (FBS), 100 U/ml penicillin, 100 µg/ml streptomycin. Primary human umbilical vein endothelial cells (HUVECs) were obtained and grown in endothelial cell growth media (EGM-2, CC-1362) from Lonza Group Ltd. HUVECs were homozygous for the R688 common form of SPG7.

The Q688 variant form of human SPG7 (clone BC036104) was purchased from Open Biosystems (Huntsville, AL). The common R688 form was generated by site-directed mutagenesis using the Stratagene QuickChange XL site-directed mutagenesis kit (Agilent Technologies, Santa Clara, CA). The R688 and Q688 variant SPG7 cDNA were cloned in frame into the pCMV-tag4 vetor and SPG7 (R688 and Q688) cDNAs were released from pCMV by NotI and Mlu I double digestion and then subcloned into pLEX vector (Open Biosystems) for stable transfections of HEK293 cells or to generate lentiviral vectors for transduction of HUVECs. The wild type form of human AFG3L2 (C-terminal Myc-DDK-tagged) was purchased from ORIGENE (Cat# RC209058, NM_006796). The Y179D and Y179F mutants of AFG3L2 were generated by site-directed mutagenesis using the Stratagene QuickChange XL site-directed mutagenesis kit (Agilent Technologies, Santa Clara, CA). All constructs were verified by sequencing.

Cells were transfected with linearized pLEX-SPG7 constructs using lipofectamine 2000 (Invitrogen, Carlsbad, CA) according to the manufacturer's instructions. Twenty four hours after transfection, cells were passaged at a 1:20 dilution into fresh growth medium (DMEM containing 20% fetal bovine serum) with 2 µg/ml puromycin to select for positive clones. Medium containing 2 µg/ml puromycin was changed every 2 days for 4 weeks. After selection, stable HEK293 cells bearing the R688 or Q688 variant of SPG7 were maintained

in DMEM containing 20% fetal bovine serum. For the mitochondrial fusion experiments, cells were transiently transfected with pQCXIP-N-Venus-Z-N-Rluc using lipofectamine 2000. Mdivi-1 (sc-215291A, Santa Cruz biotechnology) was used at a concentration of 50 µM. shRNA to AFG3L2 (sc-72464-SH), SPG7 (sc-62755-SH) and control shRNAs were purchased from Santa Cruz biotechnology. ROS scavengers NAC (A7250, Sigma) and Tiron (172553, Sigma) were used at a concentration of 10 mM.

Bromodeoxyuridine (BrdU) staining and FACS analysis.

HEK293 cells plated at equal densities were grown for 48 hours at 37°C, synchronized for 24 hours by serum withdrawal and released with fresh media containing serum. Cells were pulse-labeled with 10 µM bromodeoxyuridine (BrdU) for 45 minutes and harvested for fluorescence-activated cell sorting (FACS) analysis. Unlabeled cells were included as a negative control. Live cell umbers were determined by trypan blue exclusion. 1 x 10^6 BrdU-pulsed cells were collected and stained with anti-BrdU-FITC conjugated antibody using the BrdU Flow kit (559619, BD Pharmingen™) according to the manufacturer's instructions. Instead of 7-amino-actinomycin D (7-AAD) we added 10 mg/ml propidium iodide (PI) to label the nuclei. Stained cells were acquired on a CyAn ADP analyser (Beckman Coulter) and analyzed using Kaluza® software (Beckman Coulter).

Immunoblot analyses and Immunoprecipitation.

Duplicate blood samples were collected in EDTA-tubes and centrifuged for 10 minutes at 3000 rpm to obtain the buffy coat containing peripheral blood mononuclear cells. DNA was purified and genotyped by Affymetrix SNP microarrays from one aliquot, as described previously (203). From the second aliquot, buffy coat protein was extracted in RIPA buffer (4.25 mM Tris, pH8.0, 135 mM NaCl, 1% IGEPAL CA-630, 1% SDS 0.5%

deoxycholate) in the presence of protease and phosphatase inhibitors (Roche Molecular Systems, Branchburg, NJ).

Blue Native-PAGE. Cell extracts were solubilized in digitonin lysis buffer and 40 µg of cell protein extracts were loaded on a 3-12% polyacrylamide gradient gel. Precast gels and buffers were purchased from Lifetechnologies (Invitrogen). BN-PAGE and immunoblotting was performed as described previously (204). MCAD (medium-chain acyl-CoA dehydrogenase) was used as a loading control with a native molecular mass of about 230 kDa.

Antibodies to cyclinD1 (#2926) were from Cell Signaling, to PCNA (sc-56), c-Myc (sc-789), MCAD (sc-271931), TNF1-□ (sc-13515), p21(sc-6246), p27(sc-1641), COX1 (sc-58347), COX2 (sc-65239), COX4 (sc-59348), GAPDH (sc-59540), TFAM (sc-10412) and □-tubulin (sc-23948) from Santa Cruz Biotechnology were used 1:1000 dilutions in blocking solution (5% non-fat milk). Rabbit SPG7 (sc-135026), AFG3L2 (sc-84687), cyclin E (sc-481) antibodies were from Santa Cruz Biotechnology, PRDX3 (ab16751) and COX3 (ab81180) from Abcam, p-RB (ser799, #93015), p-AMPK (Thr172, #2531) eNOS (#5880) and p-eNOS (thr495, #9574) from Cell Signaling, and hMRPL32 (c14071) from Assay Biotechnology were used at 1:5000 dilution. Goat mouse IgG (HAF007, R&D Systems) and goat rabbit IgG (product #31460, Piercenet) were diluted in 1:15,000 in blocking solution before application.

Immunoprecipitation of AFG3L2 from HEK293 cells was carried out using the rabbit antibody and protein A/G Sepharose (SantaCruz Biotechnology) as per manufacturer's instructions. Immunoblot analysis was carried out using phospho-tyrosine (136600),

phospho-threonine (718200) and phospho-serine (618100) were purchased from Zymed (Life Technologies, Inc) using extracts from cells treated or not with 5 µM Forskolin for 8 hours.

Confocal live imaging

Mitochondrial ROS production was visualized using the MitoSOX™ Red superoxide indicator (M36008, Molecular Probes) and also using the oxidation-sensitive dye HEt. Living cells stably expressing the Q688 and R688 variant and non transfected cells (NT) were grown on coverslips in 24 well plates then incubated with 100nM MitoTracker (Green) and 5 µM MitoSOX (Red) or 5 µM HEt (Red) in the presence of 1 M HEPES buffer for 10 minutes and then were imaged using an FV1000 laser scanning confocal microscope (IX80, Olympus) equipped with a 100X objective 133 NA 1.4. All images were obtained using sequential image acquisition using the Olympus Fluoview ver. 1.7 software.

Yeast complementation assay

Studies in *S. cerevisiae* were carried out as described previously (60,168). A combination of human wild-type or mutant AFG3L2 was expressed with either R688 or Q688 variant SPG7 in a yeast strain, yta10Δyta12Δ, lacking the mAAA protease orthologues yta10 and yta12 (168). Yeast strains were grown at 28 °C on YEP medium (1% yeast extract, 2% Bacto-peptone, 2% agar for plates) or selective medium supplemented with 2% (wt/vol) glucose according to standard procedures. For complementation experiments, equal amounts of fivefold serial dilutions of cells from exponentially grown cultures were spotted onto YEP plates containing 2% (wt/vol) glucose (YPD) or 3% (vol/vol) glycerol (YPG) and incubated them at 28°C or 37 °C.

Determination of mitochondrial H^+-ATPase activity

Mitochondria and cytosol were isolated as described (205). Mitochondrial H^+-ATPase activity was measured by fluorescence bioluminescence (A22066, Molecular Probes, Burlington, ON, Canada), as described *(206).* This assay utilizes glycerol as a substrate. Mitochondria were adjusted to a protein concentration of 1 µg/µl and 10 µl of mitochondria were mixed with 90 µl of the standard reaction solution that was prepared as instructed by the kit but in the absence of ATP. Addition of ADP (Sigma, A2754) to the reaction solution triggers the conversion of ADP to ATP by H^+-ATPase of the mitochondria the intensity of the emitted light was assayed on a luminometer (Montreal-Biotech Inc., Montreal, QC, Canada) following the manufacturer's instructions. The amount of ATP in the experimental samples was calculated from a standard curve.

In situ measurement of cellular bioenergetics.

Mitochondrial bioenergetics and glycolytic flux were tested in intact cells using the Seahorse XF24 Extracellular Flux Analyzer (Seahorse Biosciences, North Billerica, MA, USA), as described previously (207). HEK293 cells were maintained in low glucose DMEM (in mM, 5 glucose, 4 glutamine, and 1 pyruvate) containing 10% FBS and 2% antibiotics-antimycotics. Cells were seeded at 50,000 cells/mL in Matrigel-coated Seahorse Tissue Culture plates and grown for 24h. Media was aspirated; cells were washed once with PBS, and then incubated for 30 min in Seahorse Incubation Medium (glucose- and HCO_3-free DMEM containing 4mM glutamine and 1mM pyruvate as respiratory substrates) at 37°C and ambient CO_2. For measurement of the contribution of fatty acids to cell bioenergetics, the Seahorse medium consisted of glucose- and HCO_3-free DMEM containing 0.1 mM oleate complexed to 0.1% w/v BSA, 1mM L-carnitine, and 4 mM glutamine. Fluorimetric sensors

enabled the measurement of O_2 consumption rate (OCR, mitochondrial bioenergetics) and extracellular acidification rate (ECAR, glycolytic flux) in the extracellular microenvironment. Following three measurement intervals of resting respiration (1 interval consists of 2 minutes mixing, 2 minutes of incubation, and 2 minutes measurement step), cells were sequentially treated with oligomycin (ATP synthase inhibitor, 0.2 μg/mL), FCCP (carbonylcyanide-p-trifluoromethoxyphenylhydrazone, a chemical proton gradient uncoupler, 2 μM), and Antimycin A (complex III inhibitor, 2 μM) to test proton leak-dependent (state 4 or nonphosphorylating) respiration, maximal respiration, and extramitochondrial respiration respectively. Total resting, proton leak-dependent, and maximal OCR values were calculated by averaging the intervals of measurement followed by correction to extramitochondrial respiration values. The percent contribution of resting respiration to aerobic ATP synthesis was calculated by subtracting the percent contribution of proton leak dependent respiration from total resting respiration. All values were expressed as mean ± SEM (unless indicated), normalized to total protein amount/well using the Bradford assay and BSA as a standard. One-way analysis of variance with Fisher's post-hoc test identified significant differences.

Structural modelling of AFG3L2 and SPG7 (Q688) heterohexamer

Molecular models of AFG3L2 and SPG7 were built as described previously (105), using the automated homology modeling server SWISS-MODEL (208) (http://swissmodel.expasy.org/SWISS-MODEL.html) and the solved structure of *T. thermophilus* FtsH (mutant G399L) (PDB: 2DHR; UniProt accession No. Q72IK4) as the coordinate template (176). The sequences were first aligned with the Clustal_X program to optimize insertions/deletions (209). The models were visualized and analyzed by the Molmol program (210).

This protein is a homohexamer which adopts a flat-cylinder-like shape (135Å diameter, 65Å height) bearing a non-crystallographic 3-fold rotational symmetry. The cylinder is divided into two disks. The lower disk, that covers the sequence of the protease domain, forms a 6-fold-symmetric structure and contains a Zn^{2+} binding site. The upper disk is composed of six AAA+ domains, each of which contains ADP. For symmetry reasons, the structure can be considered as formed by a trimer of dimers, in which the AAA+ domains are alternatively in ‘‘open’’ and ‘‘closed’’ conformations.

Intracellular reactive oxygen species (ROS) measurement

The OxiSelect™ ROS Assay Kit (STA-342, Cell Biolabs Inc., San Diego, CA) was used to assay ROS activity in HEK293 cells. This is a cell-based assay for measuring activity of reactive oxygen species using a cell-permeable fluorogenic probe 2’, 7’-Dichlorodihydrofluorescin diacetate (DCFH-DA) that is deacetylated by cellular esterases to non-fluorescent 2’, 7’-Dichlorodihydrofluorescin (DCFH) once in the cells. DCFH is rapidly oxidized to highly fluorescent 2’, 7’-Dichlorodihydrofluorescein (DCF) by ROS and fluorescence intensity is proportional to the ROS levels within the cytosol.

Electron micrography

Cells were cultured on plastic cover slips, washed in PBS, fixed in 1.6% glutaraldehyde and were embedded in LR white (Marivac, PQ, Canada), thin sections were cut with a Leica Ultracut E ultramicrotome and counterstained with lead citrate and uranyl acetate. Digital images were taken using a JEOL 1230 TEM at 60 kV adapted with a 2K x 2K bottom mount CCD digital camera (Hamamatsu, Japan) and AMT software.

Mass spectrometry

Samples were prepared by in gel digestion of Q688 and R688 variant SPG7 performed overnight using sequencing grade modified trypsin (Promega) at 37°C. Peptides were extracted from the gel with three subsequent 100 µL extractions (70% acetonitrile, 1% formic acid) and lyophilized. Samples were dissolved in 5 µL 0.1 trifluoroacetic acid and transferred to glass autosampler vials.

Peptide digests were analyzed by nanoflow reversed-phase liquid chromatography (nRPLC) coupled online to a hybrid linear Iontrap-Orbitrap mass spectrometer (LTQ-Velos Orbitrap, ThermoFisher Scientific, Inc., San Jose, CA). Separation of the peptide digests was performed using an integrated electrospray ionization (ESI)-fused silica capillary column (100 µm ID x 360 µm OD x 20 cm length) packed in-house with 5 µm 300 Å pore size C_{18}-reversed-phase stationary phase (Jupiter, Phenomenex, Torrance, CA). Mobile phase flow was supplied by a nanoflow HPLC system (Ultimate 3000, Dionex, Corp., Sunnyvale, CA). The sample was injected onto a trap column (C_{18}, 5 µm, 100 Å, 300 µm ID x 5 mm, LC Packings, Dionex Inc., CA) for 3 minutes at a flow rate of 30 µL/min of mobile phase A (2% acetonitrile, 0.1% formic acid in water) using the loading pump and valve set to waste. The nanoflow pump was then switched in line with the trap column and peptides were eluted using a linear gradient of 2% to 40 % mobile phase B (0.1% formic acid in acetonitrile) over 115 minutes at a constant flow rate of 200 nL/min followed by a column wash consisting of 95% mobile phase B for 30 minutes at a constant flow rate of 400 nL/min. Full scan MS spectra were collected in the Orbitrap using full ion scan mode over the *m/z* range 375-1800 (R = 60,000 @ 400 *m/z)*. The twenty most abundant molecular ions dynamically determined from the full MS scan were selected for sequencing by collision-induced dissociation (CID)

in the ion trap using a normalized CID energy of 35%. An inclusion mass list corresponding to potential phosphorylation peptides was also included for CID MS/MS. Dynamic exclusion of 60 s was used for ions already selected for fragmentation to minimize redundancy. MS data was recorded for 120 minutes.

Tandem mass spectra were searched against the UniProt human proteome database (http://www.expasy.org) using SEQUEST (ThermoFisher Scientific, Inc.). Peptides were considered legitimately identified if they achieved specific charge state and proteolytic cleavage-dependent cross-correlation (Xcor) scores of 1.9 for $[M + H]^{1+}$, 2.2 for $[M + 2H]^{2+}$, and 3.5 for $[M + 3H]^{3+}$, and a minimum delta correlation score (ΔCn) of 0.08.

Supplemental figures

Figure S1. Quantification of over-expressed SPG7 R688 and Q688 proteins in HEK293 cells.

Immunoblots shown in Figure 2A and 6A from whole cell extracts and Figure 1G from mitochondrial extracts for untreated cells were quantified for total SPG7 protein (precursor and mature form) by densitometry of image files using the ImageQuant software (GE Healthcare Life Science Inc.) and normalized to GAPDH for whole cells and to COX2 for mitochondrial extracts. No difference in the level of over-expressed SPG7 isoforms was detected.

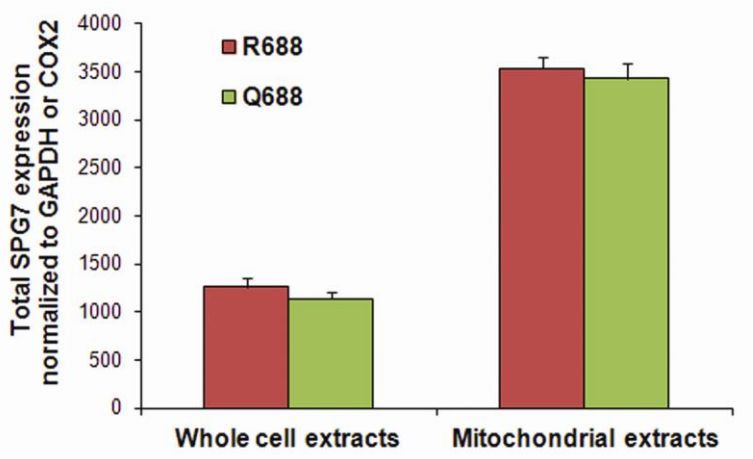
Total SPG7 expression normalized to GAPDH or COX2
4000
3500
3000
2500
2000
1500
1000
500
0
R688
Q688
Whole cell extracts
Mitochondrial extracts

Figure S2. Knockdown of SPG7 shows that both bands detected in mitochondria by immunoblot are SPG7.
shRNA to SPG7 was expressed from a lentiviral plasmid vector transiently transfected into HEK293 cells. Forty µg of mitochondrial proteins were loaded per lane. Samples were normalized to TOM20 and quantified by densitometry.

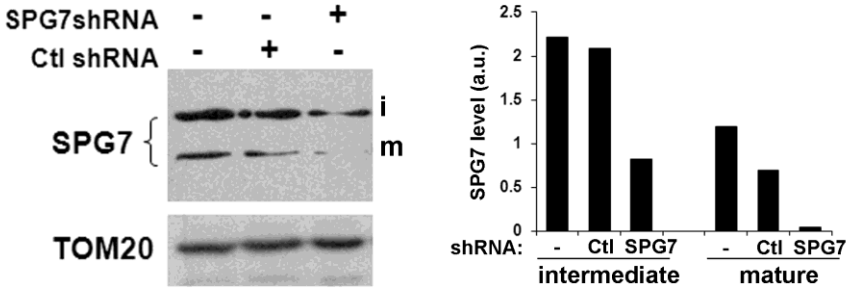
SPG7shRNA - - +
Ctl shRNA - + -
SPG7
i
m
TOM20
SPG7 level (a.u.)
2.5
2
1.5
1
0.5
0
shRNA: - Ctl SPG7 - Ctl SPG7
intermediate
mature

Figure S3. Effect of TCA cycle substrates glutamine and pyruvate on aerobic respiration (oxygen consumption rate, OCR) and glycolysis (extracellular acidification, ECAR) in HEK293 cells transfected with wild type R688 or variant Q688.
Untransfected HEK293 cells served as the control. Following measurement of OCR and ECAR under resting conditions, cells were treated with oligomycin, FCCP, and Antimycin A to induce proton leak-dependent respiration, FCCP stimulated respiration, and test extramitochondrial respiration. Only TCA cycle-linked substrates were used for analysis. (A) summary of in situ analysis of oxygen consumption rate.
n=4, mean ± SEM. (B) FCCP-stimulated OCR, corrected to extramitochondrial (antimycin A induced) respiration. n=4 independent experiments (each with 6 replicates), mean ± SEM, 1-way ANOVA with Fisher's post- hoc test. (C) Subtracting proton leak- dependent respiration from resting respiration reveals markedly increased resting respiration in Q688-expressing cells. *, $p<0.05$ comparing R688 and Q688; **, $P<0.005$, ***, $P<0.0005$ compared to NT. (D) Summary of in situ analysis of extracellular acidification rate. n=4 independent experiments (each with 6 replicates), mean ± SEM.

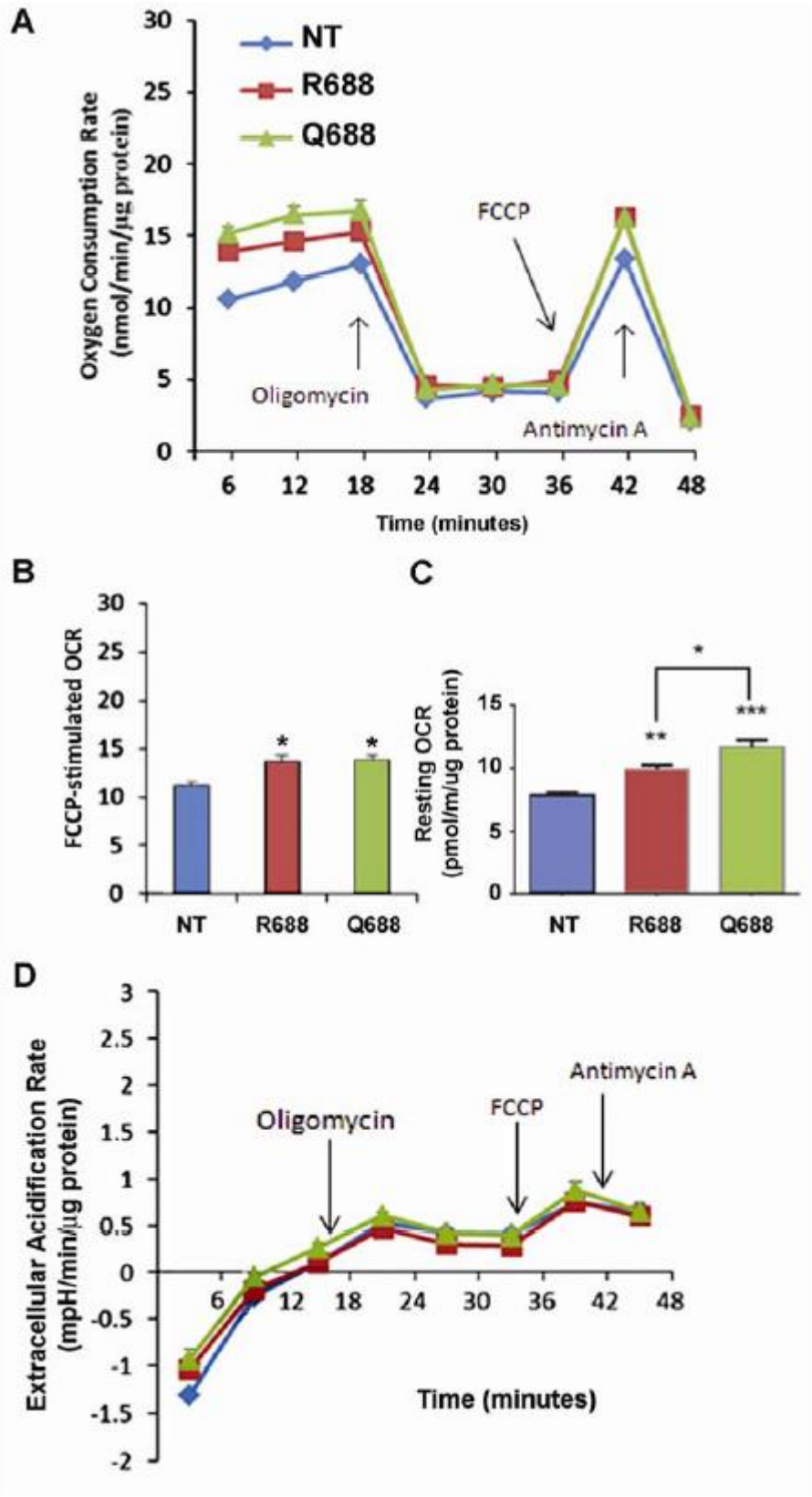
A
NT
R688
Q688
Oxygen Consumption Rate (nmol/min/µg protein)
FCCP
Oligomycin
Antimycin A
Time (minutes)
B
FCCP-stimulated OCR
NT
R688
Q688
C
Resting OCR (pmol/m/ug protein)
D
Extracellular Acidification Rate (mpH/min/µg protein)
Oligomycin
FCCP
Antimycin A
Time (minutes)

Figure S4. Effect of fatty acid oxidation on aerobic respiration (oxygen consumption rate, OCR) and glycolysis (extracellular acidification, ECAR) in HEK293 cells transfected with wild type R688 or variant Q688.

Untransfected HEK293 cells served as the control. Following measurement of OCR and ECAR under resting conditions, cells were treated with oligomycin, FCCP, and Antimycin A to induce proton leak- dependent respiration, FCCP-stimulated respiration, and test extramitochondrial respiration. Only 0.1 mM oleate and 4 mM glutamine (for anaplerosis) were used as respiratory substrates. 1 mM L-carnitine was included to encourage fatty acid oxidation. (A) Summary of in situ analysis of oxygen consumption rate. n=4, mean ± SEM. (B) FCCP- stimulated OCR corrected to extramitochondrial (antimycin A-induced) respiration. n=4, mean ± SEM, 1-way ANOVA with Fisher's post- hoc test. (C) Summary of in situ analysis of extracellular acidification rate. n=4 independent experiments (each with 6 replicates), mean ± SEM.

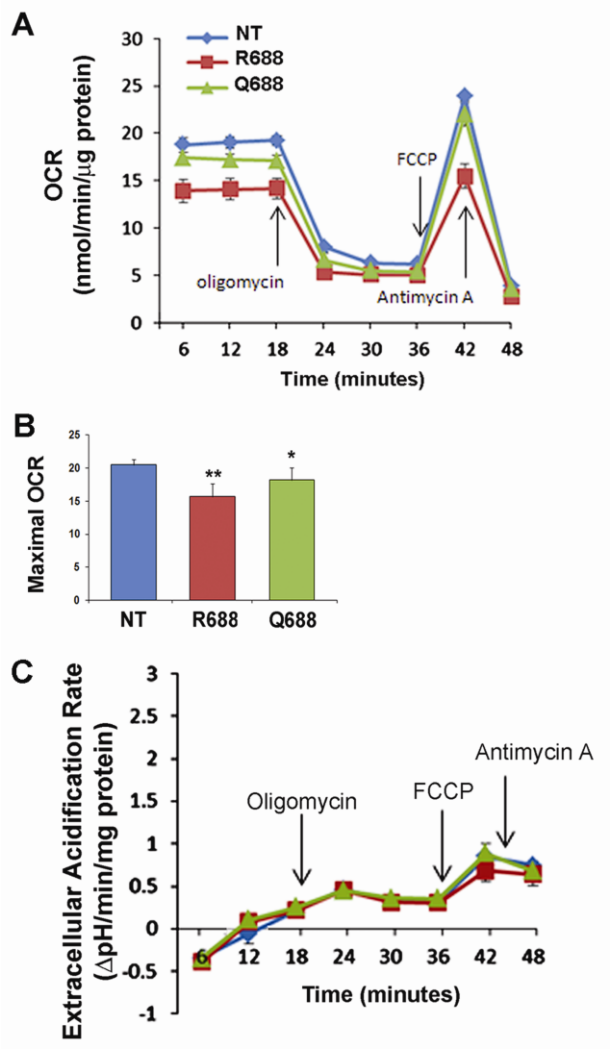
A
NT
R688
Q688
OCR
(nmol/min/μg protein)
30
25
20
15
10
5
0
FCCP
oligomycin
Antimycin A
6
12
18
24
30
36
42
48
Time (minutes)
B
Maximal OCR
25
20
15
10
5
0
**
*
NT
R688
Q688
C
Extracellular Acidification Rate
(ΔpH/min/mg protein)
3
2.5
2
1.5
1
0.5
0
-0.5
-1
Oligomycin
FCCP
Antimycin A
12
18
24
30
36
42
48
Time (minutes)

Figure S5.
Immunoblot analysis shows HUVECS transduced with lentiviral vector expressing Q688 variant have activated endothelial nitric oxide synthase (eNOS), as revealed by dephosphorylation of threonine 495 (peNOS-Thr495). Whole cell extracts of HUVECs infected with empty lentiviral vector are labeled Sham.

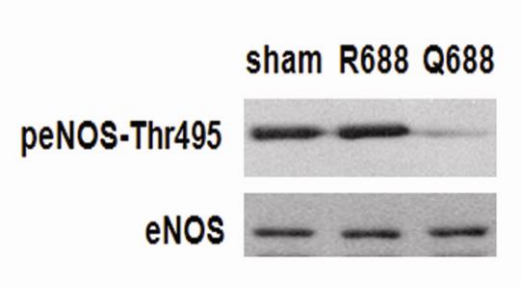
sham R688 Q688
peNOS-Thr495
eNOS

Figure S6. Specificity of immunoprecipitation.
Immunoblot probed with AFG3L2 antibody and reprobed with GAPDH antibodies shows that AFG3L2 antibody does not pull down GAPDH and GAPDH antibody does not pull down AFG3L2.

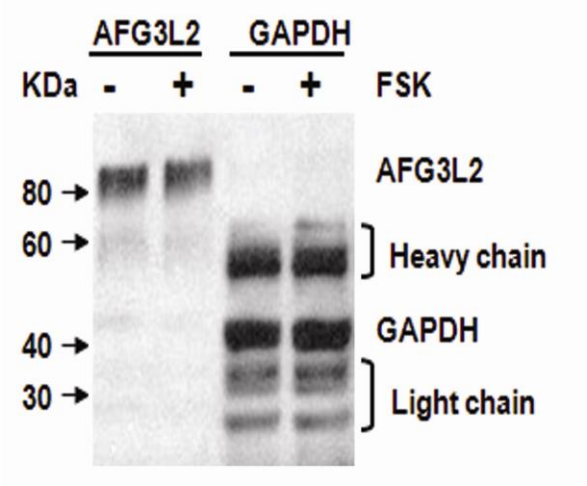
AFG3L2
GAPDH
KDa
-
+
-
+
FSK
80
60
40
30
AFG3L2
Heavy chain
GAPDH
Light chain

CHAPTER 5

Plasma PCSK9 levels are elevated with acute myocardial infarction in two independent retrospective angiographic studies

Naif A. M. Almontashiri[1,2,3], Ragnar O. Vilmundarson[1,2], Nima Ghasemzadeh[4], Sonny Dandona[5], Robert Roberts[1,6], Arshed A. Quyyumi[5], Hsiao-Huei Chen[6,7*], Alexandre F. R. Stewart[1,2,6*]

[1]Ruddy Canadian Cardiovascular Genetics Centre, University of Ottawa Heart Institute, Ottawa, Ontario, Canada, [2]Department of Biochemistry, Microbiology and Immunology, University of Ottawa, Ottawa, Ontario, Canada, [3]Center for Genetics and Inherited Diseases, Taibah University, Almadina, Saudi Arabia, [4]Department of Medicine, Emory University, Atlanta, Georgia, USA, [5]Department of Medicine, McGill University, Montreal, Canada, [6]Department of Medicine, University of Ottawa, Ottawa, Ontario, Canada, [7]Ottawa Hospital Research Institute, Ottawa, Ontario, Canada.

* address correspondence to: Hsiao-Huei Chen, Ottawa Hospital Research Institute, 451 Smyth Road, Rm 2422, Ottawa, Ontario, K1H 8M5, Canada. Email: hchen@uottawa.ca, fax: 613-562-5403, phone: 613-562-5800 x8133, and Alexandre Stewart, University of Ottawa Heart Institute, 40 Ruskin Street, Rm H3100, Ottawa, Ontario, K1Y 4W7, Canada. email: astewart@ottawaheart.ca, fax: 613-761-4647, phone: 613-761-5189

Author contributions: NAMA performed the experiments; ROV and NG performed the statistical analysis; SD read the angiogram; RR and AAQ provided plasma samples and essential reagents; NAMA, HHC, and AFRS wrote the manuscript.

Key Words: PCSK9, coronary artery disease, LDL cholesterol, statin, myocardial infarction

Abstract

Objective: Proprotein convertase subtilisin/kexin type 9 (PCSK9) is a circulating protein that promotes degradation of the low density lipoprotein (LDL) receptor. Mutations that block PCSK9 secretion reduce LDL-cholesterol and the incidence of myocardial infarction (MI). However, it remains unclear whether elevated plasma PCSK9 associates with coronary atherosclerosis (CAD) or more directly with rupture of the plaque causing MI.

Methods and Results: Plasma PCSK9 was measured by ELISA in 645 angiographically defined controls (<30% coronary stenosis) and 3,273 cases of CAD (>50% stenosis in a major coronary artery) from the Ottawa Heart Genomics Study. Because lipid lowering medications elevated plasma PCSK9, confounding association with disease, only individuals not taking a lipid lowering medication were considered (279 controls and 492 with CAD). Replication was sought in 357 controls and 465 with CAD from the Emory Cardiology Biobank study. PCSK9 levels were not associated with CAD in Ottawa, but were elevated with CAD in Emory. Plasma PCSK9 levels were elevated in 45 cases with acute MI (363.5±140.0 ng/ml) compared to 398 CAD cases without MI (302.0±91.3 ng/ml, p=0.004) in Ottawa. This finding was replicated in the Emory study in 74 cases of acute MI (445.0±171.7 ng/ml) compared to 273 CAD cases without MI (369.9±139.1 ng/ml, $p=3.7x10^{-4}$). Since PCSK9 levels were similar in CAD patients with or without a prior (non-acute) MI, our finding suggests that plasma PCSK9 is elevated either immediately prior to or at the time of MI.

Conclusion: Plasma PCSK9 levels are increased with acute MI.

Introduction

By promoting the degradation of low density lipoprotein (LDL) receptors (LDL-R) in the liver, proprotein convertase subtilisin/kexin type 9 (PCSK9) elevates plasma levels of LDL-cholesterol (LDL-C) (211). In African Americans, loss-of-function mutations in PCSK9 that prevent its secretion are associated with a 30%-40% reduction in plasma levels of LDL-C, but surprisingly reduce events associated with coronary atherosclerosis (CAD, coronary artery disease) by 88% over a 15 year period (212). A similar level of reduced LDL-C attained by statins would be associated with only a 25% reduction in the risk of coronary events. This observation has also been confirmed in individuals of European ancestry for the R46L PCSK9 variant. The MIGen consortium found markedly reduced risk of MI associated with this allele (15). In another independent study, a large meta-analysis of several Danish cohorts found that carriers of the 46L allele had a 12% reduction in LDL-C that predicted a 5% reduction, but that was in fact associated with a 28% reduction, in ischemic heart disease (213). These similar findings have been hypothesized to result from a lifetime reduction in LDL-C, reducing the burden of atherosclerosis, but could also be explained if PCSK9 does more than control LDL-R levels. Overall, plasma PCSK9 accounts for less than 8% of the variance of plasma LDL-C (214).

Statins, while lowering LDL-C, markedly elevate plasma PCSK9, most likely due to increased expression of the PCSK9 activating transcription factors SREBP2 and HNF1α (25). It would appear that the LDL-C lowering effect of statins outweighs the risk associated with elevated PCSK9, because statins dose-dependently lower LDL-C in both men and women (215) and reduce cardiovascular events in women just as well as in men (216). Recent clinical trials using antibodies against PCSK9 that block PCSK9 interaction with the LDL-R

were successful at lowering LDL-C below the levels obtained with statins over several weeks (26,217) As a proof of concept, this approach has generated considerable excitement (218). It remains to be seen whether therapies that lower plasma PCSK9 will lower the incidence of MI. Since MI occurs on a substrate of coronary atherosclerosis, whether elevated plasma PCSK9 increases MI risk through increased coronary atherosclerosis or by additional mechanisms remains unclear. Genetic studies have shown that variants contributing to the risk of coronary atherosclerosis can be distinguished from variants contributing to the risk of MI (219,220). If elevated plasma PCSK9 contributes to the risk of thrombosis and MI, rather than or in addition to the risk of atherosclerosis, then this could also account for the disproportionate reduction in MI risk associated with genetic variants that lower plasma PCSK9 levels. Importantly, if elevated plasma PCSK9 carries risk beyond its effect on LDL-C, there may be an additional benefit to lowering plasma PCSK9 in individuals treated with statins. Here, we asked whether elevated plasma PCSK9 is associated with MI or angiographically-defined CAD in two independent retrospective angiographic studies, the Ottawa Heart Genomics Study (OHGS) (203) and the Emory Cardiology Biobank (EmCB) study (221).

Materials and Methods

Study design

Plasma PCSK9 levels were measured by ELISA and tested for association with angiographic CAD and MI in two independent angiographic cross-sectional studies, the OHGS (203) with replication in a subset of the EmCB study (221).

Study participants

For the OHGS, the Research Ethics Board of the University of Ottawa Heart Institute approved this study and written informed consent was obtained from all study participants. The OHGS excluded individuals with diabetes mellitus to ensure that the genetic risk primarily associated with coronary artery disease would not be confounded by the risk associated with diabetes, as described previously (109). In addition, diabetes is known to elevate plasma PCSK9 levels (214), and a priori exclusion of diabetics in the OHGS study design removes this confounding variable.

CAD cases were identified by angiography as having a stenosis of greater than 50% in a major coronary artery, whereas angiographic controls had less than 30% stenosis. Severity of CAD was ranked according to the number of coronary arteries with stenosis, as described previously (109). Patients were further stratified as having had an acute MI, according to elevated troponin and/or ST-elevation, if it was documented at the time of catheterization. Acute MI samples were obtained within 24-48 hours of the onset of symptoms, prior to the initiation of statin therapy. Otherwise, CAD cases were classified as having prior (or historical) MI or as having no MI from chart review. Controls were individuals who underwent coronary angiography prior to heart valve surgery or symptomatic individuals but with minimal (<30%) stenosis. Individuals with intermediate stenoses between 30% and 50% were excluded. Information regarding statin use, medication to treat hypertension, and recent (at the time of recruitment or within 12 months prior to recruitment) plasma LDL-C, HDL-C, and triglycerides was measured by colorimetric assays on a Roche Modular Analytics P Module clinical chemistry analyzer (Roche Diagnostics Inc., Laval, Quebec, Canada). Plasma samples were obtained at the time of cardiac catheterization from fasting individuals, stored at -80°C and thawed once for assessment of plasma PCSK9

levels. Of note, plasma samples were drawn at various times randomly distributed throughout the day.

The EmCB study was approved by the Institutional Review Board at Emory University, Atlanta, GA, USA. All subjects provided written informed consent at the time of enrollment. For the present study, 822 plasma samples were selected from 2,357 individuals of the EmCB study who underwent elective or emergent cardiac catheterization and who were not taking a statin or fibrate nor were diabetic at the time of recruitment. CAD cases were defined as having greater than 50% stenosis whereas controls had less than 20% stenosis, as described previously (221). Similar criteria as in the OHGS were used to define CAD cases with acute, prior or no MI in the EmCB study.

PCSK9 ELISA

Plasma levels of PCSK9 were measured by ELISA using a commercial assay (Quantikine® ELISA, R&D Systems, Minneapolis, MN) that has been previously validated (19,222). Plasma samples were diluted 1:20 in dilution buffer. The minimal detectable dose of PCSK9 was 0.1 ng/ml, with a typical range of 39 to 1,400 ng/ml in human plasma. We were concerned that plasma LDL-C might affect the measurement of plasma PCSK9 using the PCSK9 ELISA assay, since PCSK9 interacts with LDL-C (223). The PCSK9 protein standard was diluted and incubated at 37°C for 30 minutes without or with the addition of LDL-C to a concentration of 2.6 mmol/L and no difference in PCSK9 levels was detected (data not shown). Thus, LDL-C does not interfere with the ELISA. PCSK9 levels in 12 individuals were tested in 6 replicates in one assay and again in a separate assay. Several different lots of the assay were used to measure PCSK9 in the OHGS samples, whereas a

single lot was used for the EmCB study. The intra-assay coefficient of variance was 8.9% and between assays was 12%.

Statistical analysis

Continuous variables are presented as mean ± standard deviation (SD) and categorical variables are presented as N (%). To determine whether differences between CAD cases and controls were significant for continuous and categorical variables the Student's *t*-test and χ^2 test were used, respectively. To determine whether mean plasma PCSK9 levels differed between 0, 1, 2 or 3 vessel disease a one-way analysis of variance (ANOVA) was used. Multiple logistic regression analysis was used to examine whether PCSK9 was associated with CAD or acute MI when correcting for known risk factors (age, male sex, BMI, smoking, antihypertensive medication use, LDL-C, HDL-C, and TG). The acute MI variable compared CAD cases with no MI to those with acute MI, excluding CAD cases with prior MI except when an individual who had suffered a prior MI had also suffered an acute MI, in which case they were labeled as having an acute MI. Spearman's rank correlation was used to determine whether plasma PCSK9 and LDL-C levels are correlated. All statistical analyses were two-sided and performed with SPSS (version 19.0, SPSS Inc., Chicago IL, USA), SAS Enterprise Guide (v. 4.3, SAS Institute Inc., Cary NC, USA) and R (v. 3.0.2, The R Foundation for Statistical Computing, Vienna, Austria). One-way ANCOVA was used to determine whether PCSK9 levels differed between controls, CAD cases with no MI, CAD cases with acute MI and CAD cases with prior MI and post-hoc tests were adjusted for multiple comparisons by Sidak correction. The threshold for significance was set at $p < 0.05$ for all analyses performed.

Results

Statins elevate plasma PCSK9

The clinical characteristics of the OHGS (203) samples are presented in Table 1, stratified by statin use because of the marked effect of statins to elevate plasma PCSK9 levels (25). Plasma PCSK9 levels were not different between cases or controls in either those taking or not taking a statin. Linear regression analysis confirmed that plasma PCSK9 is elevated by statin use as well as by young age and female sex (Table 2). Smoking, antihypertensive medication and CAD were also independent predictors of PCSK9.

Plasma PCSK9 levels are not associated with coronary atherosclerosis in the OHGS for individuals not taking a statin

To determine whether PCSK9 levels are associated with CAD, we performed a logistic regression analysis correcting for known CAD risk factors (Table 3). However, given the known marked effect of statins (24,25) and fibrates (224,225) to elevate PCSK9 levels, also seen in our study (Table 2), we stratified the analysis by statin use. PCSK9 levels were only associated with CAD in individuals taking a statin (Table 3, $p=0.0003$), suggesting that the observed effect of CAD on PCSK9 levels (Table 2) is driven by higher statin use among CAD cases. Similarly, no association between PCSK9 levels and severity of CAD, assessed by the number of diseased vessels, was observed in the OHGS by ANOVA in individuals not taking a statin (Figure 1). Given that plasma PCSK9 levels did not associate with CAD in individuals not taking a statin, we asked whether plasma PCSK9 levels might instead be associated with acute or prior MI.

Figure 1. Mean PCSK9 levels do not differ with atherosclerosis burden.
A Tukey's boxplot displaying PCSK9 levels in OHGS CAD controls (0 diseased vessels) and cases (1, 2 or 3 diseased vessels) in individuals not taking statins. The median is the line in the box, the 1st and 3rd quartiles are the upper and lower edges of the boxes and 1.5 interquartile range (IQR) is displayed as whiskers. Outliers have been removed. (0 vessel disease, N=280; 1-vessel disease, N=126; 2-vessel disease, N=102; 3-vessel disease, N=104).

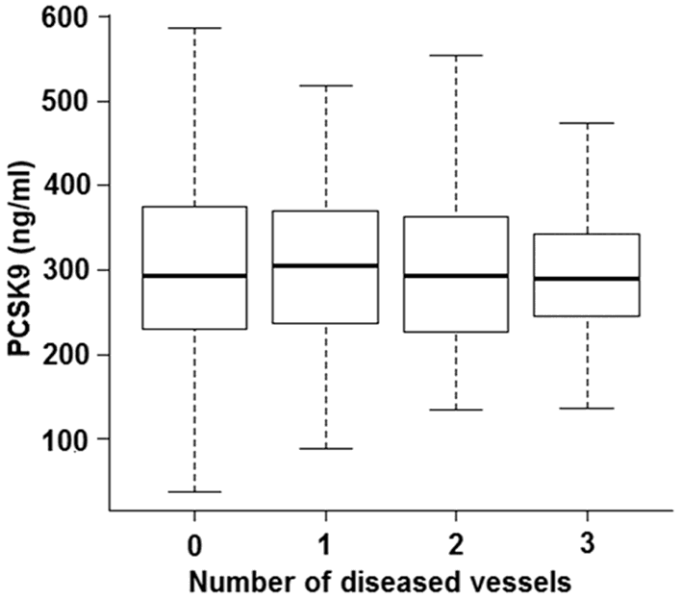
600
500
400
300
200
100
PCSK9 (ng/ml)
0
1
2
3
Number of diseased vessels

Plasma PCSK9 levels are elevated with acute MI, but not with prior MI, in the OHGS

Out of the 3,273 CAD patients in the OHGS, 1,371 had an MI (799 with prior history of MI and 572 with acute MI), and of those with an MI, 94 were not taking a statin (6.8%); 45 had acute MI and 49 had prior MI. Plasma PCSK9 levels were markedly elevated in 45 individuals with acute MI (363.5±140.0 ng/ml) compared to 398 CAD cases without MI (302.0±91.3 ng/ml, p=0.004), adjusted for age at consent, male sex, BMI, smoking, and antihypertensive meds (Figure 2). In contrast, no difference in PCSK9 levels was seen between 49 individuals with a prior MI (315.9±107.5 ng/ml) and 398 CAD cases without an MI (p=0.977). A mean of 11.4 ± 8.1 years separated the occurrence of MI from the time of recruitment in this group. Elevated PCSK9 levels seen with acute MI were not accompanied by elevated LDL-C levels (3.051±0.090 mmol/L for acute MI, 3.322±0.914 mmol/L for CAD no MI, p=0.12). Logistic regression analysis confirmed that PCSK9 levels are an independent predictor of acute MI in CAD cases not taking a statin in the OHGS (Table 4).

PCSK9 levels are associated with coronary atherosclerosis in the EmCB study

We next sought "a priori" confirmation of our findings in an independent cohort. The Emory Cardiology Biobank (EmCB) study is another large angiographic cohort consisting of more than 2,400 individuals (221). To avoid the confounding effect of statins and to replicate the selection criteria of the OHGS cohort (non-diabetic), we measured plasma PCSK9 levels in 465 CAD cases and 357 controls without diabetes mellitus and not taking a statin or fibrate at the time of recruitment (see Table 5). Linear regression analysis also showed that CAD was significantly associated with elevated plasma PCSK9 (Table 6). In contrast to the subset of individuals not taking a statin or fibrate in the OHGS, plasma

Figure 2. Plasma PCSK9 levels are increased with acute MI.
Numbers in columns reflect sample size per group for individuals not taking a lipid-lowering medication (statin or fibrate) at the time of recruitment. Values are mean±SEM. Asterisks indicate significantly elevated PCSK9 by ANCOVA, $p<0.05$ after adjusting for variables (age, male sex, BMI, antihypertensive medication use, and smoking) and correcting for multiple comparisons.

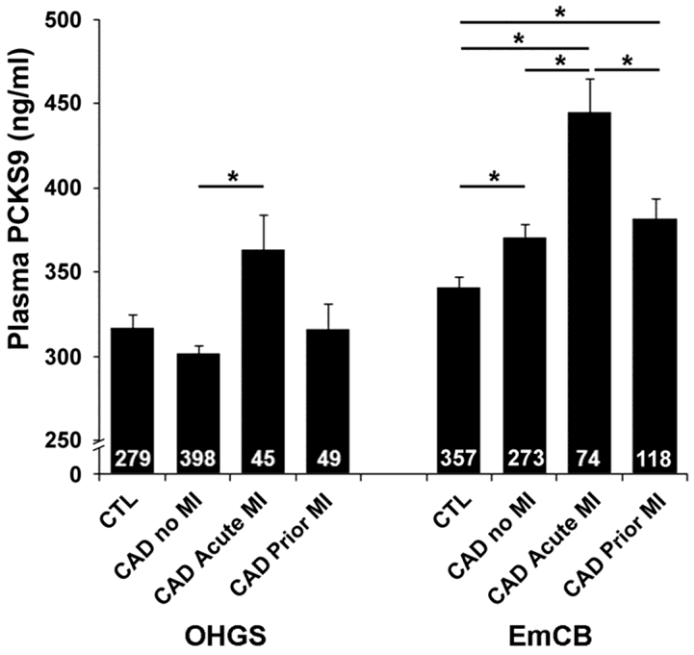
Plasma PCKS9 (ng/ml)
500
450
400
350
300
250
0
279
398
45
49
357
273
74
118
CTL
CAD no MI
CAD Acute MI
CAD Prior MI
CTL
CAD no MI
CAD Acute MI
CAD Prior MI
OHGS
EmCB
*

PCSK9 levels were elevated in angiographic CAD cases (385.0±146.9 ng/ml) compared to controls (340.4±125.2 ng/ml, p<0.001) in the EmCB sample. Logistic regression confirmed that plasma PCSK9 levels are an independent predictor of CAD in the EmCB sub-study (Table 7). The overall higher PCSK9 values in the EmCB study likely reflect a lot-specific variation in the PCSK9 ELISA.

Plasma PCSK9 levels are also elevated with acute MI, but not with prior MI, in the EmCB study

Similar to the OHGS sample, plasma PCSK9 levels were elevated in the 74 individuals with acute MI (445.0±171.7 ng/mL) compared to the 273 individuals with CAD but no MI (369.9±139.1 ng/mL, $p=3.7x10^{-4}$, after adjusting for variables, Figure 2). Here too, elevated plasma PCSK9 levels with acute MI were not associated with LDL-C levels (2.94±1.28 mmol/L for acute MI and 2.75±1.00 mmol/L for CAD no MI, p=0.423). Also similar to the OHGS, no difference was seen between the 118 individuals with prior MI (382.3±139.1 ng/mL) and 273 CAD cases without MI (369.9±139.13 ng/mL, p=0.0.954). An average of 10.1 ± 9.3 years elapsed between the MI and the time of recruitment for CAD cases of prior MI in the EmCB study. Logistic regression analysis confirmed that PCSK9 levels are an independent predictor of acute MI in CAD cases in the EmCB sub-study (Table 8).

In individuals taking statins, there was no correlation between PCSK9 levels and plasma LDL-C (r_s= -0.0288, p=0.158, N=2,410) in the OHGS. In individuals not taking statins, there was also no correlation between PCSK9 levels and LDL cholesterol (r_s=0.0813, p=0.0754, N=479). When the analysis is stratified by CAD, a weak positive correlation between the levels of PCSK9 and LDL cholesterol (r_s=0.176, p=0.0257, N=160) was

observed in controls not taking statins. No correlation was seen in CAD cases not taking statins, nor in CAD cases (r_s=-0.0268, p=0.214, N=2155) or controls (r_s=-0.0114, p=0.856, N=225) taking statins. Similarly, in the EmCB sub-study of individuals not taking statins, there was no correlation between PCSK9 levels and LDL cholesterol in either those with CAD (r_s=-0.00840, p=0.862, N=429) or controls (r_s=-0.00742, p=0.895, N=322).

Discussion

Here, for the first time to our knowledge, we found that plasma PCSK9 is elevated with acute MI in non-diabetic individuals who are not taking a statin and have angiographically proven CAD. A strength of our study is that this finding was replicated in a second independent cohort, an EmCB sub-study. Furthermore, our observation that plasma PCSK9 levels are not elevated in individuals with prior MI compared to those with angiographic CAD that did not have an MI argues that PCSK9 levels are transiently elevated with acute MI.

Since lipid lowering medications elevate plasma PCSK9 (24,25,225), it is necessary to exclude individuals on lipid lowering medications to avoid possible spurious associations due to medication. However, given the high prevalence of cholesterol-lowering prescriptions in older Americans (226), as high as 44.9% in persons over age 60, it is a challenge to obtain a large sample size. Nevertheless, we were able to identify 45 individuals in the OHGS and 74 in the EmCB study with acute MI that were not taking a lipid-lowering medication at the time of recruitment. It is likely that individuals with CAD and prior MI not taking a statin may have been intolerant to statins, since statin-induced myopathy is estimated to affect 10-15% of statin users (227).

Our findings are consistent with genetic studies that have demonstrated a causal link between lower plasma PCSK9 levels and reduced risk of MI (15,212,213,228). The mechanism whereby PCSK9 contributes to the risk of MI has been attributed largely to its effect on degrading the LDL-R, thereby elevating LDL-C and promoting atherosclerosis. Indeed, MI occurs on a foundation of coronary atherosclerosis, and most genetic factors that contribute to the elevation of coronary atherosclerosis risk were discovered through their association with the increased risk of MI (229). However, our finding that elevated plasma PCSK9 is associated with acute MI, rather than prior MI or with coronary atherosclerosis cautions that the relationship of PCSK9 to MI risk may be more complex than previously thought.

It is well recognized that elevated LDL-C is one of the most significant risk factors of atherosclerosis. Intriguingly, among the top 10 genetic variants associated with elevated LDL-C, a PCSK9 variant had the weakest association with elevated LDL-C but had the third strongest effect on the risk of MI (230). In other words, the effect of PCSK9 on MI risk far exceeds its effect on plasma LDL-C levels and on coronary atherosclerosis risk. It is noteworthy that in the present study, in individuals not taking a statin, only a weak (OHGS) or no correlation was seen between plasma PCSK9 levels and LDL-C.

PCSK9 might increase the risk of MI by a mechanism distinct from its well-known effect on LDL-C. We observed a weak correlation between plasma PCSK9 levels and LDL-C only in controls not taking a lipid lowering medication in the OHGS but not in the EmCB study. In contrast to the increased levels of PCSK9 we observed in acute MI patients (measured 1 to 2 days after MI), plasma levels of LDL-C have been reported to fall transiently following MI (231-233). Thus, PCSK9 levels are uncoupled from LDL-C, at least

at the time of MI. One possibility is that PCSK9 levels increase transiently after the trauma of an MI, as an acute phase reactant. However, a recent study reported that plasma PCSK9 levels were not elevated at the time of admission for severe trauma, but only eight days after a traumatic injury and correlated with the severity of the trauma (234), arguing that PCSK9 is not an acute phase reactant.

Another intriguing possibility is that PCSK9 levels might be elevated prior to acute MI, and even trigger MI. PCSK9 has been reported to bind to the LDL-R related protein LRP8 (235). LRP8 activation promotes platelet aggregation (236). If PCSK9 binding activates LRP8 receptor signaling, it could increase platelet aggregation and augment the risk of MI. Acute coronary events are more frequent in the morning (237), at a time when plasma PCSK9 levels are at their highest (238), and when propensity for platelets to aggregate is also increased (239). Whether PCSK9 contributes to the risk of MI through platelet activation remains to be tested. In addition, in the OHGS sample, smoking was an independent predictor of circulating PCSK9 levels. This effect has been reported previously in a study of 4 healthy cohorts from Sweden comprising 5,722 middle-aged individuals (240), and although the mechanism underlying this association has not been explored, smoking is the second most important modifiable risk factor for MI after elevated LDL-C (241).

Plasma PCSK9 levels are elevated in patients with periodontitis, independently of LDL-C levels (19). Periodontitis is a known risk factor for CAD and MI (20). The risk of MI is elevated fivefold after an acute infection (242). In mice, endotoxin elevates plasma PCSK9 levels (243) and plasma PCSK9 levels might be similarly elevated in humans after an acute infection and contribute to increased risk of subsequent MI. PCSK9-targeted therapies might

lower the risk of events after acute infections. More needs to be learned about the functions of PCSK9 beyond its effect on LDL-R degradation.

One limitation of our study is that plasma samples from the OHGS were not carried forward to control for lot-to-lot variability when the EmCB samples were assayed. Thus, the 20% higher values measured for the EmCB samples could reflect a true difference or more likely reflect a lot-to-lot difference. Another limitation of our study is that both the OHGS and the EmCB are cross-sectional rather than longitudinal studies, having recruited angiographically-defined CAD cases and controls at the time of cardiac catheterization. Thus, it remains to be determined whether plasma PCSK9 levels are elevated as a consequence of acute MI (as an acute phase reactant) or prior to MI. In addition, we do not know why PCSK9 levels were not associated with CAD in those not taking statin in the OHGS, but were in the EmCB study. This may be a reflection of the presence of less coronary atherosclerosis in EmCB angiographic controls, where 20% or less stenosis was used as an inclusion criterion compared to 30% or less for the OHGS. Another factor could be the inclusion of individuals with aortic valve disease, who showed minimal coronary stenosis, in the OHGS controls (203). It is not known whether aortic valve disease elevates plasma PCSK9 levels. A recent study of 243 angiographic cases reported a correlation between the severity of coronary artery disease and plasma PCSK9 levels (244). However, in two larger cohorts, we did not replicate this finding.

Conclusion

Among non-diabetic individuals with angiographically-defined coronary artery disease who are not taking a lipid-lowering medication, plasma PCSK9 levels are elevated at

the time of acute myocardial infarction. Future longitudinal studies will be required to determine whether PCSK9 levels are elevated prior to or as a consequence of acute coronary events.

Acknowledgments

We thank Thomas Lagace for providing LDL-C and reading of the manuscript.

Disclosures

None.

Table 1 Clinical characteristics of OHGS CAD cases and controls.

	Total			On Statin			Not taking statin		
Variable	Cases (N=3273)	Controls (N=645)	p	Cases (N=2781)	Controls (N=366)	p	Cases (N=492)	Controls (N=279)	p
Age, (years)	64 ± 11	63 ± 11	0.367	63 ± 11	64 ± 11	0.665	65 ± 11	63 ± 12	0.003
Male sex, N (%)	2503 (76.5)	302 (46.8)	<0.001	2169 (78.0)	170 (46.4)	<0.001	334 (67.9)	132 (47.3)	<0.001
BMI, kg/m^2	28.0 ± 4.9	28.7 ± 5.8	0.003	28.1 ± 4.9	28.9 ± 5.8	0.007	27.4 ± 5.0	28.4 ± 5.7	0.014
Smoking, N (%)	2354 (71.9)	374 (58.0)	<0.001	2009 (72.2)	233 (63.7)	<0.001	345 (70.1)	141 (50.5)	<0.001
HTN, N (%)	2029 (62.0)	514 (79.9)	<0.001	1784 (64.1)	307 (83.9)	<0.001	245 (49.8)	207 (74.2)	<0.001
Total-C, mmol/L	4.53 ± 1.24	4.83 ± 1.04	<0.001	4.43 ± 1.22	4.64 ± 1.03	0.002	5.26 ± 1.08	5.15 ± 0.98	0.246
LDL-C, mmol/L	2.61 ± 1.05	2.79 ± 0.87	<0.001	2.51 ± 1.02	2.62 ± 0.87	0.057	3.29 ± 0.95	3.05 ± 0.80	0.004
HDL-C, mmol/L	1.16 ± 0.41	1.37 ± 0.47	<0.001	1.15 ± 0.41	1.32 ± 0.44	<0.001	1.25 ± 0.43	1.47 ± 0.51	<0.001
TG, mmol/L	1.69 ± 1.09	1.52 ± 0.88	0.001	1.70 ± 1.10	1.58 ± 0.95	0.135	1.62 ± 1.00	1.41 ± 0.74	0.015
PCSK9, ng/mL	375.5 ± 131.2	349.7 ± 143.2	<0.001	387.3 ± 132.6	374.6 ± 146.5	0.117	309.0 ± 99.7	317.1 ± 131.9	0.376

Continuous variables presented as mean ± SD and categorical variables as N (%). Abbreviations: BMI, body mass index; HTN, anithypertensive medication, Total-C, total-cholesterol; LDL-C, Low density lipoprotein-cholesterol, HDL-C, high density lipoprotein-cholesterol, TG, triglycerides.

Table 2 Linear regression analysis of the relationships between explanatory variables and the level of PCSK9 in the OHGS.

Variable	β	p
Age, (years)	-0.086	<0.001
Male sex	-0.151	<0.001
BMI, kg/m^2	0.024	0.127
Smoking	0.033	0.033
HTN	-0.050	0.002
Statin (including fibrates)	0.225	<0.001
CAD	0.041	0.013

Abbreviations: BMI, body mass index; HTN, anithypertensive medication. N=3,918.

Table 3 Logistic regression analysis of the association of PCSK9 with CAD in the OHGS cohort, stratified by statin use.

	On statin		Not taking statin	
Variable	β or OR (95% CI)	p	β or OR (95% CI)	p
Age, (years)	0.004 (-0.009, 0.018)	0.530	0.013 (-0.007, 0.034)	0.210
Male sex	2.776 (2.075, 3.714)	6.10E-12	1.382 (0.875, 2.184)	0.166
BMI, kg/m²	-0.033 (-0.059, -0.006)	0.015	-0.035 (-0.076, 0.006)	0.091
Smoking	1.261 (0.946, 1.68)	0.113	3.343 (2.156, 5.184)	7.00E-08
HTN	0.379 (0.267, 0.538)	5.92E-08	0.442 (0.282, 0.694)	3.88E-04
LDL, mmol/L	-0.125 (-0.259, 0.009)	0.068	0.251 (-0.004, 0.506)	0.053
HDL, mmol/L	-0.612 (-0.916, -0.308)	7.86E-05	-0.887 (-1.396, -0.378)	0.001
TG, mmol/L	0.366 (-0.319, 1.050)	0.295	0.733 (-0.331, 1.797)	0.177
PCSK9, ng/mL	0.002 (0.001, 0.003)	0.0004	-0.001 (-0.002, 0.001)	0.505

Results given as beta for continuous variables and odds ratio (OR) for categorical variables. Abbreviations: BMI, body mass index; HTN, anithypertensive medication; Total-C, total-cholesterol; LDL-C, Low density lipoprotein-cholesterol; HDL-C, high density lipoprotein-cholesterol; TG, triglycerides. On statin, N=2,396; Not taking statin, N=478. Samples with missing values for variables were excluded.

Table 4 Logistic regression analysis of the association of PCSK9 with acute MI in the OHGS cohort, stratified by statin use.

	On statin		Not taking statin	
Variable	β or OR (95% CI)	p	β or OR (95% CI)	p
Age, (years)	-0.024 (-0.036, -0.012)	4.79E-05	-0.013 (-0.052, 0.027)	0.523
Male sex	0.876 (0.655, 1.172)	0.374	0.692 (0.268, 1.786)	0.447
BMI, kg/m²	-0.039 (-0.065, -0.013)	0.003	0.015 (-0.063, 0.093)	0.705
Smoking	1.287 (0.9997, 1.658)	0.050	0.94 (0.369, 2.391)	0.896
HTN	0.752 (0.594, 0.953)	0.019	0.643 (0.277, 1.49)	0.303
LDL, mmol/L	-0.049 (-0.163, 0.065)	0.403	-0.346 (-0.836, 0.143)	0.166
HDL, mmol/L	-1.068 (-1.470, -0.665)	1.97E-07	-2.038 (-3.455, -0.622)	0.005
TG, mmol/L	-0.139 (-0.751, 0.472)	0.655	-1.093 (-3.143, 0.956)	0.296
PCSK9, ng/ml	0.0004 (-0.0004, 0.001)	0.307	0.005 (0.002, 0.009)	0.002

Results given as beta for continuous variables and odds ratio (OR) for categorical variables. Abbreviations: BMI, body mass index; HTN, anithypertensive medication; Total-C, total-cholesterol; LDL-C, Low density lipoprotein-cholesterol; HDL-C, high density lipoprotein-cholesterol; TG, triglycerides. On statin, N=1,568; Not taking statin, N=287.

Table 5 Clinical characteristics of CAD cases and controls from the EmCB sub-study.

Variable	Cases (N=465)	Controls (N=357)	p
Age, (years)	65±12	56±12	<0.001
Male sex, N (%)	352(75.7)	193 (54.1)	<0.001
BMI, kg/m^2	28.3±5.5	29.8±6.8	<0.001
Smoking, N (%)	92 (19.8)	48(13.4)	0.01
HTN, N (%)	327(70.3)	201 (56.3)	<0.001
Total-C, mmol/L	4.52±1.22	4.73±1.13	0.028
LDL-C, mmol/L	2.73±1.05	2.86±0.88	0.070
HDL-C, mmol/L	1.07±0.34	1.15±0.37	0.005
TG, mmol/L	1.68±1.27	1.54±1.05	0.140
PCSK9, ng/mL	385.0±146.9	340.4±125.2	0.000003

All EmCB samples were from non-diabetic individuals not taking a statin or fibrate at the time of recruitment. Continuous variables presented as mean ± SD and categorical variables as N (%). Abbreviations: BMI, body mass index; HTN, anithypertensive medication; Total-C, total-cholesterol; LDL-C, Low density lipoprotein-cholesterol; HDL-C, high density lipoprotein-cholesterol; TG, triglycerides.

Table 6 Linear regression analysis of the relationships between explanatory variables and the level of PCSK9 in the EmCB sub-study.

Variable	β	P-value
Age, (years)	-0.077	0.054
Male sex	-0.010	0.775
BMI, kg/m^2	-0.015	0.686
Smoking	-0.034	0.348
HTN	-0.058	0.103
CAD	0.199	<0.001

Abbreviations: BMI, body mass index; HTN, anithypertensive medication. N=822.

Table 7 Logistic regression analysis of the association of PCSK9 with CAD in the EmCB sub-study.

Variable	β or OR (95% CI)	p
Age, (years)	-0.005 (-0.034, 0.024)	<2E-16
Male sex	3.408 (2.28, 5.094)	2.24E-09
BMI, kg/m²	0.034 (-0.019, 0.088)	0.103
Smoking	2.774 (1.654, 4.651)	0.0001
HTN	2.002 (1.368, 2.929)	0.0003
LDL-C, mmol/L	0.003 (-0.003, 0.010)	0.235
HDL-C, mmol/L	-0.018 (-0.044, 0.008)	0.089
TG, mmol/L	-0.438 (-1.716, 0.841)	0.256
PCSK9, ng/mL	0.003 (0.001, 0.005)	5.26E-06

All EmCB samples were from non-diabetic individuals not taking a statin at the time of recruitment. Results given as beta for continuous variables and odds ratio (OR) for categorical variables. Abbreviations: BMI, body mass index; HTN, anithypertensive medication; Total-C, total-cholesterol; LDL-C, Low density lipoprotein-cholesterol; HDL-C, high density lipoprotein-cholesterol; TG, triglycerides. N=677.

Table 8 Logistic regression analysis of the association of PCSK9 with acute MI in the EmCB sub-study.

Variable	β or OR (95% CI)	p
Age, (years)	-0.005 (-0.034, 0.024)	0.718
Male sex	0.745 (0.402, 1.378)	0.200
BMI, kg/m²	0.034 (-0.019, 0.088)	0.209
Smoking	1.127 (0.576, 2.207)	0.542
HTN	0.627 (0.358, 1.097)	0.370
LDL, mmol/L	0.003 (-0.003, 0.010)	0.316
HDL, mmol/L	-0.018 (-0.044, 0.008)	0.182
TG, mmol/L	-0.438 (-1.716, 0.841)	0.502
PCSK9, ng/mL	0.003 (0.001, 0.005)	0.0008

Results given as beta for continuous variables and odds ratio (OR) for categorical variables. Abbreviations: BMI, body mass index; HTN, anithypertensive medication; Total-C, total-cholesterol; LDL-C, Low density lipoprotein-cholesterol; HDL-C, high density lipoprotein-cholesterol; TG, triglycerides. N=296.

CHAPTER 6

General discussion

GWASs have long been criticized for the lack of complementary functional characterization of the resulting SNPs and how they associate with the risk of certain diseases. In my PhD work, I have done complementary functional characterization of some of the GWAS SNPs that were showed to be involved in the risk of CAD or CAD-associated events such as MI. Seven years after the discovery of 9p21.3 CAD risk locus, I showed that SNPs at the 9p21.3 CAD risk locus disrupt the binding of TEAD transcription factors and TEAD/TGFβ induction of p16 at the 9p21.3 risk locus. This mechanism accounts for the reduced expression of p16 and in part for the increased VSMCs proliferation seen in the presence of this risk locus. I also showed that the rs12960 risk variant in the protease domain of SPG7 is a gain-of-function that increases the activity of m-AAA protease, ATP and ROS production in the mitochondria. The increased mROS production caused an increase in cell proliferation. The risk SNPs at the 9p21.3 and SPG7 loci increased the risk of CAD in part by increasing cell proliferation as an established risk factor for atherosclerosis. Recently, by measuring plasma PCSK9 in two independent case-control studies, I have also shown that the association of PCSK9 variants with CAD and MI, seen by GWAS and linkage studies, is likely not by inducing atherosclerosis but rather precipitating MI through mechanisms independent and not limited to LDL-C. In general, my work has provided mechanisms or changed the way we approach genes like *PCSK9.* If PCSK9 play causative role in acute MI, then that role is

independent of LDL-C and could be through other targets that are yet to be discovered and could provide a therapeutic target for MI.

The regulation of gene expression at the 9p21.3 CAD risk locus

The 9p21.3 risk locus is as complex as the associated phenotypes. It was first described for its association with CAD. Several reports identified the association with other phenotypes such as type 2 diabetes (T2D), abdominal aortic aneurysm (AAA), open angle glaucoma, and periodontitis (38). The 9p21.3 risk locus contains several enhancers with defined risk haplotypes that are linked to distinct phenotypes suggesting that 9p21.3 risk locus exerts tissue- and disease-specific effects (38,78). For example, the CAD risk haplotype that is tagged by rs1333049 is associated with CAD and atherosclerosis burden but not with MI in patients with CAD when compared to patient with CAD only suggesting phenotype specific enhancer effect (245).

Gene transcript profiling showed no association of the CAD risk variants with genes in the vicinity of the 9p21.3 in donors' macrophages (79,246). Primary HAoSMCs from atherosclerotic plaques showed reduced expression of p16 and p15 proteins and increased proliferation when homozygous for the risk allele (65). The knockout of the 9p21.3 orthologous sequences in mice resulted in significant reduction of CDKN2A and CDKN2B expression, along with increased aortic smooth muscle cells proliferation and failure to enter senescence with the strongest effect seen in the aortic tissues (83). Consistent with these findings, I showed that 9p21.3 CAD risk locus is associated with reduced expression of p15 and p16, increased proliferation of HAoSMCs and failure to enter senescence. Given these data, the increased proliferation and reduced expression

p15 and p16 are the established biological phenotypes linked to the 9p21.3 CAD risk locus so far. Overall these data suggest a phenotype and tissue specific effects of the variants at the 9p21.3 locus.

VSMC proliferation seen with the 9p21.3 risk locus is well known to be involved in the pathogenesis of atherosclerosis and plaque growth. However, in order to intervene with the pathogenesis of this locus, we have to know the mechanisms by which p15 and p16 levels are reduced to affect VSMCs proliferation. Several attempts have been made to identify the mechanism. The knockout of the mouse orthologue has provided a model to study the disease in the animal context (83). This model supported the previous findings of the reduced p15 and p16 expression in patients with CAD (80). 45% of the knockout mice developed tumors and neoplasms, phenotypes that were not reported to associate with 9p21.3 CAD risk locus by GWASs. In an attempt to know the mechanism, another study claimed that interferon-γ long range induction of p15, p16 and other genes expression is disrupted by the risk variant that disrupts STAT1 binding at locus (78). However, my work did not support this hypothesis and showed that p15 and p16 were induced by interferon-γ independent of 9p21.3 risk locus. I used a larger sample size and many different types of cells. Consistent with our finding, *Erridge et al.* (2013) showed that the interferon-γ signaling to the interferon family of genes is not disrupted by the presence of the 9p21.3 risk locus (246). The lack of the differential effect of the 9p21.3 risk locus on p15 and p16 in LCLs is possibly because these basal differences may be masked by the repression of the *CDKN2A* locus by the Epstein-Barr virus nuclear antigens 3A and 3C (113,114). In fact, gene expression profiling of macrophages from CAD patients and controls did not show significant 9p21.3 genotype dependent-

differential expression of the genes in the vicinity suggesting tissue specific effect of 9p21.3 locus on the expression of p15 and p16 (79).

Pilbrow et al. (2013) showed that the expression of genes involved in the TGFβ pathway was affected by the 9p21.3 risk locus in multiple human tissues (143). Using the knockout mouse model of 9p21.3 risk locus, *Loinard et al*. (2014) showed reduced TGFβ dependent Smad2 signaling linked to reduced p15 (p16 was not affected) expression and increased proliferation in AoSMCs from the knockout mice. Moreover, they showed that these mice were susceptible to aneurysm and plaque rupture that were preventable by CDK inhibitor. My unbiased scanning approach for the disruption of transcription factor binding at the 9p21.3 locus identified TEAD3 as a mediator of TGFβ induction of p16 (p15 was not affected) that is disrupted by the presence of the risk locus. My findings are consistent with those of *Pilbrow et al*. (2013) with regard to the involvement of TGFβ pathway in the risk mechanism. However, my study does not support the findings of *Loinard et al*. (2014) as I show the opposite of their finding. This contradiction could be explained by species differences between mouse and human and also by models differences. They used a knockout mouse model and I used primary HAoSMCs that carry the CAD linked SNPs which is more relevant biologically and clinically to the 9p21.3 risk locus. A limitation of my study is that it does not explain the observed reduction in the levels of p15 expression seen in the presence of the 9p21.3 risk locus. The reduction in the level of p15 expression can be explained by the post-transcriptional effect of the *ANRIL* anti-sense transcript that is up-regulated with the risk locus and shown to repress the expression of *CDKN2B* locus and transcript (37,80,81). My studies provide a novel mechanism by which TEAD3 and TEAD4 induce p16 expression and mediate TGFβ

induction of p16 at the 9p21.3 locus. A peptide that activates TEADs factors to control the cell cycle and suppress gastric cancer growth in vivo has been developed (147). Future studies can employ similar strategies to prevent or mitigate atherosclerosis in CAD patients who are not homozygotes for the 9p21.3 risk allele. In my work, the mechanism by which the 9p21.3 risk locus affects the expression of CDKN2A and smooth muscle proliferation does not explain or account for the effect of 9p21.3 to confer risk of coronary artery (247) and aortic calcification (248), and this mechanism awaits future studies.

Mitochondrial ROS signaling and atherosclerosis

Increased mROS production as a by-product of ATP synthesis or due to the inability of the mitochondria to buffer ROS through proton leak dependent respiration (181) is involved in the development of chronic diseases such as atherosclerosis, diabetes and hypertension (86,89). However, there are two sides of the mROS effect; the first one is redox signaling where a small increase in the levels of mROS acts as signaling molecule for a critical cell function. The second side of mROS is the oxidative stress or damage where an excessive ROS production triggers a pathological effect by damaging DNA, proteins or lipids (249). mROS can display its two sides on one biological process such as proliferation. For example in the proliferation of normal cells, mROS antioxidants such as PRDXs are temporarily inactivated to allow for a small increase in the level of the "redox signaling" type of mROS that inactivates the cellular phosphatases that dephosphorylate growth factors such as EGFR and inhibit cell proliferation (250). Moreover, this kind of mROS is required for stem cell renewal and adult tissue

replenishment (251). On the other hand, in the pathological proliferation of cells, such as in cancer cells for example, accumulation of higher levels of mROS leads to activation of oncogenes and inactivation of tumor suppressor such as p53 leading to DNA instability (249,252). With the higher levels of mROS, activation of antioxidants such PRDX3 is required to buffer mROS and control cancer cells proliferation (253). The antioxidant, Vitamin E, prevents human breast and prostate cancers growth by inhibiting cell proliferation (254,255). The pathological proliferation of VSMCs and higher levels of mROS are involved in the development of atherosclerosis (166,188). I showed that CAD risk variant in SPG7 protein is associated with higher levels of mROS that is linked to increased cell proliferation. Using ROS scavenger, such as Tiron (vitamin E analog), rescued the cell proliferation phenotype. The higher levels of mROS were accompanied by an increased expression in level of PRDX3 likely as a counteract mechanism for mROS. My work is entirely consistent with the "oxidative stress and damage" theory of higher levels of mROS.

Although not at genome-wide significance, I pursued the rs12960 variant in *SPG7* for functional characterization because of its interesting involvement in other clinical phenotypes that might limit its association. The characterization of this variant revealed a novel mechanism whereby SPG7 processing and activity is controlled by tyrosine phosphorylation of AFG3L2. A recent study characterized an obesity risk (endpoint) variant in the Bardet-Biedl syndrome (characterized by vision loss, obesity and impaired speech) gene (*BBS10*) with *p*-value below the threshold of significance of 1.38×10^{-6}. They showed in a zebrafish model that rs202042386 variant is pathogenic and associated with T2D and obesity in Finnish and non-Finnish European (256). This study along with

my work serve as an example to not rely on the threshold of genome-wide significance for association with complex diseases could leave behind interesting pleiotropic variants. The threshold of the genome wide significance should be used to generate and guide hypotheses not to exclude variant based merely on probability and statistical tests.

The pathogenic roles of PCSK9 in CAD

PCSK9 was first discovered to associate with increased levels of LDL-C and increased risk of CAD related events such as MI. Until recently, the link between plasma PCSK9 levels and CAD and its events were not investigated. However, the linkage and GWAS studies showed that the correlation between the reduction in LDL-C levels and the CAD related events attributed to loss-of-function mutations or variants in PCSK9 was not proportional (7,212). In other words, a relatively moderate reduction in LDL-C (~25%) was accompanied by 88% reduction in CAD related events. Because this observation was made over 15 years of follow-up, the unexpectedly large reduction in the cardiovascular events is explained by the beneficial life time effect of the lower level of LDL-C over long time. Although this hypothesis is plausible, it is not experimentally or epidemiologically proven yet. An alternative explanation would be the presence of another pathological function of PCSK9 in addition to LDL-C. I have shown that plasma PCSK9 levels are associated with acute MI but not with CAD without MI or CAD with previous MI (not acute) (107). This association was independent of LDL-C and could be causal or an acute response (acute phase reactant). A recent study showed positive correlation between plasma PCSK9 and CAD severity, independent of LDL-C (244). Our large study of two independent cohorts could not support the association with CAD

severity but is consistent with the fact the PCSK9 levels do not correlate with LDL-C. In recent studies, plasma PCSK9 levels showed positive correlations with white blood cell count (WBCC) and fibrinogen levels in patients with stable CAD (257,258). Increased fibrinogen levels and WBCC are correlated with acute myocardial infarction (259). Through the binding of PCSK9 to LRP8 receptor which promotes platelet aggregation, higher levels of plasma PCSK9 could cause MI through conversion of fibrinogen to fibrin to trigger thrombosis (235,236). My study has the limitation of the cross sectional design; therefore future experimental and longitudinal studies are required to examine the exact role played by PCSK9 in AMI and whether or not that involves new targets for PCSK9.

My study has important implications for therapies that target PCSK9 with the intent to lower cholesterol beyond levels that can be achieved with statins. In particular, therapies aimed at blocking PCSK9 interaction with the LDL-receptor may achieve robust LDL-C reductions by preventing degradation of the LDL-receptor (26,27,217,260). However, since LDL-receptor is one of the mechanisms required for PCSK9 clearance, the antibody strategy would prevent PCSK9 uptake and co-degradation with the LDL-receptor and this approach is likely to associate with elevated levels of circulating PCSK9. The plasma PCSK9 levels in these clinical trials were not reported and are likely to be elevated by the antibody therapy because it prevents PCSK9 degradation. The elevated plasma PCSK9 after the administration of the antibody could potentially increase the risk of AMI.

Future insights

Strengths of my PhD studies are the clinical aspect and impact derived from the GWASs of the CAD risk loci derived from human cohorts. The use of large sample size and the disease-relevant cells such as HAoSMCs are other strengths of my studies. These strengths move the field steps ahead in term of their future medical applications. Moreover, my studies show the power of GWASs to identify variants that provide novel mechanisms and therapeutic targets for atherosclerosis. In the future with the advancement and reduced cost of next generation sequencing (NGS), the generation of big and genome wide data will not be difficult. The hard task will be to mine, analyze and functionally understand these data using sophisticated bioinformatics tools and most importantly applying the experimental biology to validate the significance and the clinical relevance of these data.

rs10811656 and rs4977757 are two functional SNPs at the 9p21.3 risk locus that increase the proliferation of HAoSMCs by the lowering of p15 and p16 expression through the disruption of TEAD and TEAD-mediated TGF-B induction of p16. Designing polypeptide that mimics TEAD3 and interacts with Smad3 to induce p16 expression could prove useful in attenuating the risk of atherosclerosis in suseptible patients who are heterozygotes or homozygotes for the non-risk locus. Future bioinformatics and functional studies are warranted to scan the 9p21.3 locus for non-coding RNAs that might be involved in CAD risk by the locus.

To further understand the physiological and clinical importance of the mechanism of the regulation of SPG7 processing by phosphoryrlation, generation of transgenic mice carrying the AFG3L2 mutants is required. Such studies provide valuable information about regulation of the m-AAA protease activity not only in CAD but also in the

neurdegenrative diseases that are caused by loss-of-function mutation in AFG3L2 or SPG7. A refined metanalysis in cohorts that exclude controls and cases with phenotypes such as diabetes and hypertension could result in a genome-wide-signifcant association with CAD due to the minimization of the effect of pleiotropy.

Alternative approaches to knockdown or knockout *PCSK9* will be ideal to avoid the possible side effects of the antibody strategy of elevated circulating PCSK9. For example, studies in hypercholesterolemic non-human primates showed that strategies that specifically lower circulating PCSK9 levels using antisense oligonucleotides was successful at lowering LDL-C (261). A recent study used the CRISPR-Cas9 genome editing to conditionally knock out PCSK9 expression in mouse liver was successful at lowering plasma PCSK9 and LDL-C together (262). These strategies could be developed to be used in human to reduce PCSK9 and LDL-C levels. However, these strategies have major limitations of the off-target effect and the introduction of deleterious mutations to the human genome. Addressing these limitations will make them medically safe and attractive.

Appendices

RE: JACC061312-2422DR (Interferon-{lower case gamma} activates expression of p15 and p16 regardles ...)

From:	jaccsd <jaccsd@acc.org>
To:	"nalmontashiri@ottawaheart.ca" <nalmontashiri@ottawaheart.ca>
Date:	Friday - May 16, 2014 10:26 PM
Subject:	RE: JACC061312-2422DR (Interferon-{lower case gamma} activates expression of p15 and p16 regardless of ...)
Attachments:	Mime.822

Dear Mr. Almontashiri,

I've consulted our executive editor, Glenn Collins, and he has granted permission for you to use the paper for your thesis dissertation. You would only need a formal copyright release if they were to be re-used in anothe publication. For the purpose of your thesis, you may simply state that the paper is "Reprinted with permission"and cite the JACC reference.

Best of luck with your dissertation!

Regards,
Michelle McMullen
JACC Editorial Office
jaccsd@acc.org
Submit online at http://www.jaccsubmit.org
Read online at http://content.onlinejacc.org/

Appendix 1. Permission from the Journal of the American College of Cardiology to reprint paper (106) in the PhD dissertation.

REFERENCES

1. Libby P. Inflammation in atherosclerosis. Nature 2002;420:868-74.
2. Wald NJ, Law MR. A strategy to reduce cardiovascular disease by more than 80%. BMJ 2003;326:1419.
3. Lusis AJ. Atherosclerosis. Nature 2000;407:233-41.
4. Nora JJ, Lortscher RH, Spangler RD, Nora AH, Kimberling WJ. Genetic--epidemiologic study of early-onset ischemic heart disease. Circulation 1980;61:503-8.
5. Rissanen AM. Familial occurrence of coronary heart disease: effect of age at diagnosis. Am J Cardiol 1979;44:60-6.
6. Roberts R, Stewart AF. The genetics of coronary artery disease. Curr Opin Cardiol 2012;27:221-7.
7. Schunkert H, Konig IR, Kathiresan S et al. Large-scale association analysis identifies 13 new susceptibility loci for coronary artery disease. Nat Genet 2011;43:333-8.
8. Roberts R, Stewart AF. Genes and coronary artery disease: where are we? J Am Coll Cardiol 2012;60:1715-21.
9. Finn AV, Nakano M, Narula J, Kolodgie FD, Virmani R. Concept of vulnerable/unstable plaque. Arterioscler Thromb Vasc Biol 2010;30:1282-92.
10. Falk E. Pathogenesis of atherosclerosis. J Am Coll Cardiol 2006;47:C7-12.
11. Allahverdian S, Chehroudi AC, McManus BM, Abraham T, Francis GA. Contribution of intimal smooth muscle cells to cholesterol accumulation and macrophage-like cells in human atherosclerosis. Circulation 2014;129:1551-9.
12. Glass CK, Witztum JL. Atherosclerosis. the road ahead. Cell 2001;104:503-16.
13. Abifadel M, Rabes JP, Jambart S et al. The molecular basis of familial hypercholesterolemia in Lebanon: spectrum of LDLR mutations and role of PCSK9 as a modifier gene. Hum Mutat 2009;30:E682-91.
14. Seidah NG, Benjannet S, Wickham L et al. The secretory proprotein convertase neural apoptosis-regulated convertase 1 (NARC-1): liver regeneration and neuronal differentiation. Proc Natl Acad Sci U S A 2003;100:928-33.
15. Kathiresan S. A PCSK9 missense variant associated with a reduced risk of early-onset myocardial infarction. N Engl J Med 2008;358:2299-300.
16. Grefhorst A, McNutt MC, Lagace TA, Horton JD. Plasma PCSK9 preferentially reduces liver LDL receptors in mice. J Lipid Res 2008;49:1303-11.
17. Gotto AM, Jr. The cardiology patient page. Statins: powerful drugs for lowering cholesterol: advice for patients. Circulation 2002;105:1514-6.
18. Allen Maycock CA, Muhlestein JB, Horne BD et al. Statin therapy is associated with reduced mortality across all age groups of individuals with significant coronary disease, including very elderly patients. J Am Coll Cardiol 2002;40:1777-85.
19. Miyazawa H, Honda T, Miyauchi S et al. Increased serum PCSK9 concentrations are associated with periodontal infection but do not correlate with LDL cholesterol concentration. Clin Chim Acta 2012;413:154-9.
20. DeStefano F, Anda RF, Kahn HS, Williamson DF, Russell CM. Dental disease and risk of coronary heart disease and mortality. BMJ 1993;306:688-91.
21. Kostner GM, Gavish D, Leopold B, Bolzano K, Weintraub MS, Breslow JL. HMG CoA reductase inhibitors lower LDL cholesterol without reducing Lp(a) levels. Circulation 1989;80:1313-9.
22. Careskey HE, Davis RA, Alborn WE, Troutt JS, Cao G, Konrad RJ. Atorvastatin increases human serum levels of proprotein convertase subtilisin/kexin type 9. J Lipid Res 2008;49:394-8.
23. Awan Z, Seidah NG, Macfadyen JG et al. Rosuvastatin, Proprotein Convertase Subtilisin/Kexin Type 9 Concentrations, and LDL Cholesterol Response: the JUPITER Trial. Clin Chem 2012;58:183-9.
24. Dubuc G, Chamberland A, Wassef H et al. Statins upregulate PCSK9, the gene encoding the proprotein convertase neural apoptosis-regulated convertase-1 implicated in familial hypercholesterolemia. Arterioscler Thromb Vasc Biol 2004;24:1454-9.

25. Dong B, Wu M, Li H et al. Strong induction of PCSK9 gene expression through HNF1alpha and SREBP2: mechanism for the resistance to LDL-cholesterol lowering effect of statins in dyslipidemic hamsters. J Lipid Res 2010;51:1486-95.
26. Stein EA, Mellis S, Yancopoulos GD et al. Effect of a monoclonal antibody to PCSK9 on LDL cholesterol. N Engl J Med 2012;366:1108-18.
27. Stein EA, Raal F. Reduction of low-density lipoprotein cholesterol by monoclonal antibody inhibition of PCSK9. Annu Rev Med 2014;65:417-31.
28. Hannon GJ, Beach D. p15INK4B is a potential effector of TGF-beta-induced cell cycle arrest. Nature 1994;371:257-61.
29. Hara E, Smith R, Parry D, Tahara H, Stone S, Peters G. Regulation of p16CDKN2 expression and its implications for cell immortalization and senescence. Mol Cell Biol 1996;16:859-67.
30. Lund G, Andersson L, Lauria M et al. DNA methylation polymorphisms precede any histological sign of atherosclerosis in mice lacking apolipoprotein E. J Biol Chem 2004;279:29147-54.
31. Sharma P, Garg G, Kumar A et al. Genome wide DNA methylation profiling for epigenetic alteration in coronary artery disease patients. Gene 2014;541:31-40.
32. Sharma P, Kumar J, Garg G et al. Detection of altered global DNA methylation in coronary artery disease patients. DNA Cell Biol 2008;27:357-65.
33. Kim J, Kim JY, Song KS et al. Epigenetic changes in estrogen receptor beta gene in atherosclerotic cardiovascular tissues and in-vitro vascular senescence. Biochim Biophys Acta 2007;1772:72-80.
34. Krishnamurthy J, Torrice C, Ramsey MR et al. Ink4a/Arf expression is a biomarker of aging. J Clin Invest 2004;114:1299-307.
35. Kuilman T, Michaloglou C, Mooi WJ, Peeper DS. The essence of senescence. Genes Dev 2010;24:2463-79.
36. Rayess H, Wang MB, Srivatsan ES. Cellular senescence and tumor suppressor gene p16. Int J Cancer 2012;130:1715-25.
37. Zhuang J, Peng W, Li H et al. Methylation of p15INK4b and expression of ANRIL on chromosome 9p21 are associated with coronary artery disease. PLoS One 2012;7:e47193.
38. Chen HH, Almontashiri NA, Antoine D, Stewart AF. Functional genomics of the 9p21.3 locus for atherosclerosis: clarity or confusion? Current cardiology reports 2014;16:502.
39. Ross R. Atherosclerosis--an inflammatory disease. N Engl J Med 1999;340:115-26.
40. Rekhter MD, Gordon D. Active proliferation of different cell types, including lymphocytes, in human atherosclerotic plaques. Am J Pathol 1995;147:668-77.
41. Kragel AH, Reddy SG, Wittes JT, Roberts WC. Morphometric analysis of the composition of atherosclerotic plaques in the four major epicardial coronary arteries in acute myocardial infarction and in sudden coronary death. Circulation 1989;80:1747-56.
42. Grainger DJ. Transforming growth factor beta and atherosclerosis: so far, so good for the protective cytokine hypothesis. Arterioscler Thromb Vasc Biol 2004;24:399-404.
43. Kojima S, Harpel PC, Rifkin DB. Lipoprotein (a) inhibits the generation of transforming growth factor beta: an endogenous inhibitor of smooth muscle cell migration. J Cell Biol 1991;113:1439-45.
44. Grainger DJ, Metcalfe JC, Grace AA, Mosedale DE. Transforming growth factor-beta dynamically regulates vascular smooth muscle differentiation in vivo. J Cell Sci 1998;111 (Pt 19):2977-88.
45. Berk BC. Vascular smooth muscle growth: autocrine growth mechanisms. Physiol Rev 2001;81:999-1030.
46. Tashiro H, Shimokawa H, Sadamatu K, Yamamoto K. Prognostic significance of plasma concentrations of transforming growth factor-beta in patients with coronary artery disease. Coron Artery Dis 2002;13:139-43.
47. Reifenberg K, Cheng F, Orning C et al. Overexpression of TGF-ss1 in macrophages reduces and stabilizes atherosclerotic plaques in ApoE-deficient mice. PLoS One 2012;7:e40990.
48. Borkowski P, Robinson MJ, Kusiak JW, Borkowski A, Brathwaite C, Mergner WJ. Studies on TGF-beta 1 gene expression in the intima of the human aorta in regions with high and low

probability of developing atherosclerotic lesions. Modern pathology : an official journal of the United States and Canadian Academy of Pathology, Inc 1995;8:478-82.
49. Jiang X, Zeng HS, Guo Y, Zhou ZB, Tang BS, Li FK. The expression of matrix metalloproteinases-9, transforming growth factor-beta1 and transforming growth factor-beta receptor I in human atherosclerotic plaque and their relationship with plaque stability. Chin Med J (Engl) 2004;117:1825-9.
50. Inamoto S, Kwartler CS, Lafont AL et al. TGFBR2 mutations alter smooth muscle cell phenotype and predispose to thoracic aortic aneurysms and dissections. Cardiovasc Res 2010;88:520-9.
51. Loeys BL, Chen J, Neptune ER et al. A syndrome of altered cardiovascular, craniofacial, neurocognitive and skeletal development caused by mutations in TGFBR1 or TGFBR2. Nat Genet 2005;37:275-81.
52. Reynisdottir I, Polyak K, Iavarone A, Massague J. Kip/Cip and Ink4 Cdk inhibitors cooperate to induce cell cycle arrest in response to TGF-beta. Genes Dev 1995;9:1831-45.
53. Vijayachandra K, Higgins W, Lee J, Glick A. Induction of p16ink4a and p19ARF by TGFbeta1 contributes to growth arrest and senescence response in mouse keratinocytes. Mol Carcinog 2009;48:181-6.
54. Fujii M, Toyoda T, Nakanishi H et al. TGF-beta synergizes with defects in the Hippo pathway to stimulate human malignant mesothelioma growth. J Exp Med 2012;209:479-94.
55. Stewart AF, Suzow J, Kubota T, Ueyama T, Chen HH. Transcription factor RTEF-1 mediates alpha1-adrenergic reactivation of the fetal gene program in cardiac myocytes. Circ Res 1998;83:43-9.
56. Pobbati AV, Hong W. Emerging roles of TEAD transcription factors and its coactivators in cancers. Cancer Biol Ther 2013;14:390-8.
57. Yoshida T. MCAT elements and the TEF-1 family of transcription factors in muscle development and disease. Arterioscler Thromb Vasc Biol 2008;28:8-17.
58. The International HapMap Project. Nature 2003;426:789-96.
59. Almontashiri NA, Chen HH, Mailloux RJ et al. SPG7 Variant Escapes Phosphorylation-Regulated Processing by AFG3L2, Elevates Mitochondrial ROS, and Is Associated with Multiple Clinical Phenotypes. Cell Rep 2014;7:834-47.
60. Bonn F, Pantakani K, Shoukier M, Langer T, Mannan AU. Functional evaluation of paraplegin mutations by a yeast complementation assay. Hum Mutat 2010;31:617-21.
61. Bush WS, Moore JH. Chapter 11: Genome-wide association studies. PLoS Comput Biol 2012;8:e1002822.
62. Dube JB, Hegele RA. Genetics 100 for cardiologists: basics of genome-wide association studies. Can J Cardiol 2013;29:10-7.
63. Manolio TA, Collins FS, Cox NJ et al. Finding the missing heritability of complex diseases. Nature 2009;461:747-53.
64. Preuss M, Konig IR, Thompson JR et al. Design of the Coronary ARtery DIsease Genome-Wide Replication And Meta-Analysis (CARDIoGRAM) Study: A Genome-wide association meta-analysis involving more than 22 000 cases and 60 000 controls. Circ Cardiovasc Genet 2010;3:475-83.
65. Davies RW, Dandona S, Stewart AFR et al. Improved prediction of cardiovascular disease based on a panel of single nucleotide polymorphisms identified through genome-wide association studies. Circ Cardiovasc Genet 2010;3:468-74.
66. Estivill X, Armengol L. Copy number variants and common disorders: filling the gaps and exploring complexity in genome-wide association studies. PLoS Genet 2007;3:1787-99.
67. Lanktree MB, Hegele RA. Gene-gene and gene-environment interactions: new insights into the prevention, detection and management of coronary artery disease. Genome Med 2009;1:28.
68. Shirts BH, Hasstedt SJ, Hopkins PN, Hunt SC. Evaluation of the gene-age interactions in HDL cholesterol, LDL cholesterol, and triglyceride levels: the impact of the SORT1 polymorphism on LDL cholesterol levels is age dependent. Atherosclerosis 2011;217:139-41.
69. Ardissino D, Berzuini C, Merlini PA et al. Influence of 9p21.3 genetic variants on clinical and angiographic outcomes in early-onset myocardial infarction. J Am Coll Cardiol 2011;58:426-34.

70. McPherson R, Pertsemlidis A, Kavaslar N et al. A common allele on chromosome 9 associated with coronary heart disease. Science 2007;316:1488-91.
71. Genome-wide association study of 14,000 cases of seven common diseases and 3,000 shared controls. Nature 2007;447:661-78.
72. Helgadottir A, Thorleifsson G, Magnusson KP et al. The same sequence variant on 9p21 associates with myocardial infarction, abdominal aortic aneurysm and intracranial aneurysm. Nat Genet 2008;40:217-24.
73. Wellcome_Trust_Case_Control_Consortium. Genome-wide association study of 14,000 cases of seven common diseases and 3,000 shared controls. Nature 2007;447:661-78.
74. Helgadottir A, Thorleifsson G, Manolescu A et al. A common variant on chromosome 9p21 affects the risk of myocardial infarction. Science 2007;316:1491-3.
75. Samani NJ, Erdmann J, Hall AS et al. Genomewide association analysis of coronary artery disease. N Engl J Med 2007;357:443-53.
76. Musunuru K. Enduring mystery of the chromosome 9p21.3 locus. Circ Cardiovasc Genet 2013;6:224-5.
77. Dandona S, Stewart AF, Chen L et al. Gene dosage of the common variant 9p21 predicts severity of coronary artery disease. J Am Coll Cardiol 2010;56:479-86.
78. Harismendy O, Notani D, Song X et al. 9p21 DNA variants associated with coronary artery disease impair interferon-gamma signalling response. Nature 2011;470:264-8.
79. Zollbrecht C, Grassl M, Fenk S et al. Expression pattern in human macrophages dependent on 9p21.3 coronary artery disease risk locus. Atherosclerosis 2013;227:244-9.
80. Jarinova O, Stewart AF, Roberts R et al. Functional analysis of the chromosome 9p21.3 coronary artery disease risk locus. Arterioscler Thromb Vasc Biol 2009;29:1671-7.
81. Yap KL, Li S, Munoz-Cabello AM et al. Molecular interplay of the noncoding RNA ANRIL and methylated histone H3 lysine 27 by polycomb CBX7 in transcriptional silencing of INK4a. Mol Cell 2010;38:662-74.
82. Motterle A, Pu X, Wood H et al. Functional analyses of coronary artery disease associated variation on chromosome 9p21 in vascular smooth muscle cells. Hum Mol Genet 2012;21:4021-9.
83. Visel A, Zhu Y, May D et al. Targeted deletion of the 9p21 non-coding coronary artery disease risk interval in mice. Nature 2010;464:409-12.
84. Chen Q, Moghaddas S, Hoppel CL, Lesnefsky EJ. Ischemic defects in the electron transport chain increase the production of reactive oxygen species from isolated rat heart mitochondria. Am J Physiol Cell Physiol 2008;294:C460-6.
85. Liesa M, Palacin M, Zorzano A. Mitochondrial dynamics in mammalian health and disease. Physiol Rev 2009;89:799-845.
86. Wallace DC. A mitochondrial bioenergetic etiology of disease. J Clin Invest 2013;123:1405-12.
87. Azumi H, Inoue N, Ohashi Y et al. Superoxide generation in directional coronary atherectomy specimens of patients with angina pectoris: important role of NAD(P)H oxidase. Arterioscler Thromb Vasc Biol 2002;22:1838-44.
88. Delafontaine P, Ku L. Reactive oxygen species stimulate insulin-like growth factor I synthesis in vascular smooth muscle cells. Cardiovasc Res 1997;33:216-22.
89. Madamanchi NR, Vendrov A, Runge MS. Oxidative stress and vascular disease. Arterioscler Thromb Vasc Biol 2005;25:29-38.
90. Sigala F, Kotsinas A, Savari P et al. Oxidized LDL in human carotid plaques is related to symptomatic carotid disease and lesion instability. J Vasc Surg 2010;52:704-13.
91. Hansen JM, Go YM, Jones DP. Nuclear and mitochondrial compartmentation of oxidative stress and redox signaling. Annu Rev Pharmacol Toxicol 2006;46:215-34.
92. McBride HM, Neuspiel M, Wasiak S. Mitochondria: more than just a powerhouse. Curr Biol 2006;16:R551-60.
93. Araki M, Nanri H, Ejima K et al. Antioxidant function of the mitochondrial protein SP-22 in the cardiovascular system. J Biol Chem 1999;274:2271-8.
94. Matsushima S, Ide T, Yamato M et al. Overexpression of mitochondrial peroxiredoxin-3 prevents left ventricular remodeling and failure after myocardial infarction in mice. Circulation 2006;113:1779-86.

95. Yamashita N, Hoshida S, Otsu K, Asahi M, Kuzuya T, Hori M. Exercise provides direct biphasic cardioprotection via manganese superoxide dismutase activation. J Exp Med 1999;189:1699-706.
96. Li Y, Huang TT, Carlson EJ et al. Dilated cardiomyopathy and neonatal lethality in mutant mice lacking manganese superoxide dismutase. Nat Genet 1995;11:376-81.
97. Bota DA, Davies KJ. Lon protease preferentially degrades oxidized mitochondrial aconitase by an ATP-stimulated mechanism. Nat Cell Biol 2002;4:674-80.
98. Maltecca F, Casari G. In vivo detection of oxidized proteins: a practical approach to tissue-derived mitochondria. Methods Mol Biol 2010;648:257-67.
99. Almajan ER, Richter R, Paeger L et al. AFG3L2 supports mitochondrial protein synthesis and Purkinje cell survival. J Clin Invest 2012;122:4048-58.
100. Nolden M, Ehses S, Koppen M, Bernacchia A, Rugarli EI, Langer T. The m-AAA protease defective in hereditary spastic paraplegia controls ribosome assembly in mitochondria. Cell 2005;123:277-89.
101. Rugarli EI, Langer T. Mitochondrial quality control: a matter of life and death for neurons. EMBO J 2012;31:1336-49.
102. Koppen M, Bonn F, Ehses S, Langer T. Autocatalytic processing of m-AAA protease subunits in mitochondria. Mol Biol Cell 2009;20:4216-24.
103. Atorino L, Silvestri L, Koppen M et al. Loss of m-AAA protease in mitochondria causes complex I deficiency and increased sensitivity to oxidative stress in hereditary spastic paraplegia. J Cell Biol 2003;163:777-87.
104. De Michele G, De Fusco M, Cavalcanti F et al. A new locus for autosomal recessive hereditary spastic paraplegia maps to chromosome 16q24.3. Am J Hum Genet 1998;63:135-9.
105. Di Bella D, Lazzaro F, Brusco A et al. Mutations in the mitochondrial protease gene AFG3L2 cause dominant hereditary ataxia SCA28. Nat Genet 2010;42:313-21.
106. Almontashiri NA, Fan M, Cheng BL, Chen HH, Roberts R, Stewart AF. Interferon-gamma activates expression of p15 and p16 regardless of 9p21.3 coronary artery disease risk genotype. J Am Coll Cardiol 2013;61:143-7.
107. Almontashiri NA, Vilmundarson RO, Ghasemzadeh N et al. Plasma PCSK9 Levels Are Elevated with Acute Myocardial Infarction in Two Independent Retrospective Angiographic Studies. PLoS One 2014;9:e106294.
108. Samani NJ, Erdmann J, Hall AS et al. Genomewide association analysis of coronary artery disease. N Engl J Med 2007;357:443-53.
109. Dandona S, Stewart AFR, Chen L et al. Gene dosage of the common variant 9p21 predicts severity of coronary artery disease. J Am Coll Cardiol 2010;56:479-86.
110. Chan K, Motterle A, Laxton RC, Ye S. Common variant on chromosome 9p21 predicts severity of coronary artery disease. J Am Coll Cardiol 2011;57:1497-8; author reply 1498-9.
111. Sandhu C, Garbe J, Bhattacharya N et al. Transforming growth factor beta stabilizes p15INK4B protein, increases p15INK4B-cdk4 complexes, and inhibits cyclin D1-cdk4 association in human mammary epithelial cells. Mol Cell Biol 1997;17:2458-67.
112. Lal A, Kim HH, Abdelmohsen K et al. p16(INK4a) translation suppressed by miR-24. PLoS One 2008;3:e1864.
113. Maruo S, Zhao B, Johannsen E, Kieff E, Zou J, Takada K. Epstein-Barr virus nuclear antigens 3C and 3A maintain lymphoblastoid cell growth by repressing p16INK4A and p14ARF expression. Proc Natl Acad Sci U S A 2011;108:1919-24.
114. Skalska L, White RE, Franz M, Ruhmann M, Allday MJ. Epigenetic repression of p16(INK4A) by latent Epstein-Barr virus requires the interaction of EBNA3A and EBNA3C with CtBP. PLoS Pathog 2010;6:e1000951.
115. Chaturvedi V, Cesnjaj M, Bacon P et al. Role of INK4a/Arf locus-encoded senescent checkpoints activated in normal and psoriatic keratinocytes. Am J Pathol 2003;162:161-70.
116. Hu G, Gong AY, Liu J, Zhou R, Deng C, Chen XM. miR-221 suppresses ICAM-1 translation and regulates interferon-gamma-induced ICAM-1 expression in human cholangiocytes. Am J Physiol Gastrointest Liver Physiol 2010;298:G542-50.
117. Tedgui A, Mallat Z. Cytokines in atherosclerosis: pathogenic and regulatory pathways. Physiol Rev 2006;86:515-81.

118. Stewart AFR, Larkin SB, Farrance IKG, Mar JH, Hall DE, Ordahl CP. Muscle-enriched TEF-1 isoforms bind M-CAT elements from muscle-specific promoters and differentially activate transcription. J Biol Chem 1994;269:3147-3150.
119. Nabel EG, Braunwald E. A tale of coronary artery disease and myocardial infarction. N Engl J Med 2012;366:54-63.
120. WTCCC. Genome-wide association study of 14,000 cases of seven common diseases and 3,000 shared controls. Nature 2007;447:661-78.
121. Dandona S, Chen L, Fan M et al. The transcription factor GATA-2 does not associate with angiographic coronary artery disease in the Ottawa Heart Genomics and Cleveland Clinic GeneBank Studies. Hum Genet 2010;127:101-5.
122. Patel RS, Su S, Neeland IJ et al. The chromosome 9p21 risk locus is associated with angiographic severity and progression of coronary artery disease. Eur Heart J 2010;31:3017-23.
123. Loinard C, Basatemur G, Masters L et al. Deletion of 9p21 Non-Coding Cardiovascular Risk Interval in Mice Alters Smad2 Signaling and Promotes Vascular Aneurysm. Circ Cardiovasc Genet 2014.
124. Nordon IM, Hinchliffe RJ, Loftus IM, Thompson MM. Pathophysiology and epidemiology of abdominal aortic aneurysms. Nat Rev Cardiol 2011;8:92-102.
125. Almontashiri NA, Fan M, Cheng BL, Chen HH, Roberts R, Stewart AFR. Interferon-gamma Activates Expression of p15 and p16 Regardless of 9p21.3 Coronary Artery Disease Risk Genotype. J Am Coll Cardiol 2013;61:143-7.
126. Stewart AFR, Richard CW, 3rd, Suzow J et al. Cloning of human RTEF-1, a transcriptional enhancer factor-1-related gene preferentially expressed in skeletal muscle: evidence for an ancient multigene family. Genomics 1996;37:68-76.
127. Chen HH, Mullett SJ, Stewart AFR. Vgl-4, a novel member of the vestigial-like family of transcription cofactors, regulates alpha1-adrenergic activation of gene expression in cardiac myocytes. J Biol Chem 2004;279:30800-6.
128. Mahoney WM, Jr., Hong JH, Yaffe MB, Farrance IK. The transcriptional co-activator TAZ interacts differentially with transcriptional enhancer factor-1 (TEF-1) family members. Biochem J 2005;388:217-25.
129. Maeda T, Chapman DL, Stewart AFR. Mammalian Vestigial-like 2, a Cofactor of TEF-1 and MEF2 Transcription Factors That Promotes Skeletal Muscle Differentiation. J Biol Chem 2002;277:48889-98.
130. Benhaddou A, Keime C, Ye T et al. Transcription factor TEAD4 regulates expression of myogenin and the unfolded protein response genes during C2C12 cell differentiation. Cell Death Differ 2012;19:220-31.
131. Cao X, Pfaff SL, Gage FH. YAP regulates neural progenitor cell number via the TEA domain transcription factor. Genes Dev 2008;22:3320-34.
132. Gan Q, Yoshida T, Li J, Owens GK. Smooth muscle cells and myofibroblasts use distinct transcriptional mechanisms for smooth muscle alpha-actin expression. Circ Res 2007;101:883-92.
133. Leask A, Holmes A, Black CM, Abraham DJ. Connective tissue growth factor gene regulation. Requirements for its induction by transforming growth factor-beta 2 in fibroblasts. J Biol Chem 2003;278:13008-15.
134. Farrance IK, Mar JH, Ordahl CP. M-CAT binding factor is related to the SV40 enhancer binding factor, TEF-1. J Biol Chem 1992;267:17234-40.
135. Maeda T, Maeda M, Stewart AFR. TEF-1 transcription factors regulate activity of the mouse mammary tumor virus LTR. Biochem Biophys Res Commun 2002;296:1279-85.
136. Hellman LM, Fried MG. Electrophoretic mobility shift assay (EMSA) for detecting protein-nucleic acid interactions. Nat Protoc 2007;2:1849-61.
137. Chen Z, Friedrich GA, Soriano P. Transcriptional enhancer factor 1 disruption by a retroviral gene trap leads to heart defects and embryonic lethality in mice. Genes Dev 1994;8:2293-301.
138. Milewski RC, Chi NC, Li J, Brown C, Lu MM, Epstein JA. Identification of minimal enhancer elements sufficient for Pax3 expression in neural crest and implication of Tead2 as a regulator of Pax3. Development 2004;131:829-37.

139. Zheng Y, Devitt C, Liu J, Mei J, Skapek SX. A distant, cis-acting enhancer drives induction of Arf by Tgfbeta in the developing eye. Dev Biol 2013;380:49-57.
140. MacLellan WR, Lee TC, Schwartz RJ, Schneider MD. Transforming growth factor-β response elements of the skeletal α-actin gene. Combinatorial action of serum response factor, YY1, and the SV40 enhancer-binding protein, TEF-1. J Biol Chem 1994;269:16754-60.
141. Lenk GM, Tromp G, Weinsheimer S, Gatalica Z, Berguer R, Kuivaniemi H. Whole genome expression profiling reveals a significant role for immune function in human abdominal aortic aneurysms. BMC Genomics 2007;8:237.
142. Reifenberg K, Cheng F, Orning C et al. Overexpression of TGF-b1 in macrophages reduces and stabilizes atherosclerotic plaques in ApoE-deficient mice. PLoS One 2012;7:e40990.
143. Pilbrow AP, Folkersen L, Pearson JF et al. The chromosome 9p21.3 coronary heart disease risk allele is associated with altered gene expression in normal heart and vascular tissues. PLoS One 2012;7:e39574.
144. Gibbons GH, Pratt RE, Dzau VJ. Vascular smooth muscle cell hypertrophy vs. hyperplasia. Autocrine transforming growth factor-beta 1 expression determines growth response to angiotensin II. J Clin Invest 1992;90:456-61.
145. Sharpless NE, Bardeesy N, Lee KH et al. Loss of p16Ink4a with retention of p19Arf predisposes mice to tumorigenesis. Nature 2001;413:86-91.
146. Gizard F, Amant C, Barbier O et al. PPAR alpha inhibits vascular smooth muscle cell proliferation underlying intimal hyperplasia by inducing the tumor suppressor p16INK4a. J Clin Invest 2005;115:3228-38.
147. Jiao S, Wang H, Shi Z et al. A peptide mimicking VGLL4 function acts as a YAP antagonist therapy against gastric cancer. Cancer Cell 2014;25:166-80.
148. Ueyama T, Zhu C, Valenzuela YM, Suzow JG, Stewart AFR. Identification of the functional domain in the transcription factor RTEF-1 that mediates α_1-adrenergic signaling in hypertrophied cardiac myocytes. J Biol Chem 2000;275:17476-17480.
149. Ueyama T, Zhu C, Valenzuela YM, Suzow JG, Stewart AF. Identification of the functional domain in the transcription factor RTEF-1 that mediates alpha 1-adrenergic signaling in hypertrophied cardiac myocytes. J Biol Chem 2000;275:17476-80.
150. Maeda T, Mazzulli JR, Farrance IK, Stewart AFR. Mouse DTEF-1 (ETFR-1, TEF-5) is a transcriptional activator in alpha1-adrenergic agonist-stimulated cardiac myocytes. J Biol Chem 2002.
151. Kariya K, Karns LR, Simpson PC. An enhancer core element mediates stimulation of the rat beta-myosin heavy chain promoter by an alpha 1-adrenergic agonist and activated beta-protein kinase C in hypertrophy of cardiac myocytes. J Biol Chem 1994;269:3775-82.
152. Almontashiri NA, Chen HH, Mailloux RJ et al. SPG7 Variant Escapes Phosphorylation-Regulated Processing by AFG3L2, Elevates Mitochondrial ROS, and Is Associated with Multiple Clinical Phenotypes. Cell reports 2014;7:834-47.
153. Pearse RN, Feinman R, Shuai K, Darnell JE, Jr., Ravetch JV. Interferon gamma-induced transcription of the high-affinity Fc receptor for IgG requires assembly of a complex that includes the 91-kDa subunit of transcription factor ISGF3. Proc Natl Acad Sci U S A 1993;90:4314-8.
154. Dennler S, Itoh S, Vivien D, ten Dijke P, Huet S, Gauthier JM. Direct binding of Smad3 and Smad4 to critical TGF beta-inducible elements in the promoter of human plasminogen activator inhibitor-type 1 gene. EMBO J 1998;17:3091-100.
155. Suzuki YJ, Day RM, Tan CC et al. Activation of GATA-4 by serotonin in pulmonary artery smooth muscle cells. J Biol Chem 2003;278:17525-31.
156. Furuita K, Ishizaki I, Fukada H et al. Studies of DNA recognition mechanism of transcription factor IRF-4. Nucleic Acids Symp Ser (Oxf) 2006:259-60.
157. Chen HH, Maeda T, Mullett SJ, Stewart AF. Transcription cofactor Vgl-2 is required for skeletal muscle differentiation. Genesis 2004;39:273-9.
158. Okada Y, Nagai R, Sato T et al. Homeodomain proteins MEIS1 and PBXs regulate the lineage-specific transcription of the platelet factor 4 gene. Blood 2003;101:4748-56.
159. Horard B, Tatout C, Poux S, Pirrotta V. Structure of a polycomb response element and in vitro binding of polycomb group complexes containing GAGA factor. Mol Cell Biol 2000;20:3187-97.

160. Rehli M, Poltorak A, Schwarzfischer L, Krause SW, Andreesen R, Beutler B. PU.1 and interferon consensus sequence-binding protein regulate the myeloid expression of the human Toll-like receptor 4 gene. J Biol Chem 2000;275:9773-81.
161. Madamanchi NR, Runge MS. Mitochondrial dysfunction in atherosclerosis. Circ Res 2007;100:460-73.
162. Lowell BB, Shulman GI. Mitochondrial dysfunction and type 2 diabetes. Science 2005;307:384-7.
163. Arlt H, Tauer R, Feldmann H, Neupert W, Langer T. The YTA10-12 complex, an AAA protease with chaperone-like activity in the inner membrane of mitochondria. Cell 1996;85:875-85.
164. Hornig-Do HT, Tatsuta T, Buckermann A et al. Nonsense mutations in the COX1 subunit impair the stability of respiratory chain complexes rather than their assembly. EMBO J 2012;31:1295-307.
165. Sena LA, Chandel NS. Physiological roles of mitochondrial reactive oxygen species. Mol Cell 2012;48:158-67.
166. Formentini L, Sanchez-Arago M, Sanchez-Cenizo L, Cuezva JM. The Mitochondrial ATPase Inhibitory Factor 1 Triggers a ROS-Mediated Retrograde Prosurvival and Proliferative Response. Mol Cell 2012;45:731-42.
167. West AP, Brodsky IE, Rahner C et al. TLR signalling augments macrophage bactericidal activity through mitochondrial ROS. Nature 2011;472:476-80.
168. Koppen M, Metodiev MD, Casari G, Rugarli EI, Langer T. Variable and tissue-specific subunit composition of mitochondrial m-AAA protease complexes linked to hereditary spastic paraplegia. Mol Cell Biol 2007;27:758-67.
169. Pierson TM, Adams D, Bonn F et al. Whole-exome sequencing identifies homozygous AFG3L2 mutations in a spastic ataxia-neuropathy syndrome linked to mitochondrial m-AAA proteases. PLoS Genet 2011;7:e1002325.
170. Casari G, De Fusco M, Ciarmatori S et al. Spastic paraplegia and OXPHOS impairment caused by mutations in paraplegin, a nuclear-encoded mitochondrial metalloprotease. Cell 1998;93:973-83.
171. Deeken JF, Cormier T, Price DK et al. A pharmacogenetic study of docetaxel and thalidomide in patients with castration-resistant prostate cancer using the DMET genotyping platform. Pharmacogenomics J 2010;10:191-9.
172. Morris AP, Voight BF, Teslovich TM et al. Large-scale association analysis provides insights into the genetic architecture and pathophysiology of type 2 diabetes. Nat Genet 2012;44:981-90.
173. Schunkert H, König IR, Kathiresan S et al. Large-scale association analysis identifies 13 new susceptibility loci for coronary artery disease. Nat Genet 2011;43:333-8.
174. Kiliszek M, Burzynska B, Michalak M et al. Altered gene expression pattern in peripheral blood mononuclear cells in patients with acute myocardial infarction. PLoS One 2012;7:e50054.
175. Wingrove JA, Daniels SE, Sehnert AJ et al. Correlation of peripheral-blood gene expression with the extent of coronary artery stenosis. Circ Cardiovasc Genet 2008;1:31-8.
176. Suno R, Niwa H, Tsuchiya D, Zhang X, Yoshida M, Morikawa K. Structure of the whole cytosolic region of ATP-dependent protease FtsH. Mol Cell 2006;22:575-85.
177. Langer T. AAA proteases: cellular machines for degrading membrane proteins. Trends Biochem Sci 2000;25:247-51.
178. Augustin S, Gerdes F, Lee S, Tsai FT, Langer T, Tatsuta T. An intersubunit signaling network coordinates ATP hydrolysis by m-AAA proteases. Mol Cell 2009;35:574-85.
179. Hardie DG. Minireview: the AMP-activated protein kinase cascade: the key sensor of cellular energy status. Endocrinology 2003;144:5179-83.
180. Bravo R, Vicencio JM, Parra V et al. Increased ER-mitochondrial coupling promotes mitochondrial respiration and bioenergetics during early phases of ER stress. J Cell Sci 2011;124:2143-52.
181. Brookes PS. Mitochondrial H(+) leak and ROS generation: an odd couple. Free Radic Biol Med 2005;38:12-23.
182. Sohal RS, Toroser D, Bregere C, Mockett RJ, Orr WC. Age-related decrease in expression of mitochondrial DNA encoded subunits of cytochrome c oxidase in Drosophila melanogaster. Mech Ageing Dev 2008;129:558-61.

183. Rosca MG, Vazquez EJ, Chen Q, Kerner J, Kern TS, Hoppel CL. Oxidation of fatty acids is the source of increased mitochondrial reactive oxygen species production in kidney cortical tubules in early diabetes. Diabetes 2012;61:2074-83.
184. Echtay KS, Murphy MP, Smith RA, Talbot DA, Brand MD. Superoxide activates mitochondrial uncoupling protein 2 from the matrix side. Studies using targeted antioxidants. J Biol Chem 2002;277:47129-35.
185. Thomas SR, Chen K, Keaney JF, Jr. Hydrogen peroxide activates endothelial nitric-oxide synthase through coordinated phosphorylation and dephosphorylation via a phosphoinositide 3-kinase-dependent signaling pathway. J Biol Chem 2002;277:6017-24.
186. Nisoli E, Falcone S, Tonello C et al. Mitochondrial biogenesis by NO yields functionally active mitochondria in mammals. Proc Natl Acad Sci U S A 2004;101:16507-12.
187. Bell EL, Klimova TA, Eisenbart J et al. The Qo site of the mitochondrial complex III is required for the transduction of hypoxic signaling via reactive oxygen species production. J Cell Biol 2007;177:1029-36.
188. Guevara NV, Kim HS, Antonova EI, Chan L. The absence of p53 accelerates atherosclerosis by increasing cell proliferation in vivo. Nat Med 1999;5:335-9.
189. Ritter SL, Hall RA. Fine-tuning of GPCR activity by receptor-interacting proteins. Nat Rev Mol Cell Biol 2009;10:819-30.
190. Miyazaki T, Neff L, Tanaka S, Horne WC, Baron R. Regulation of cytochrome c oxidase activity by c-Src in osteoclasts. J Cell Biol 2003;160:709-18.
191. Lee I, Salomon AR, Ficarro S et al. cAMP-dependent tyrosine phosphorylation of subunit I inhibits cytochrome c oxidase activity. J Biol Chem 2005;280:6094-100.
192. Cagnoli C, Mariotti C, Taroni F et al. SCA28, a novel form of autosomal dominant cerebellar ataxia on chromosome 18p11.22-q11.2. Brain 2006;129:235-42.
193. Greenberg AJ, Stockwell SR, Clark AG. Evolutionary constraint and adaptation in the metabolic network of Drosophila. Mol Biol Evol 2008;25:2537-46.
194. Salvi M, Brunati AM, Bordin L, La Rocca N, Clari G, Toninello A. Characterization and location of Src-dependent tyrosine phosphorylation in rat brain mitochondria. Biochim Biophys Acta 2002;1589:181-95.
195. Hitosugi T, Fan J, Chung TW et al. Tyrosine phosphorylation of mitochondrial pyruvate dehydrogenase kinase 1 is important for cancer metabolism. Mol Cell 2011;44:864-77.
196. Grey JY, Connor MK, Gordon JW, Yano M, Mori M, Hood DA. Tom20-mediated mitochondrial protein import in muscle cells during differentiation. Am J Physiol Cell Physiol 2000;279:C1393-400.
197. Kim KY, Rhim T, Choi I, Kim SS. N-acetylcysteine induces cell cycle arrest in hepatic stellate cells through its reducing activity. J Biol Chem 2001;276:40591-8.
198. Yamagishi SI, Edelstein D, Du XL, Kaneda Y, Guzman M, Brownlee M. Leptin induces mitochondrial superoxide production and monocyte chemoattractant protein-1 expression in aortic endothelial cells by increasing fatty acid oxidation via protein kinase A. J Biol Chem 2001;276:25096-100.
199. Bartels K, Grenz A, Eltzschig HK. Hypoxia and inflammation are two sides of the same coin. Proc Natl Acad Sci U S A 2013;110:18351-2.
200. Danesh J, Collins R, Peto R. Chronic infections and coronary heart disease: is there a link? Lancet 1997;350:430-6.
201. Roberts R, Stewart AFR. 9p21 and the genetic revolution for coronary artery disease. Clin Chem 2012;58:104-12.
202. Little J, Higgins JP, Ioannidis JP et al. STrengthening the REporting of Genetic Association Studies (STREGA): an extension of the STROBE statement. PLoS Med 2009;6:e22.
203. Stewart AFR, Dandona S, Chen L et al. Kinesin family member 6 variant Trp719Arg does not associate with angiographically defined coronary artery disease in the Ottawa Heart Genomics Study. J Am Coll Cardiol 2009;53:1471-2.
204. Wittig I, Braun HP, Schagger H. Blue native PAGE. Nat Protoc 2006;1:418-28.
205. Schauss AC, Huang H, Choi SY et al. A novel cell-free mitochondrial fusion assay amenable for high-throughput screenings of fusion modulators. BMC Biol 2010;8:100.

206. Qian L, Song X, Ren H, Gong J, Cheng S. Mitochondrial mechanism of heat stress-induced injury in rat cardiomyocyte. Cell Stress Chaperones 2004;9:281-93.
207. Mailloux RJ, Seifert EL, Bouillaud F, Aguer C, Collins S, Harper ME. Glutathionylation acts as a control switch for uncoupling proteins UCP2 and UCP3. J Biol Chem 2011;286:21865-75.
208. Schwede T, Kopp J, Guex N, Peitsch MC. SWISS-MODEL: An automated protein homology-modeling server. Nucleic Acids Res 2003;31:3381-5.
209. Thompson JD, Gibson TJ, Plewniak F, Jeanmougin F, Higgins DG. The CLUSTAL_X windows interface: flexible strategies for multiple sequence alignment aided by quality analysis tools. Nucleic Acids Res 1997;25:4876-82.
210. Koradi R, Billeter M, Wuthrich K. MOLMOL: a program for display and analysis of macromolecular structures. J Mol Graph 1996;14:51-5, 29-32.
211. Horton JD, Cohen JC, Hobbs HH. Molecular biology of PCSK9: its role in LDL metabolism. Trends Biochem Sci 2007;32:71-7.
212. Cohen JC, Boerwinkle E, Mosley TH, Jr., Hobbs HH. Sequence variations in PCSK9, low LDL, and protection against coronary heart disease. N Engl J Med 2006;354:1264-72.
213. Benn M, Nordestgaard BG, Grande P, Schnohr P, Tybjaerg-Hansen A. PCSK9 R46L, low-density lipoprotein cholesterol levels, and risk of ischemic heart disease: 3 independent studies and meta-analyses. J Am Coll Cardiol 2010;55:2833-42.
214. Lakoski SG, Lagace TA, Cohen JC, Horton JD, Hobbs HH. Genetic and metabolic determinants of plasma PCSK9 levels. J Clin Endocrinol Metab 2009;94:2537-43.
215. Truong QA, Murphy SA, McCabe CH, Armani A, Cannon CP. Benefit of intensive statin therapy in women: results from PROVE IT-TIMI 22. Circ Cardiovasc Qual Outcomes 2011;4:328-36.
216. Kostis WJ, Cheng JQ, Dobrzynski JM, Cabrera J, Kostis JB. Meta-analysis of statin effects in women versus men. J Am Coll Cardiol 2012;59:572-82.
217. McKenney JM, Koren MJ, Kereiakes DJ, Hanotin C, Ferrand AC, Stein EA. Safety and efficacy of a monoclonal antibody to proprotein convertase subtilisin/kexin type 9 serine protease, SAR236553/REGN727, in patients with primary hypercholesterolemia receiving ongoing stable atorvastatin therapy. J Am Coll Cardiol 2012;59:2344-53.
218. Norata GD, Tibolla G, Catapano AL. Targeting PCSK9 for hypercholesterolemia. Annu Rev Pharmacol Toxicol 2014;54:273-93.
219. Fan M, Dandona S, McPherson R et al. Two Chromosome 9p21 Haplotype Blocks Distinguish Between Coronary Artery Disease and Myocardial Infarction Risk. Circ Cardiovasc Genet 2013;6:372-80.
220. Reilly MP, Li M, He J et al. Identification of ADAMTS7 as a novel locus for coronary atherosclerosis and association of ABO with myocardial infarction in the presence of coronary atherosclerosis: two genome-wide association studies. Lancet 2011;377:383-92.
221. Chan K, Patel RS, Newcombe P et al. Association between the chromosome 9p21 locus and angiographic coronary artery disease burden: a collaborative meta-analysis. J Am Coll Cardiol 2013;61:957-70.
222. Persson L, Henriksson P, Westerlund E, Hovatta O, Angelin B, Rudling M. Endogenous estrogens lower plasma PCSK9 and LDL cholesterol but not Lp(a) or bile acid synthesis in women. Arterioscler Thromb Vasc Biol 2012;32:810-4.
223. Kosenko T, Golder M, Leblond G, Weng W, Lagace TA. Low Density Lipoprotein Binds to Proprotein Convertase Subtilisin/Kexin Type-9 (PCSK9) in Human Plasma and Inhibits PCSK9-mediated Low Density Lipoprotein Receptor Degradation. J Biol Chem 2013;288:8279-88.
224. Costet P, Hoffmann MM, Cariou B, Guyomarc'h Delasalle B, Konrad T, Winkler K. Plasma PCSK9 is increased by fenofibrate and atorvastatin in a non-additive fashion in diabetic patients. Atherosclerosis 2010;212:246-51.
225. Mayne J, Dewpura T, Raymond A et al. Plasma PCSK9 levels are significantly modified by statins and fibrates in humans. Lipids Health Dis 2008;7:22.
226. Gu Q, Dillon CF, Burt VL. Prescription drug use continues to increase: U.S. prescription drug data for 2007-2008. NCHS data brief 2010:1-8.
227. Abd TT, Jacobson TA. Statin-induced myopathy: a review and update. Expert opinion on drug safety 2011;10:373-87.

228. Cohen J, Pertsemlidis A, Kotowski IK, Graham R, Garcia CK, Hobbs HH. Low LDL cholesterol in individuals of African descent resulting from frequent nonsense mutations in PCSK9. Nat Genet 2005;37:161-5.
229. Roberts R, Stewart AFR. Genes and coronary artery disease: where are we? J Am Coll Cardiol 2012;60:1715-21.
230. Voight BF, Peloso GM, Orho-Melander M et al. Plasma HDL cholesterol and risk of myocardial infarction: a mendelian randomisation study. Lancet 2012;380:572-80.
231. Gaziano JM, Hennekens CH, Satterfield S et al. Clinical utility of lipid and lipoprotein levels during hospitalization for acute myocardial infarction. Vasc Med 1999;4:227-31.
232. Wattanasuwan N, Khan IA, Gowda RM, Vasavada BC, Sacchi TJ. Effect of acute myocardial infarction on cholesterol ratios. Chest 2001;120:1196-9.
233. Pfohl M, Schreiber I, Liebich HM, Haring HU, Hoffmeister HM. Upregulation of cholesterol synthesis after acute myocardial infarction--is cholesterol a positive acute phase reactant? Atherosclerosis 1999;142:389-93.
234. Le Bras M, Roquilly A, Deckert V et al. Plasma PCSK9 Is a late biomarker of severity in patients with severe trauma injury. J Clin Endocrinol Metab 2013;98:E732-6.
235. Poirier S, Mayer G, Benjannet S et al. The proprotein convertase PCSK9 induces the degradation of low density lipoprotein receptor (LDLR) and its closest family members VLDLR and ApoER2. J Biol Chem 2008;283:2363-72.
236. Quinn KL, Henriques M, Tabuchi A et al. Human neutrophil peptides mediate endothelial-monocyte interaction, foam cell formation, and platelet activation. Arterioscler Thromb Vasc Biol 2011;31:2070-9.
237. Morning peak in the incidence of myocardial infarction: experience in the ISIS-2 trial. ISIS-2 (Second International Study of Infarct Survival) Collaborative Group. Eur Heart J 1992;13:594-8.
238. Persson L, Cao G, Stahle L et al. Circulating proprotein convertase subtilisin kexin type 9 has a diurnal rhythm synchronous with cholesterol synthesis and is reduced by fasting in humans. Arterioscler Thromb Vasc Biol 2010;30:2666-72.
239. Tofler GH, Brezinski D, Schafer AI et al. Concurrent morning increase in platelet aggregability and the risk of myocardial infarction and sudden cardiac death. N Engl J Med 1987;316:1514-8.
240. Chernogubova E, Strawbridge R, Mahdessian H et al. Common and low-frequency genetic variants in the PCSK9 locus influence circulating PCSK9 levels. Arterioscler Thromb Vasc Biol 2012;32:1526-34.
241. Yusuf S, Hawken S, Ounpuu S et al. Effect of potentially modifiable risk factors associated with myocardial infarction in 52 countries (the INTERHEART study): case-control study. Lancet 2004;364:937-52.
242. Smeeth L, Thomas SL, Hall AJ, Hubbard R, Farrington P, Vallance P. Risk of myocardial infarction and stroke after acute infection or vaccination. N Engl J Med 2004;351:2611-8.
243. Feingold KR, Moser AH, Shigenaga JK, Patzek SM, Grunfeld C. Inflammation stimulates the expression of PCSK9. Biochem Biophys Res Commun 2008;374:341-4.
244. Li S, Guo YL, Xu RX et al. Plasma PCSK9 levels are associated with the severity of coronary stenosis in patients with atherosclerosis. Int J Cardiol 2014;174:863-4.
245. Fan M, Dandona S, McPherson R et al. Two chromosome 9p21 haplotype blocks distinguish between coronary artery disease and myocardial infarction risk. Circ Cardiovasc Genet 2013;6:372-80.
246. Erridge C, Gracey J, Braund PS, Samani NJ. The 9p21 locus does not affect risk of coronary artery disease through induction of type 1 interferons. J Am Coll Cardiol 2013;62:1376-81.
247. O'Donnell CJ, Kavousi M, Smith AV et al. Genome-wide association study for coronary artery calcification with follow-up in myocardial infarction. Circulation 2011;124:2855-64.
248. van Setten J, Isgum I, Smolonska J et al. Genome-wide association study of coronary and aortic calcification implicates risk loci for coronary artery disease and myocardial infarction. Atherosclerosis 2013;228:400-5.
249. Schieber M, Chandel NS. ROS function in redox signaling and oxidative stress. Curr Biol 2014;24:R453-62.

250. Woo HA, Yim SH, Shin DH, Kang D, Yu DY, Rhee SG. Inactivation of peroxiredoxin I by phosphorylation allows localized H(2)O(2) accumulation for cell signaling. Cell 2010;140:517-28.
251. Ito K, Hirao A, Arai F et al. Reactive oxygen species act through p38 MAPK to limit the lifespan of hematopoietic stem cells. Nat Med 2006;12:446-51.
252. Gao P, Zhang H, Dinavahi R et al. HIF-dependent antitumorigenic effect of antioxidants in vivo. Cancer Cell 2007;12:230-8.
253. Neumann CA, Krause DS, Carman CV et al. Essential role for the peroxiredoxin Prdx1 in erythrocyte antioxidant defence and tumour suppression. Nature 2003;424:561-5.
254. Cheng G, Zielonka J, McAllister DM et al. Mitochondria-targeted vitamin E analogs inhibit breast cancer cell energy metabolism and promote cell death. BMC Cancer 2013;13:285.
255. Ni J, Chen M, Zhang Y, Li R, Huang J, Yeh S. Vitamin E succinate inhibits human prostate cancer cell growth via modulating cell cycle regulatory machinery. Biochem Biophys Res Commun 2003;300:357-63.
256. Lim ET, Liu YP, Chan Y et al. A Novel Test for Recessive Contributions to Complex Diseases Implicates Bardet-Biedl Syndrome Gene BBS10 in Idiopathic Type 2 Diabetes and Obesity. Am J Hum Genet 2014;95:509-20.
257. Li S, Guo YL, Xu RX et al. Association of plasma PCSK9 levels with white blood cell count and its subsets in patients with stable coronary artery disease. Atherosclerosis 2014;234:441-5.
258. Zhang Y, Zhu CG, Xu RX et al. Relation of circulating PCSK9 concentration to fibrinogen in patients with stable coronary artery disease. J Clin Lipidol 2014;8:494-500.
259. Madjid M, Fatemi O. Components of the complete blood count as risk predictors for coronary heart disease: in-depth review and update. Tex Heart Inst J 2013;40:17-29.
260. Stein EA, Gipe D, Bergeron J et al. Effect of a monoclonal antibody to PCSK9, REGN727/SAR236553, to reduce low-density lipoprotein cholesterol in patients with heterozygous familial hypercholesterolaemia on stable statin dose with or without ezetimibe therapy: a phase 2 randomised controlled trial. Lancet 2012;380:29-36.
261. Lindholm MW, Elmen J, Fisker N et al. PCSK9 LNA antisense oligonucleotides induce sustained reduction of LDL cholesterol in nonhuman primates. Mol Ther 2012;20:376-81.
262. Ding Q, Strong A, Patel KM et al. Permanent alteration of PCSK9 with in vivo CRISPR-Cas9 genome editing. Circ Res 2014;115:488-92.